POLITECNICO DI TORINO

Master's Degree in Energy and Nuclear Engineering

Master's Degree Thesis

ANALYSIS OF RENEWABLE ENERGY AND CARBON CAPTURE: APPLICATION TO SARDINIA ISLAND

Supervisors

Prof. GIOVANNI BRACCO

Prof. DOUGLAS KELLER

Prof. PHILIPPE DROBINSKI

Candidate

GABRIELE CELLAI

OCTOBER 2023

Abstract

The imperative shift towards renewable energy sources has become more critical than ever in the current global context. Among several options, offshore wind energy has emerged as a promising avenue for sustainable power generation.
Within this context, the Mediterranean region, specifically the area surrounding the island of Sardinia, with its exceptional wind patterns and vast expanses of unexplored offshore territory, stands out as an exciting opportunity to exploit this kind of green energy.

In this perspective, the following study delves into the meticulous research and analysis that underpins the selection of an offshore region where to locate a wind power plant. Such a facility, determined with the utilization of program tools as ERA5 and CMEMS for the evaluation of wind and wave characteristics, will be used to run a series of devices for the synthesis of methanol, through the capture of atmospheric CO_2 and the combination of it with hydrogen gas.

Basing on wind pattern considerations and environmental constraints, the location has been found in the southern region of Sardinia, close to Gulf di Cagliari, a promising area where to put the plant.
Considering the power production of that facility, simulated with FLORIS program, that power, in turn, has been used to simulate the final fuel output production, numerically built on pyseafuel python package. Given a substantial wind plant facility with a total net power capacity of 600 MW and a seawater inflow rate of 10 L/s, the expected daily methanol output has been calculated to be 1400 liters/day.

This kind of plants, eventually implemented with a wave capture energy device to improve the performances, represent a promising step towards future implementation. However, it is worth noting that additional studies, primarily focused on economic aspects and technological enhancements, will be essential to fully realize the potential of this innovative approach.

I

Table of Contents

List of Tables

List of Figures

VIII

x

Acronyms

AEM

    Anion Exchange Membrane

BECCS

    Bio-energy with Carbon Capture and Storage

BECCU

    Bio-energy with Carbon Capture and Utilization

BPM

    Bipolar Membrane

BPMED

    Bipolar Membrane Electrodialysis

BPZ

    Biological Protection Zone

CDR

    Carbon Dioxide Removal

CEM

    Cation Exchange Membrane

CER

    Chlorine Evolution Reaction

CMEMS

    Copernicus Marine Environment Monitoring Service

COP27

United Nations Climate Change Conference

DAC

Direct Air Capture

DIC

Dissolved Inorganic Carbon

DME

Dimethyl ether

DMFC

Direct methanol fuel cell

ECMWF

European Centre for Medium-Range Weather Forecasts

ED

Electrodialysis

ESD

Effort-sharing Decision

ESR

Effort-sharing Regulation

ETS

Emission Trading System

EU

European Union

EUA

European Union Allowances

EUA-A

European Union Aviation Allowances

GHG

Greenhouse Gas

HER

Hydrogen Evolution Reaction

IEM

Ion Exchange Membrane

ICE

Internal Combustion Engine

LNG

Liquified Natural Gas

MEA

Membrane-Electrode Assembly

MISE

Ministry of Economic Development, called now Ministry of Enterprises and Made in Italy

MIT

Ministry of Infrastructure and Transport

MTBE

Methyl tert-butyl ether

NAP

National Adaptation Plan

NECP

National Energy and Climate Plan

NSDS

National Sustainable Development Strategy

OER

Oxigen Evolution Reaction

OWC

Oscillating Water Column

PEARS

Energy and Environment Plan of the Sardinia Region

PEM

Proton Exchange Membrane

PNRR

National Recovery and Resilience Plan

PTO

Power Take Off

RES

Renewable Energy Source

REDII

Renewable Energy Directive II

RWGS

Reverse Water Gas Shift

SAC

Special Area of Conservation

SCI

Site of Community Importance

SOE

Solid Oxide Electrolyzer

SPA

Special Protection Area

SSLNG

Small Scale Liquifie Natural Gas

TRL

Technology Readiness Level

WEC

Wave Energy Converter

Chapter 1

Introduction

The topic of renewable energy is a growing concern among both specialists and the general population. Over the recent years, there has been a significant rise in studies focusing on renewable energy sources (RES), both in absolute numbers and in relation to other research areas. These RES have the potential to play a vital role in addressing two critical issues: the depletion of fossil fuels and global warming. Energy sources can be broadly categorized into three main types: fossil fuels, nuclear resources, and renewable resources. Among these, RES such as solar, wind, biomass, geothermal, and hydro-power, hold immense importance as they offer a viable means to combat the energy crises. One of the most significant reasons for the importance of renewable energy is its ability to mitigate climate change. [1] By harnessing these renewable sources, it is possible to replenish the energy needs and mitigate the challenges posed by finite fossil fuel supplies. Plus, relying on renewable energy sources will enhance energy security and independence for countries. Price fluctuations of fossil fuels have triggered economic instability in numerous countries and the uneven distribution of these finite resources worldwide has led to some nations becoming reliant on others to fulfill their energy demands, thereby amplifying their economic vulnerabilities. These challenges collectively pose significant threats to a country's energy security, which is a crucial prerequisite for sustainable growth. To safeguard their energy security, countries must adopt various measures to address these threats and a prominent approach is to enhance the utilization of renewable energy sources. By diversifying their energy mix and embracing renewable technologies, countries can reduce their reliance on fluctuating fossil fuel supplies and enhance their resilience against energy-related risks. [2] Unlike fossil fuels, which often need to be imported from other regions, renewable energy can be harnessed domestically, reducing dependence on foreign energy resources and mitigating geopolitical risks. Moreover they have the potential to improve energy affordability and accessibility, particularly in rural and remote areas, with difficult access to the main grid. Especially in this very turbulent geopolitical

period, after years of Covid that hit the economy and with the Ukrainian war now, the tension that Europe is living has disrupt the traditional energy supply chains, affecting the availability and affordability of energy. [3] That's why diversifying energy sources and promoting energy security through regional cooperation and alternative energy routes can help mitigate this risk as well as being able to self-produce its own energy will allow individuals, communities and countries to reduce their dependence on external energy sources. They can gain more control over their energy supply reducing vulnerability to energy price fluctuations, supply disruptions, and geopolitical tensions associated with it.

In the last years Europe has emerged as a leading force in the global fight against climate change, recognizing the need to reduce greenhouse gas emissions and transition towards a sustainable, low-carbon future. As the world grapples with the impact of climate change, the European Union and its member states have set ambitious goals for decarbonization. With a steadfast commitment to combat climate change, Europe aims to create a greener, cleaner and more resilient continent. These European goals go beyond the mere environmental preservation; they encompass economic, social and geopolitical aspects as well. Europe seeks to foster innovation, enhance energy security and improve the overall well-being of its citizens. Decarbonization is at the core of Europe's long-term vision, encapsulated in European Green Deal, a comprehensive roadmap to transform the continent into the world's first climate-neutral continent by 2050. Under this ambitious framework, the EU aims to reduce its net greenhouse gas emissions to zero and decouple economic growth from resource consumption. To achieve these goals, Europe has set specific targets for emissions reduction and renewable energy deployment. It has committed to reduce the emissions by at least 55% by 2030, compared to 1990 levels. The main goal of the European Green Deal strategy is to place sustainability and human well-being at the centre of economic policy and as a fundamental dimension of all policy decisions and the resulting actions. [4] Europe's commitment to decarbonization is further reinforced by international collaborations such as the Paris Agreement, which aims to limit global warming to well below 2 °C above pre-industrial levels.

Therefore, all the methods to capture, store and utilize the carbon dioxide, could play a fundamentl role to prevent a significant amount of greenhouse gases from entering the atmosphere, helping to limit global warming and minimize the impacts of climate change, such as rising temperatures, sea-level rise and extreme weather events. For instance, carbon dioxide removal (CDR) technology is being extensively studied as a way to potentially reverse emissions enough to return warming trends to only a 1.5 °C global temperature increase. [5] [6] Carbon capture technologies can be also integrated into existing industrial and power generation facilities, allowing

for the continued use of fossil fuels while reducing emissions. This compatibility enables a smoother transition towards a low-carbon economy, as it does not require an immediate and complete overhaul of existing energy infrastructure. Plus, carbon capture, when combined with carbon utilization or storage, can contribute to achieve negative emissions. Negative emissions technologies remove CO_2 from the atmosphere, effectively reversing the carbon emissions process. This can help offset emissions from sectors that are challenging to decarbonize and assist in achieving carbon neutrality or net-zero emissions goals.

So, following these goals and these directives that Europe has adopted, Italy has set its sights on a greener an more sustainable future too. This commitment is reflected in key documents and initiatives that guide Italy's path towards decarbonization. One of the primary documents is the National Energy and Climate Plan (NECP). Aligned with European Union's objectives, it serves as a roadmap to guide Italy's energy transition until 2030, taking into account the targets set by the EU climate-energy policy and Paris Agreement. The NECP emphasizes the importance of renewable energy, energy efficiency, and sustainable mobility as crucial pillars of Italy's decarbonization strategy. Italy has set an ambitious target of achieving a 30% share of renewable energy in its final energy consumption by 2030. This target encompasses a diversified mix of renewable sources, including solar, wind, hydro, and biomass. Plus a reduction in GHG vs 2005 for all non-ETS sectors of 33% respect to 2005 levels. The NECP also highlights the need to promote energy efficiency measures, aiming for a 43% improvement in energy efficiency by 2030 compared to 2007 levels. [7] In Table 1.1 are visible the goals of Europe and Italy in the fight to climate change.

In addition to the NECP, Italy has established the National Adaptation Plan (NAP) to address the impacts of climate change and enhance the country's resilience. The NAP focuses on identifying vulnerabilities, implementing adaptation measures, and integrating climate considerations into policy planning. Moreover, Italy's commitment to decarbonization extends to regional and local levels. Many Italian cities have embraced sustainable urban development and have implemented initiatives to reduce emissions and enhance energy efficiency. These efforts align with nation's broader decarbonization goals and contribute to the country's overall sustainability objectives. In this optic the perspective of capturing CO_2 from the atmosphere and utilizing it to produce a synthetic fuel through a process of CO_2 hydrogenation offers a multifaceted approach to address pressing environmental and energy challenges. Capturing CO_2 and converting it into a fuel like methanol will help to reduce its levels, thereby directly contributing to climate change mitigation efforts aligned with national plans and international agreements aimed at reducing these emissions. Methanol moreover is widely used in the chemical

	2030 objectives	
	EU	ITALY (NECP)
Renewable energies (RES)		
Share of energy from RES in the gross final consumption of energy	32%	30%
Share of energy from RES in the gross final consumption of energy in the transport sector	14%	22%
Energy efficiency		
Reduction in primary energy consumption compared to PRIMES 2007 scenario	-32.5%	-43%
Greenhouse gas emissions		
Reduction in GHG vs 2005 for all plants subject to ETS rules	-43%	
Reduction in GHG vs 2005 for all non-ETS sectors	-30%	-33%

Table 1.1: Primary energy and climate objectives 2030, EU and Italy. The PRIMES model represents a European Union energy system model that mimics energy consumption and the energy supply infrastructure.

industry, in the production of formaldehyde, MTBE (methyl tert-butyl ether) and acetic acid, it has excellent combustion properties, which allows its use as a fuel in vehicles, although it has only about half the energy density of gasoline and last it is less polluting than conventional fossil fuels. Methanol and its derivative, dimethyl ether (DME), display remarkable efficiency as fuels in internal combustion engines (ICE) and can subsequently be utilized in the production of a wide array of hydrocarbon-based products. [8] [9] Hence this path of methanol and/or dimethyl ether production involving chemical recycling of carbon dioxide, presents a novel approach to achieving renewable fuels with a remarkable carbon-neutral or even carbon-negative impact on the environment. Carbon recycling creates a circular economy approach, where carbon is reused and transformed into useful products like methanol. The energy needed to run the process will be taken from renewable energies like the one from the wind or the sun making the system carbon-neutral and closing the anthropogenic carbon cycle, as also visible in Fig. 1.1 So, by capturing CO_2 from the atmosphere and using it to produce methanol through CO_2 hydrogenation, a proactive step towards combating climate change is taken, fostering a sustainable energy system, and unlocking new economic opportunities, all while supporting the goals outlined in national plans for a greener and more resilient future.
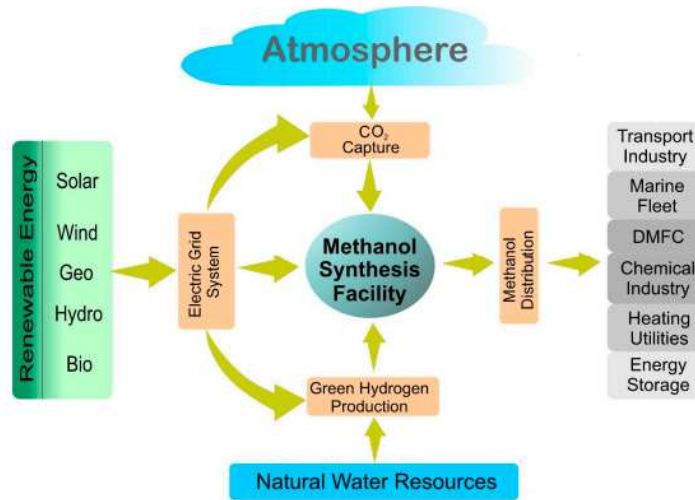
Figure 1.1: Clean methanol synthesis and its utilization in a carbon neutral cycle. Starting from renewable energy to produce electricity. Then using it to extract CO_2 from atmosphere and hydrogen from a natural water resource and combining them to obtain methanol. This could have several final utilization after a distillation process.

1.1 Advancing Energy Sustainability: Exploring CO_2 Capture and Self-Fuel Production for a Greener Future

Basing on all the benefits linked with the implementation of a renewable energy power device, the ones associated with the capture of CO_2 and all the documents published to push the energy transition towards a greener future, the realization and implementation of a self-fuel production structure coupled with CO_2 capture offers several advantages, starting from energy sustainability, passing through emissions reduction and finishing with environmental stewardship. That's why the scope of this project has been the research on the realization of a structure able to capture CO_2 from the Mediterranean sea, reducing so the level into the atmosphere and using the carbon dioxide captured to self-produce a synthetic fuel which could be used for several purposes. The choice of which kind of fuel will be based on the actual state of economy allowing the best income and depending on which are the future trends Sardinia's region wants to pursue. However, this particular decision will not be analyzed within this study. Instead, the focus here is solely centered on performing a preliminary analysis to evaluate the project's technical feasibility, with no consideration given to potential energy scenarios or economic assessments.

1.2 Driving Italy's Energy Transition: Policies, Targets, and Regional Initiatives

At the national level, Italy intends to accelerate the transition from traditional fuels to renewable sources, promoting the gradual phasing out of coal for electricity generation in favor of an electric mix, based on an increasing share of renewables and, for the residual part, gas. A contibution is done by the National Energy and Climate Plan, NECP, a strategic plan developed by the Italian government to set targets and actions related to greenhouse gas emissions reduction, renewable energy deployment, energy efficiency improvements, and other aspects of the energy transition. It serves as a roadmap for Italy's energy and climate policies, aligning with international and European Union commitments and goals.

Italy will implement the necessary policies and measures to achieve greenhouse gas reduction targets agreed upon at the international and European level. For sectors covered by the EU-ETS, European Emission Trading System, explained in section 1.3, such as thermal power generation and energy-intensive industries, in addition to higher CO_2 prices compared to previous years, the phase-out of coal, scheduled by 2025, will contribute along with a significant acceleration of renewables and energy efficiency in industrial processes. Among other measures, the phase-out of coal can be achieved through the construction of additional gas-fired power units. In terms of renewables, Italy will promote their further development while safeguarding and enhancing existing productions, aiming to exceed the 30% target, which should still be considered as a contribution towards the EU objective. For energy supply security, Italy aims to reduce dependency on imports through increased use of renewables and energy efficiency, as well as diversification of supply sources (e.g. by utilizing natural gas, including liquified natural gas LNG, with infrastructure consistent with the deep decarbonization scenario by 2050). Furthermore, to pursue security and flexibility objectives, Italy intends to explore the possibility of greater integration between electricity and gas infrastructure networks. In this context, it will be important to assess the costs and benefits of power-to-gas technologies, which, especially in the long term, could help absorbing any imbalances between renewable electricity production, particularly with high levels of photovoltaic penetration, and energy demand.[7]

Given that gas will continue to serve an essential function in the short to medium term, in conjunction with renewable sources, for industrial and domestic uses (including transportation) and especially for electricity generation, it is important to maintain a strong focus on diversifying the sources of supply. Currently, gas supplies predominantly come from countries with high geopolitical risks. To mitigate this unfavorable situation, efforts have been made to diversify non-European suppliers, optimizing the utilization of LNG import capacity in existing terminals, and

promoting the production of renewable sources of gas for the integration into the network, with the long-term goal of serving all end uses, including electricity generation.

Furthermore, many current laws are based on various resolutions and decrees established by COP27, where discussions were held on addressing the climate emergency, building resilience, adapting to impacts, and financing climate action. According to several official legislative decrees ratified in 2022, it is foreseen that the Ministry of the Interior will directly use or grant concessions for the use of state-owned assets, in whole or in part, to install renewable energy production plants, including, under certain conditions, utilizing resources from the PNRR (National Recovery and Resilience Plan) to cover the related costs. Moreover, the guidelines established by the European Renewable Energy Directive II, REDII, are followed with the aim of accelerating the country's sustainable transition in line with the European objectives towards climate neutrality by 2050, defining the necessary tools, mechanisms, incentives, and institutional, financial, and legal frameworks to achieve the targets for increasing the share of renewable energy by 2030.

With the "Green Package" presented on July 14, 2021, the European Commission proposed the "Fit for 55%" package, aimed at achieving a 55% reduction in emissions by 2030 compared to 1990 levels, as outlined in the Green Deal and made legally binding by the European Climate Law, and also containing relevant elements for adaptation.

Additionally, on January 21, 2020, the Ministry of Economic Development finalized the NEPC, structured into five categories: decarbonization, energy efficiency, energy security, internal energy market, research, innovation, and competitiveness. The main objectives of this plan include achieving a percentage of energy production from renewable sources (RES) in Gross Final Energy Consumption of 30% and a share of energy from RES in Gross Final Energy Consumption in transport of 21.6%, compared to the EU's target of 14%. It also aims to reduce greenhouse gas emissions by 33% in non-ETS sectors compared to 2005 levels, surpassing the Brussels target by an additional 3%. [10]

1.3   Forecast of CO$_2$ in Italy

Speaking about the current regulations in Italy regarding the control of CO$_2$ emissions, they refer to the European Emissions Trading System, also known as ETS. This system represents a true carbon market based on a methodology of limitation and exchange of emission allowances for high-energy-intensive industries and the energy production sector. It is the instrument adopted by the European Union to address emission reduction.

The emissions trading system implemented across the European Union encompasses emissions from electricity generation and industry. The objective of reducing greenhouse gas emissions by at least 40% by 2030 at the European level, compared to 1990 levels, is divided between the ETS sectors (energy-intensive industries, energy-intensive sectors, and aviation) and non-ETS sectors (transportation, residential, tertiary, non-ETS industrial sectors, agriculture, and waste). The ETS sectors are expected to achieve a reduction of -43% compared to 2005 levels, while the non-ETS sectors are expected to achieve a reduction of -30% compared to 2005 levels for Europe and -33% for Italy. [7] This objective is to be achieved through a linear reduction trajectory that will set an emissions cap for each year. Apart from the ETS, the EU has additional legislation, known as the effort-sharing legislation, which addresses emissions from sectors not covered by the ETS, including transport, buildings, agriculture, and waste. Italy was required to decrease its non-ETS greenhouse gas emissions by 13% compared to 2005 levels during the 2013-2020 period, as per the Effort-sharing Decision (ESD). Under the Effort-sharing Regulation (ESR) for the 2021-2030 period, Italy is now obligated to reduce its emissions by 33% against 2005 levels. Fig. 1.3.

The EU ETS functions are based on the concept of "Cap and Trade". It sets a limit, or cap, on the maximum amount of emissions allowed by participating installations. Within this cap, companies have the flexibility to buy or sell emission allowances according to their requirements. These allowances serve as the primary currency within the system, granting the holder the right to emit one metric ton of CO$_2$ or an equivalent amount of other greenhouse gases. Once a year, all companies participating in the EU ETS is required to submit emission allowances equivalent to their emitted CO$_2$eq. A limited number of allowances are allocated for free to certain companies based on standardized rules applied across Europe. Companies that do not receive enough free allowances to cover their emissions or those that do not receive any at all must obtain additional allowances through auctions or from other companies. Conversely, companies with excess allowances can sell them to those in need. Severe penalties are imposed on companies that fail to comply with the emissions reduction obligations. Fig. 1.2.
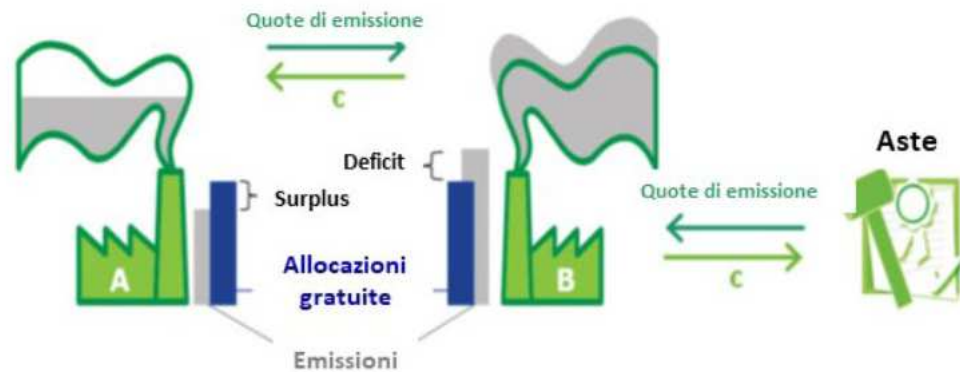
Figure 1.2: Cap&Trade mechanism. Companies can buy and sell emission allowances, which represent the right to emit a certain amount of a pollutant.

Auctions serve as the mechanism for allocating emission allowances to meet the compliance requirements of the EU ETS. Since 2013, auctioning has been the primary method of allocation, although there are exceptions to support the competitiveness of manufacturing sectors in international markets. [11]

The allocation process, starting from that date, promotes efficiency in establishing a reference price for CO_2 in Europe, encourages the internalization of environmental costs, facilitates the transition to sustainable energy mixes, and stimulates investments in energy efficiency. Auctions are used to allocate 50% of the European Union Allowances (EUA), which are climate credits (or carbon credits) utilized within the EU ETS to fulfill emission offsetting obligations for all participating operators. Additionally, 15% of the European Union Aviation Allowances (EUA-A) are allocated through auctions exclusively for aviation operators. Auctions take place on specific platforms determined through competitive bidding processes and are managed in accordance with Regulation 1031/2010 (Auctioning Regulation).

When discussing carbon credits, it's important to note that there are two types operating in two different markets.

- First, there is the mandatory market, which applies to around 12,000 large, high-emitting companies operating in specific sectors such as energy, oil and gas, steel, etc. These companies are obligated to purchase GHG emission permits.

- The other type is the voluntary market, which involves all companies and individuals who choose to voluntarily offset their emissions by purchasing carbon credits.

In the mandatory market, following the Cap and Trade logic, governments

establish annual caps on maximum allowable emissions. If a company exceeds its allocated quota, it is required to purchase additional carbon credits to cover the excess emissions. The price in this market is determined by a regulated system that sets the prices for purchasing these permits. On the other hand, in the voluntary market, carbon credits are traded through individual transactions between sellers and buyers. As a result, prices can vary significantly depending on factors such as the project type, location, volume of purchase, and co-benefits generated by the project itself.

In Italy, the quantities of emissions in the non-ETS sectors are primarily influenced by the transportation and civil sectors (residential and tertiary). The implementation techniques to reduce these emissions will involve a greater focus on energy efficiency improvements in existing buildings for the civil sector. As for the transportation sector, the reduction in emissions will be achieved through a combination of the gradual and natural replacement of the vehicle fleet, the development of shared/public mobility, and the progressive adoption of vehicles with lower energy consumption and significantly reduced or zero CO_2 emissions.
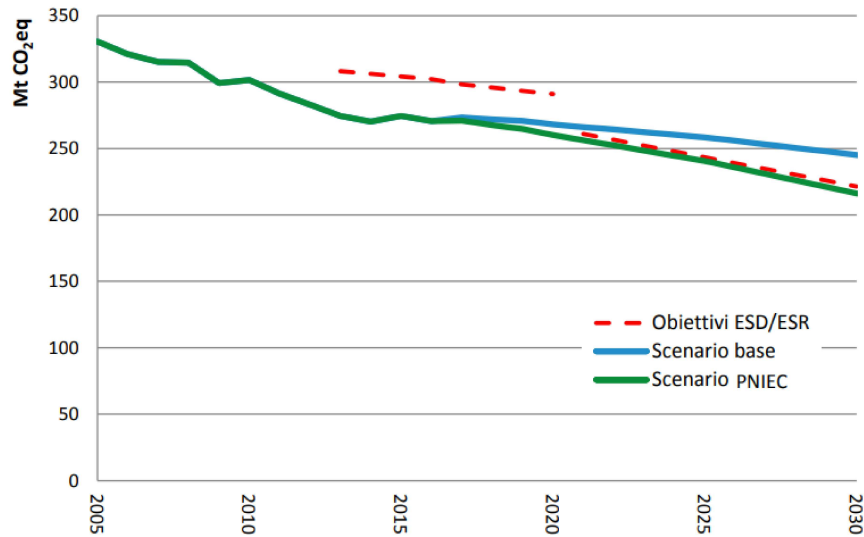
Figure 1.3: Historical trends in emissions in the non-ETS sectors and future scenarios. Blue line stands for the basic scenario, dashed line refers to ESD/ESR goals and green line is the NEPC scenario.

1.4   A Focus on Sardinia's Energy Transition

The focus of the study has been pointed out on the island of Sardinia, looking for the best location where to put a potential offshore wind farm to run a floating platform for the production of a synthetic fuel. The choice to exclusively focus on the island of Sardinia is due to its current electrical and energetic condition. This allows the exploitation of its rich energetic potential, as visible using the software Solargis and Global Wind Atlas, to perform the carbon dioxide capture process. Further explanations will be provided within this section, once have seen its energetic mix.
As stated in the National Energy and Environmental Plan, the electrical grid in Sardinia needs to be expanded. Additionally, in terms of methane supply, Sardinia is the only island without access to the national gas network, which results in excessive coal consumption and usage of residues from oil refining processes. Given this very marginal penetration of methane and the relevance of services like tourism, commerce, agriculture, Sardinia needs to be electrified, since nowadays electricity is mainly produced by leveraging coal and residues from oil refining processes. The goal of the electrification initiative by 2030 is to eliminate coal-based energy production, enhance the proportion of renewable energy derived from solar photovoltaic and wind sources in the energy mix and facilitate the electrification of various end uses.

But before delving into the projects and objectives to implement Sardinia's energy plan, it is important to provide a general overview of the energy supply and dispatch situation in different sectors, considering their sources and purposes. According to the information reported by PEARS (Energy and Environment Plan of the Sardinia Region) it is possible to observe from Fig. 1.4 both the structure of the regional energy system and the energy exchanges that occur among different entities. The highest import to the island is in terms of the quantity of oil, which is 12,105 ktep (kilotons of oil equivalent), followed by coal, which accounts for one-tenth of the quantity of oil. Once all the necessary transformations of the raw products are completed, heat production consists of 94.8% from fossil sources, while for the electricity sector, it covers 69%. Second position for wind energy production with a substantial smaller amount of 12%. About the net electricity produced, electrical losses stand at 6.4%, a slightly higher amount than the national average. Out of all the electricity generated, only 70% is consumed regionally, while the remaining portion is exported to other regions, with a smaller quantity being exported abroad. Analyzing in detail the Sankey diagram of Sardinia region, Fig. 1.5, it is possible to have a better look of the path followed for electricity.

11
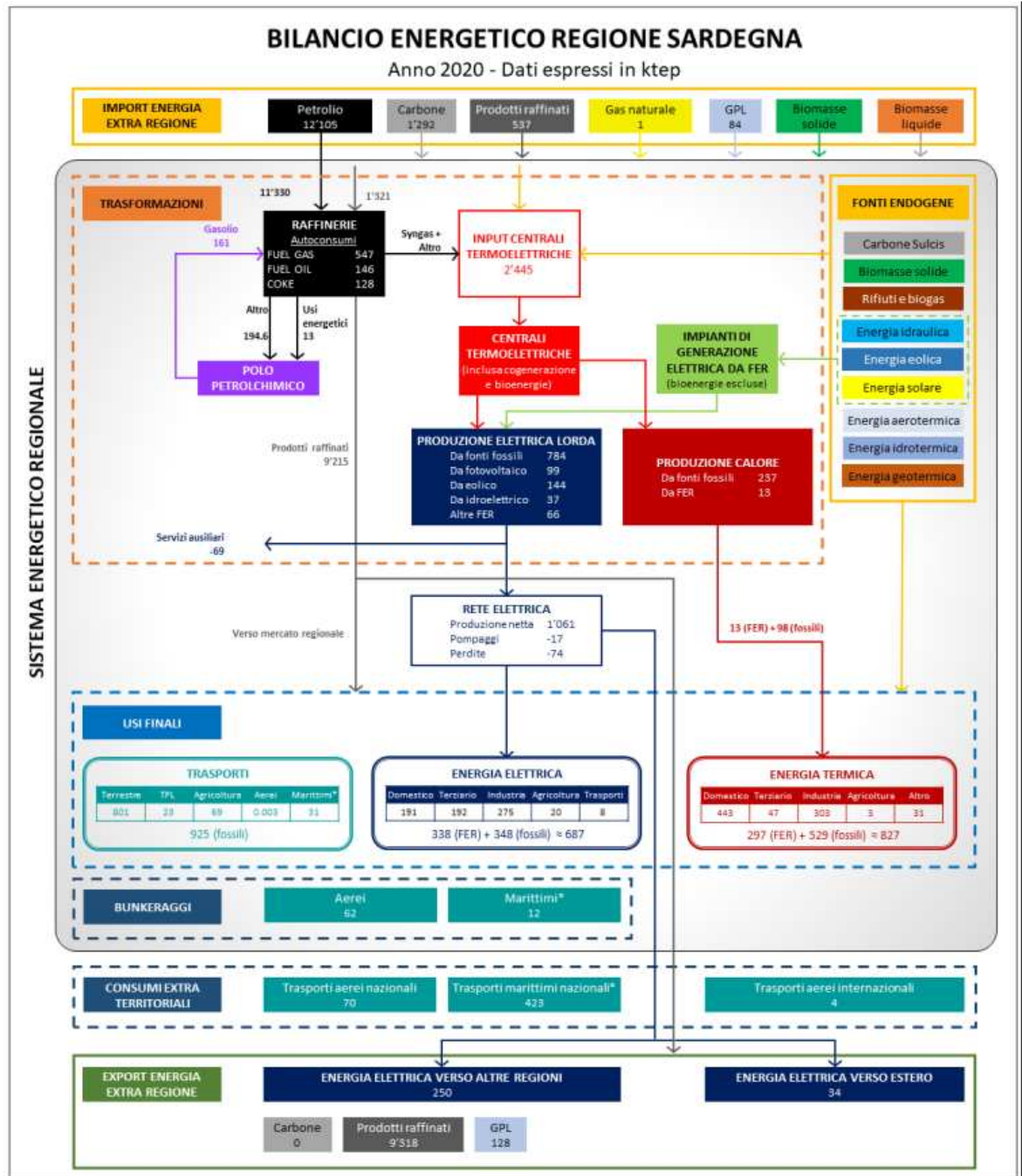
Figure 1.4: Regional Energy Balance 2020 for Sardinia island. The scheme is divided into 4 macro-areas: - Import of energy from outside the region, - Regional energy system, - Extraterritorial consumption and -Export of energy outside the region.
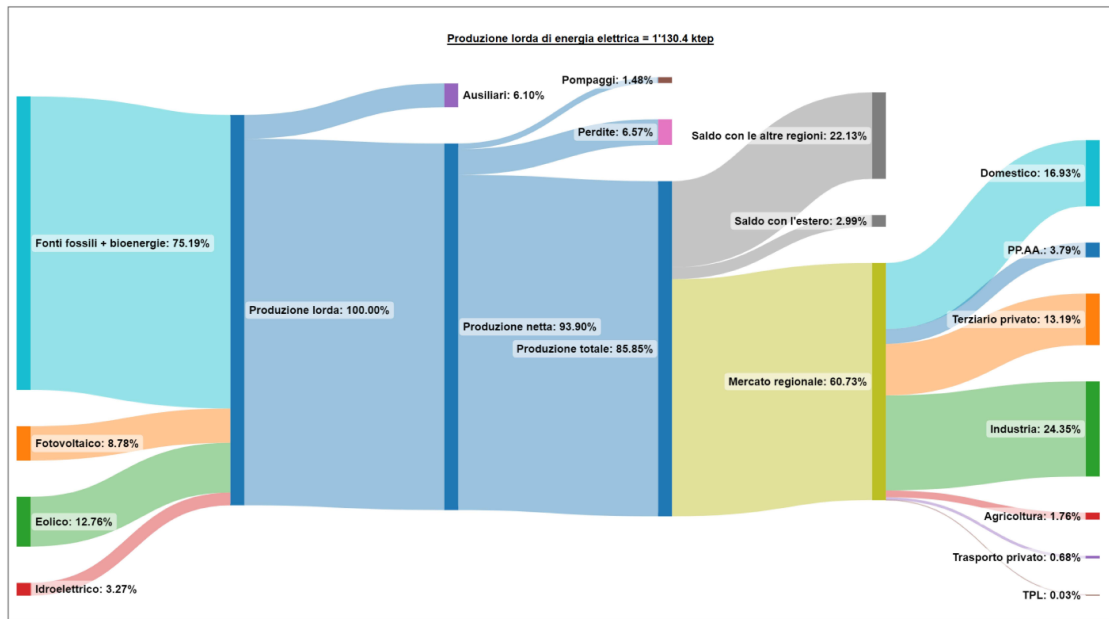
Figure 1.5: Sankey Diagram of electrical sector for 2020 for Sardinia island. Percentages referred to eletrical gross production, corresponding to 1130 ktep. Only 70% is for regional purposes.

In 2020, the electricity generated in Sardinia from fossil fuel-based thermal power plants and cogeneration facilities fueled by fossil or bioenergy sources accounted for a significant 75.2% of the total electricity production, while 12.8% comes from wind energy and 8.8% from solar plant, Fig. 1.6. Coal remained a prominent energy source in thermal power plants, representing 51% of the total energy consumption and contributing to 33% of the electricity produced. This was slightly lower than the electricity generated from refinery gas, which accounted for 34% of production. However, the consumption of refinery gas only made up 40% of the total energy consumption in thermal power plants. Out of the total electricity produced, approximately 70.7% was consumed within the region, while the remaining portion, after accounting for losses, self-consumption, and pumping, was either consumed in other regions (26.1%) or exported abroad (3.2%), Fig.1.7. Of the approximately 687 ktep of electricity consumed within the region, the industrial sector accounted for 40% of consumption, followed by the tertiary sector with 29%.

So, considering the significant surplus of available electrical production and the substantial generation of electricity from renewable sources, there exists a remarkable potential in Sardinia for methanol production through CO_2 hydrogenation. That explains the choice to focus on the island of Sardinia as location for the project, due to its great availability of resources and excess of electricity.
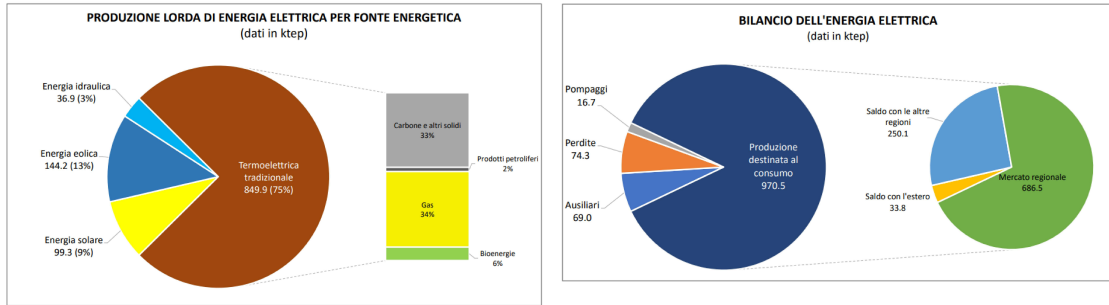
Figure 1.6: Gross electricity production. The majority of the production stems from the use of coal and gas, amounting to a total of 75% of the overall.

Figure 1.7: Electricity balance. With an electrical production efficiency of 93.9%, only 70.7% is consumed locally. The remainder is exported abroad and to other Italian regions.

In the heat sector, it is interesting to note in Fig. 1.8 that the residential sector accounts for just over half of the thermal energy consumption (approximately 54%), with a prevalence of energy derived from renewable sources (biomass). The industrial sector follows, representing about 37% of thermal energy consumption, with a predominance of petroleum-based energy consumption. The tertiary sector contributes to around 6% of the total thermal energy consumption, with a slight prevalence of renewable energy sources over petroleum products. The remaining portion (about 4%) is attributed to the agricultural sector or cannot be uniquely assigned to a specific sector.

Finally, in the transportation sector, Fig. 1.9, just over half is attributed to private land transport. The majority of the fuel consumed here is diesel followed by gasoline. Maritime transport to domestic destinations accounts for about 30% of the total primarily fueled by fuel oil, while air transport to domestic destinations represents less than 5% of the total.

The endeavors towards electrification align with the NSDS, Italian National Strategy for Sustainable Development, particularly under the Decarbonization pillar. This strategy encompasses initiatives to improve energy efficiency and promote sustainable mobility.

Numerous projects have already been developed to improve these aspects but even if there is a big desire to become self-sufficient using RES power, the picture of the near-future in Sardinia is not so clearly based on RES. For the moment, the approved regional plan for energy forecasts the extension of natural gas grid to the entire island, building a new connection with the mainland through the Tuscany region or using liquefied gas terminals in the seaports. Subsequently, the entire internal major grid must be created. [12]

Figure 1.8: Distribution of thermal energy consumption. The bigger contribution is the residential sector fueled mainly by RES.

Figure 1.9: Heat distribution in transport sector. It was not possible to specify all the items accounting for less than 0.5% of the total, such as regional and international air transport consumption, maritime bunker fuel consumption, and regional maritime transport consumption.

Indeed, given the significant surplus of electrical production in Sardinia that exceeds regional consumption, it is therefore a plausible option to exploit this surplus and use it partially for the production of high-quality, "clean" and "renewable" synthetic fuels through appropriate processes of CO_2 hydrogenation. This CO_2 will be obtained through capture processes, with hydrogen produced from electrolytic processes. Such a system, properly and strategically integrated with the Sardinian electric generation system, could provide a significant contribution to a more effective management of dispatching electricity from non-programmable renewable energy plants and improve the operational efficiency of fossil fuel thermal power plants. Additionally, it would contribute to reducing CO_2 emissions into the atmosphere. [13]

1.5 Natural Gas Infrastructure in Sardinia

In Italy the gas comes from abroad and it is injected into the national gas pipeline network through 5 entry points corresponding to the interconnections with the imported natural gas pipelines (Tarvisio, Gorizia, Passo Gries, Mazara del Vallo, Gela) and from the regasification terminals of LNG in Panigaglia, in the offshore of the Upper Adriatic Sea, and in the Tyrrhenian Sea off the coast of Tuscany. As it is possible to see from Fig. 1.10, Sardinia is not included in the national natural gas network.

Figure 1.10: Italian natural gas network infrastructure from SNAM's Sustainability Report 2020. Sardinia is outside the national gas network.

Regarding the analysis of the natural gas network in the region, there is a specific chapter in the PEARS [10] that describes the current situation and the planned natural gas projects to be implemented. In the text it is possible to read: "The natural gasification of the Sardinia Region is considered one of the strategic actions for achieving the objectives of the PEARS. In fact, the supply and use of natural gas, as a replacement for other currently used fossil fuels, has been considered in the analyzed scenarios as a transitional fossil solution for 2030." In fact, the island is the only region completely devoid of access to the national natural gas network. The natural gas is intended for the production of part of the thermal energy in industrial processes, to meet the energy demands of naval and road mobility, for freight transportation and to provide partial heating for residential use. Furthermore, the possibility of using methane for cogeneration of electricity and thermal energy in agro-industrial processes and energy districts, as well as for covering peak electric loads, has been evaluated in order to increase the flexibility and security of the island's power system.

Possible solutions to be adopted have been indicated, including a connection pipeline from Tuscany to the National Gas Grid, a regasification plant serving a regional backbone, and Small Scale LNG (SSLNG) systems, which are coastal LNG storage facilities. In the gas sector, several small-scale coastal LNG storage projects are currently being authorized and evaluated by the Ministry of Economic Development (MISE), and the Ministry of Infrastructure and Transport (MIT). These projects involve the unloading of LNG from small-sized methane ships, storage, and subsequent loading into bunker vessels and cryogenic tankers for the supply of civilian and industrial customers, as well as fueling stations. Specifically, in Sardinia, two out of three submitted initiatives involve the coupling of SSLNG and mini regasification plants. It is advantageous and cost-effective to supply natural gas to Sardinian industries, existing city distribution networks (replacing propane), which are already compatible with natural gas and under construction. Additionally, it is beneficial to replace fuels for heavy transportation and traditional marine fuels with LNG, gradually introducing the 0.1% sulfur limit for port vehicles and ferries. Furthermore, natural gas should be used to power the planned thermal power plants as part of the phase-out of coal-fired power plants.

1.6 Synthetic fuel production analysis

The global pursuit of sustainable energy solutions and the urgent need to address climate change challenges have led to innovative approaches in the realm of synthetic fuel production. Among these, the process of capturing carbon dioxide (CO_2) and utilizing hydrogen (H_2) from renewable resources presents a promising avenue for the development of clean and eco-friendly synthetic fuels. This revolutionary method involves harnessing CO_2 from CO_2-rich sources and combining it with green H_2 generated through water electrolysis, leveraging renewable energy sources. In this paper, the possibilities and advantages of utilizing captured CO_2 and green H_2 for synthetic fuel production are analysed. The research will delve into the cutting-edge technologies driving this process, the potential scale of implementation, and the environmental impact, comparing it to traditional fossil fuel-based methods. By examining the benefits of transitioning towards a "methanol economy" that closes the carbon loop and striving for carbon neutrality, the aim is to shed light on how these advancements can play a pivotal role in shaping a sustainable and greener future for the energy landscape. The first fuel analysed is the methanol.

1.6.1 Methanol

Methanol (CH_3OH) is a colourless water-soluble liquid with a mild alcoholic odour. It freezes at -97.6°C, boils at 64.6°C and has a density of 0.791 kilograms per cubic metre at 20°C.

Methanol serves a crucial role within the chemical industry and it is gradually emerging as an energy fuel, predominantly derived from fossil fuels. However, a shift towards renewable methanol production, sourced from biomass or synthesized using green hydrogen and carbon dioxide, holds the potential to enhance its applications as both a chemical feedstock and a fuel. Thanks to its high octane rating, it serves as a versatile option for internal combustion engines by acting as either an additive or a potential substitute for gasoline, as well as for hybrid and fuel cell vehicles and vessels. An important parameter to notice is that methanol has only half of the volumetric energy density of gasoline and diesel so, if it is used as a fuel, adjustments to the tank size have to be done to reach similar range. Additionally, methanol can be utilized in modified diesel engines. [14] [15] It remains in a liquid state under typical atmospheric conditions, making it easy to store, transport, and distribute. It is compatible with the current distribution infrastructure and can be mixed with traditional fuels. [9] [16] Hence, adopting renewable methanol could facilitate the industrial and transportation sectors in achieving net carbon-neutral objectives. Plus, direct methanol fuel cells (DMFCs) have the remarkable ability to directly convert the chemical energy present in methanol into electrical power. This characteristic makes DMFCs an attractive option for portable power sources and

other applications where a direct conversion of methanol to electricity is desirable without the need for high-temperature operation. [17]

Presently, the production of renewable methanol comes with high costs and limited output volumes. Nevertheless, with the implementation of appropriate policies and strategic initiatives, it is plausible for renewable methanol to become cost-competitive by 2050 or possibly even earlier. Such a transformation would pave the way for a more sustainable and environmentally friendly approach to utilizing methanol, fostering progress towards a greener energy landscape and carbon-neutral future. [18]

Renewable methanol offers a promising avenue for sustainable fuel production, utilizing renewable energy sources and feedstocks through two distinct pathways:

- Bio-methanol
  This route involves deriving methanol from sustainable biomass resources. Notable feedstock options include forestry and agricultural waste, by-products, biogas from landfill, sewage, municipal solid waste, and black liquor from the pulp and paper industry.

- Green methanol
  In this approach, CO_2 captured from renewable sources, such as bioenergy with carbon capture and storage and direct air capture (DAC), is combined with green hydrogen. The green hydrogen, produced using renewable electricity, forms the essential component for obtaining e-methanol.

The growing interest in renewable methanol stems from its potential to address climate change by significantly reducing or eliminating CO_2 emissions. It aligns with the imperative of limiting global temperature rise to no more than 1.5°C, necessitating net carbon-neutral emissions across all economic sectors by the mid-century. By capitalizing on these environmentally friendly production pathways, renewable methanol has the potential to pave the way for a greener and more sustainable energy future. [19]

E-methanol is categorized as an electrofuel (e-fuel) and falls under the electrochemical category, which involves utilizing electricity from renewable sources (such as wind or solar power) to produce hydrogen through water electrolysis. About the carbon dioxide, to be considered renewable, it has to be obtained from the atmosphere either directly by DAC or through biomass. Fig. 1.11.
When the CO_2 generated from the production of e-methanol or other bioenergy processes is captured and either stored or utilized for various purposes, it is commonly referred to as "bio-energy with carbon capture and storage" (BECCS) or "bio-energy with carbon capture and utilization" (BECCU). [20]
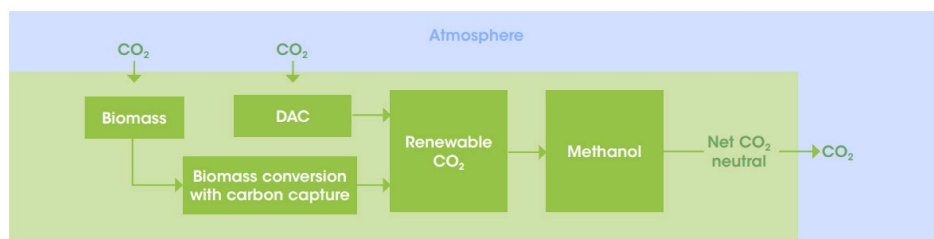
Figure 1.11: CO_2 feedstock for the production of e-methanol.

The process of producing e-methanol involves three primary steps, each with its own significance:

- Hydrogen (H_2) generation through water electrolysis

  Water electrolysis, a mature technology, efficiently splits water into hydrogen and oxygen gases. Alkaline and PEM-based electrolysers currently achieve efficiencies of approximately 75-85% in this process. PEM-type electrolysers offer a significant advantage in the production of e-methanol due to their capability to deliver hydrogen at higher output pressures, typically 30 bar and even higher. This higher H_2 output pressure can be directly utilized in the downstream methanol synthesis process, potentially reducing the overall cost associated with pressurizing hydrogen for this step. There are also Solid oxide electrolyzers (SOE) which are another type of electrolyzer technology that is currently being developed and shows great promise. Unlike PEM-type electrolyzers that operate at relatively low temperatures, SOEs are designed to work at much higher temperatures, typically exceeding 700°C. [21]

- Carbon dioxide (CO_2) capture

  The focus is on capturing CO_2 emissions either for storage or utilization. It is a crucial aspect of ensuring that the carbon footprint of e-methanol production is minimized.

- Methanol synthesis

  Synthesis of methanol using the hydrogen generated in the first step and the captured carbon dioxide.

But these processes will be evaluated in detail in the next chapters.

The overall efficiency of methanol production from electricity and CO_2 is about 50-60%. This is largely due to the need to produce hydrogen through water electrolysis.

And finally, in Fig. 1.12 it is possible to see the values of volumetric energy content of different fuels.
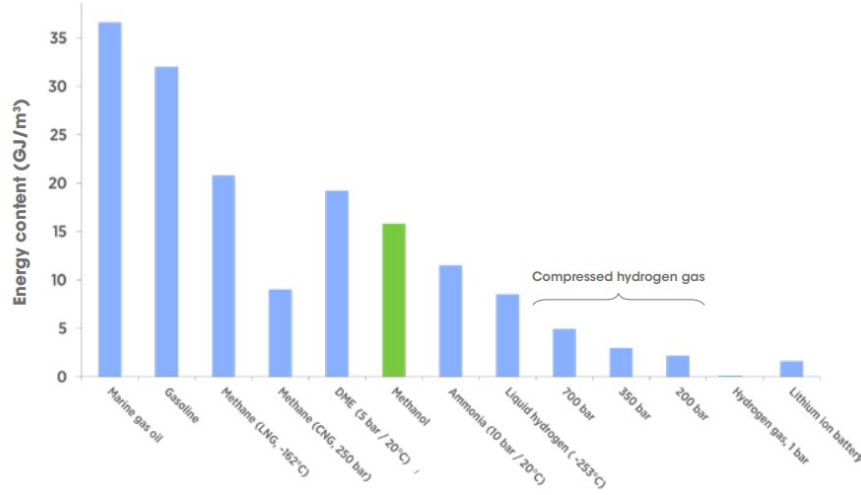
Figure 1.12: Volumetric energy content of different fuels. Methanol has a value smaller than gasoline and diesel. Much higher than compressed hydrogen gas.

1.6.2   Dimethyl ether

Despite methanol has been used in diesel engines, it is not the most suitable candidate to replace diesel fuel due to its low cetane number. From Olah et al. (2009) [8] it is possible to obtain several informations about the characteristics of dimethyl ether, CH_3OCH_3, and its possible applications. The cetane number is a measure of a fuel's tendency to self-ignite under high heat and pressure conditions. For efficient diesel engine operation, a high cetane number is required. In comparison, DME possesses a cetane number of 55-60, significantly higher than the 40-55 range found in conventional diesel fuel. [22] Currently, DME is produced through the bimolecular dehydration of methanol. Dimethyl ether, the most basic form of ethers, is a clear and colorless chemical compound that possesses several advantageous qualities. It is nontoxic, noncorrosive, noncarcinogenic, and environmentally friendly, making it a safe and sustainable option. DME finds its primary usage in certain countries for household heating and cooking. Additionally, it serves as a viable substitute for diesel fuel and can be utilized as a fuel source for high-temperature fuel cells. The conversion of a diesel engine to burn DME requires only moderate modifications, making it a relatively straightforward process.

DME stands apart from other homologous ethers as it does not create explosive peroxides [23], ensuring its safe storage and handling. Despite having a boiling point of -24.9 °C, which classifies it as a gas under normal conditions, DME is

commonly handled as a liquid and stored in pressurized tanks, similar to liquefied petroleum gas. [24] A further analysis, introduced in section 2.6.5, will present the procedure to synthesize it, involving the integration of a methanol synthesis catalyst with a methanol dehydratation catalyst.

1.7 Résumé

In summary, the primary aim and overarching goal of this comprehensive study is to introduce a potential and innovative application, which involves the establishment of a synthetic fuel production floating plant situated on the island of Sardinia. This plant is conceived to harness the island's abundant wind energy resources and eventually the incorporation of an advanced wave energy converter system, which could potentially enhance the plant's power generation capabilities.

Chapter 1 serves as a critical stepping stone to the exploration within this study. It elucidates the existing energy landscape in Sardinia, the current legislation and future energetic goals of the country, providing an overview of the energy composition, laying the groundwork for evaluating the application of a methanol production island.

Chapter 2 provides a thorough and systematic examination of the methodological aspects followed in the analysis and a detailed description of the numerical model adopted to obtain results.

Chapter 3 is dedicated to the presentation of tangible outcomes and findings derived from the research. It represents an analytical examination of the model's performance, providing a comprehensive and transparent account of the results obtained.

Finally, chapter 4 serves as the endpoint of the research, leaving with an understanding of the potential for synthetic fuel production in Sardinia and the impact it could have on the island's energy landscape as well as the further efforts and progress to be made to enable the application of these technologies.

Chapter 2

Methods

In the context of this chapter, the focus is upon a comprehensive exploration, wherein it is introduced and examined an array of programs, software tools, and computational methodologies used to move forward with the analysis.

These include a diverse spectrum of resources, ranging from indispensable databases that serve to obtain and elaborate essential variables required to compute the data needed for the calculation of important parameters, fundamental for the ultimate decision of the final location. Additionally, a dive into the field of potential implementations and prospective applications for the project is performed, showing the possible pathways through which the research can be applied now and in future projects.

2.1 Site Selection for Offshore Wind Farm in the Mediterranean Sea

The Mediterranean Sea, with its abundant wind resources and proximity to coastal regions, presents a compelling opportunity for the development of offshore wind energy projects. However, the process of selecting an optimal site for an offshore wind farm requires careful consideration of various factors, including wind patterns, environmental impacts and regulatory constraints. To ensure an informed and effective decision-making process, harnessing reliable and detailed weather and climate data is crucial. The ERA5 dataset, provided by the European Centre for Medium-Range Weather Forecasts (ECMWF), offers comprehensive and high-resolution information about past weather conditions globally. In addition the research must account for territorial and normative constraints. Factors such as maritime regulations, environmental protection measures, shipping lines, fishing grounds and other spatial restrictions play a significant role in determining the feasibility and viability of a proposed project. These constraints ensure the sustainable

development of offshore wind energy plant while mitigating potential conflicts with other sectors and safeguarding marine ecosystems. By integrating meteorological insights with comprehensive spatial analysis, this study seeks to identify suitable areas for offshore wind farm development while addressing environmental, economic and regulatory considerations.

2.2   Methodology to estimate the final output

Within this section, a comprehensive step-by-step process is provided, detailing the systematic approach adopted to reach the ultimate objective, which is the calculation of synthetic fuel production achievable from the offshore facility. This procedural elucidation is complemented by an illustrative diagram, Fig. 2.1, which delineates each sequential step. Additionally, the diagram showcases the pertinent variables to be leveraged and the specific software programs employed throughout the research endeavor, offering a visual representation of the entire analytical process.
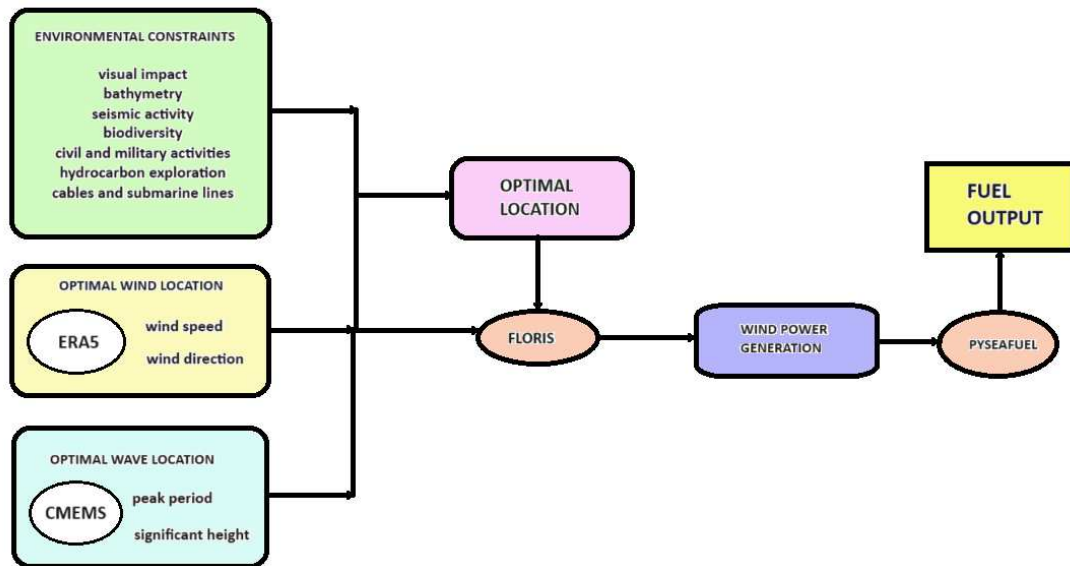
Figure 2.1: data flow and structure of the analysis in the study. The wave analysis was not considered a determining factor in the choice of the location but rather as a potential and future enhancement to the project to increase its efficiency.

As it is possible to see, the first steps consist of the selection of the optimal location relying on several parameters. The first variable concerns the wind that affects the area of interest, extracting data from ERA5, explained in section 2.3 and processing them using Python program, starting with the analysis of wind speed and its direction. Secondly, it is necessary to analyze the feasibility of the project according to the numerous landscape constraints present in the area, the visual impact, the biodiversity characterizing those areas, and additionally, all other constraints related to the seabed bathymetry, seismic risk in the area, as well as various civil and military activities that could potentially interfere with the implementation of the project in question. These aspects are evaluated in section 2.6.3.

As a final stone, wave conditions. Even if this last aspect is not applied in the aforementioned study, it would be an interesting implementation for future application, when its TRL would be greater.

Once selected the zone, the wind characteristics of that will be imported on FLORIS software, section 2.4, to obtain the power generated by the installed wind farm. In conclusion, that power would be related to the generation of a synthetic fuel through the Pyseafuel Python program, explained in section 2.6.4, to obtain the final fuel output.

2.3   ERA5

ERA5 is a state-of-the-art reanalysis dataset produced by the European Centre for Medium-Range Weather Forecasts providing hourly data on many atmospheric, land-surface and sea-state parameters together with estimates of uncertainty. Re-analysis refers to a process that combines historical short-range weather forecasts with observations through data assimilation to generate a comprehensive and consistent global weather dataset. This process mirrors the methodology employed in generating day-to-day weather forecasts, starting from an analysis of the Earth's current state. By filling gaps in the observational record, reanalysis products provide a comprehensive and continuous dataset that minimizes potential artifacts in detecting climate change signals. Furthermore, they offer spatially continuous information that facilitates the evaluation of climate models. [25]

ERA5 is the fifth generation of the ECMWF's atmospheric reanalysis. It provides a wide range of weather and climate information, including variables such as temperature, wind, precipitation, humidity and atmospheric pressure. The dataset covers the entire globe, extending from the Earth's surface to the upper atmosphere. As stated in the Copernicus Climate Change Service [26], ERA5 data are available in the Climate Data Store on regular latitude-longitude grids at 0.25° x 0.25° resolution, with atmospheric parameters on 37 pressure levels, it's available from 1940 and continues to be extended forward in time, with daily updates being made available 5 days behind real time. What sets ERA5 apart is its high temporal resolution. It provides hourly data, allowing for detailed analysis of short-term weather events and capturing the diurnal variability of atmospheric processes. This high temporal resolution makes ERA5 particularly valuable for climate studies, weather forecasting, and research on extreme events.

ERA5 incorporates advancements in data assimilation techniques, improved modeling capabilities, and an expanded range of observational data compared to its predecessors. It assimilates a vast amount of observations from various sources, including satellites, weather stations, aircraft, ships, and buoys, using advanced data assimilation algorithms. This integration of observations with the model helps improve the accuracy and consistency of the dataset, assuring great reliability for the validation of climate models, having great potential also when observational data are not available or quality is not good enough, as well as for future studies related to the wind field such as wind energy production estimates. [27] ERA5 supports climate research, weather forecasting, climate monitoring, understanding climate change impacts, assessing renewable energy resources, and analyzing extreme weather events.

2.4 FLORIS

FLORIS (FLOw Redirection and Induction in Steady State) is a controls-focused wind farm simulation software that enables the evaluation of wind energy facilities to characterize their performances and eventually improve their productivity, maximizing profits by optimizing flow control strategies. The FLORIS model is based mainly on the Jensen (Park) wake model [28] and wake deflection model of Jimenez [29].

The FLORIS model involves its ability to forecast the locations of steady-state wake patterns, effective flow velocities at individual turbines, and the subsequent electrical energy production levels, all contingent on the axial induction and yaw angle adjustments of distinct rotor systems. It relies on a set of parameters, which are derived from the observed data of turbine electrical power production and are thus limited in number. [30].

2.5 Copernicus Marine Environment Monitoring Service

Copernicus Marine Environment Monitoring Service, shorter CMEMS, is a European Union initiative aimed at providing accurate and up-to-date information on the state of the world's oceans and marine environment, coordinated and managed by the European Commission in partnership with the European Space Agency (ESA) and other stakeholders. It collects and processes a vast amount of data from various sources, including satellite observations, in-situ measurements, and numerical models covering a wide range of oceanographic variables providing comprehensive and reliable information about the state and dynamics of the marine environment.

To be specif it has been used the Medsea Multiyear Wav 006-012, the multi-year wave product derived from the Mediterranean Sea Waves forecasting system. It consists of two datasets: the Reanalysis dataset and the Interim dataset. The first provides a comprehensive analysis of wave parameters at an hourly interval and a horizontal spatial resolution of 0.042° x 0.042°, starting from January 1993. The Interim dataset covers the period from the end of the Reanalysis dataset until one month prior to the present time, providing updated wave information.[31]

2.6   Wave description

Thanks to CMEMS, it is now possible to access the essential data required for the analysis and study of marine behavior. Once these data are acquired, it is possible to analyze them to determine the most suitable device for harnessing wave energy. Once again it's importat to underline that this won't be included in the project but only introduced as a possible future implementatio. However, before delving into this, it is necessary to provide an overview of how marine energy capture devices are conceived, developed, classified, and function.

First of all, it is important to consider the waves behaviour to evaluate, from a safety standpoint, the feasibility and strength of the project, taking into account the disturbances and stresses they could bring. Secondly, linked with the energy aspect, there is the possibility of harnessing the same wave motion for energy generation. The latter would be a very valid and promising alternative that would also provide a constant energy supply. By combining wind and wave energy, it would be possible to bridge the intermittent gaps that characterize traditional renewable sources such as wind and solar energy. In fact, wave energy is more predictable, more constant and considering the realization of a power plant, it would have a lower visual impact as well as for the environmental one. Last but not least, an higher energy density compared to other sources mentioned. [32] Furthermore, an interesting aspect of marine energy is the global wave power potential, with an estimated value on the order of 1 TW (terawatt), making it an enormous resource of renewable energy. The problem for this kind of technology, despite of all the potential it will have, is related to its immaturity in the economical and technological aspects.
   This kind of energy can be exploited implementing a Wave Energy Converter, a device able to transform the wave motion into useful energy. Several types of WECs exist and there are several possible classifications to define the type and operating functions, like the one proposed by Lehmann et al. (2017) [33] in five main categories:

- working principle:
  oscillating water column, heaving buoy, submerged pressure differential, wave activated bodies, bulge wave, oscillating wave surge, rotating mass and cycloidal wave absorber.

- location:
  shore-based, nearshore and offshore.

- orientation:
  point absorber, attenuator, and terminator.

The first is a device with horizontal dimensions negligible with respect to the wavelength. Both the terminator and the attenuator have definite dimensions and the first physically intercept the incoming wave, the other is able to extract energy as the wave passes through its length.

- PTO system, which is the one that converts the prime mover's mechanical energy to smooth electric power:
  hydraulic, direct drive, hydro, and pneumatic.

- TRLs: Technology Readiness Levels

Therefore, the device extracting energy must engage with the waves in a manner that diminishes the quantity of wave-energy naturally found in the ocean. The device is designed to produce a wave that clashes destructively with the existing sea waves. [34]

Of course the working principle of a WEC will depend strongly on the specific design and technology adopted, however the general concept involves a first phase of wave capture, where the WEC is exposed to incoming waves to capture its energy and transfer it to the device, an energy conversion, which can be achieved through various mechanisms, such as the oscillation of floating bodies, the movement of hydraulic pistons, or the stretching and contracting of flexible materials.

The initial conversion of wave energy happens through the occurrence of destructive wave interference in which energy is transferred from the ocean to the oscillating system, where it exists as either kinetic or potential energy. This oscillating system, called the prime mover, can be of one or multiple floating bodies that oscillate, as well as oscillating solid or flexible components. In a subsequent step of conversion, the mechanical energy harnessed by the oscillating system can be further enhanced through the utilization of conversion machinery capable to delivery useful energy. Then a power generation phase where the converted energy is used to perform a useful work; normally the mechanical energy is used to drive a generator for the production of electrical power.

2.6.1   Wind

By selecting the research area in the Mediterranean region, it is possible to extract the data obtained from ERA5 for the analysis using the Python programming language in order to generate graphs that can facilitate the rapid identification of the most favorable area based on predefined criteria. Specifically, data from ERA5 ranging from 01 January 1959 to 30 November 2022 have been retrieved, considering the following variables:

1. U and V component of wind at 100m.

2. U and V component of wind at 10m.

3. Sea surface temperature.

4. Surface pressure.

In the context of wind components, U and V represent the horizontal components of the wind vector. They are commonly used to describe the east-west (U) and north-south (V) directions of the wind flow.

- U component: it represents the eastward component of wind or horizontal wind speed along the x-axis. It is positive when the wind is blowing from the west to the east and negative when the wind is blowing from the east to the west.

- V component: it represents the northward component of wind or horizontal wind speed along the y-axis. It is positive when the wind is blowing from the south to the north and negative when the wind is blowing from the north to the south.

By combining the U and V components, it is possible calculate the total wind speed, WS, and wind direction, WD. The magnitude of the wind speed vector is given by the formula:

$$WS = sqrt(U^2 + V^2) \tag{2.1}$$

And the wind direction can be calculated using the signed arctangent function:

$$WD = atan2(\frac{V}{U}) \tag{2.2}$$

The values at 100 m above sea level is representative for the wind that will hit the blades of the turbines, while the one at 10 m above sea level would not be taken into considerations in the following study.

Once those values were obtained, a further step was to calculate the average wind speed, the standard deviation, and the ratio between the two quantities. As

well, percentile at 95%, 97% and 99% have been obtained for wind speed at 100 m and finally all of them have been plotted. Fig. 2.6 Fig.2.8 and Fig.2.9.

Since the percentile expresses the amount that the usage is below the number of the percentile, the 95th percentile shows how wind speed velocity in roughly under the value of 15 m/s, as visible in Fig. 2.7. For the 97th percentile, it includes a bigger contribution since it avoids only the 3% of wind speed values, showing how it is approximately below 16 - 17 m/s. Finally, the 99th percentile, the once that includes almost all, discarding only the most infrequent values, it shows the predominance of values below the speed of 20 m/s.
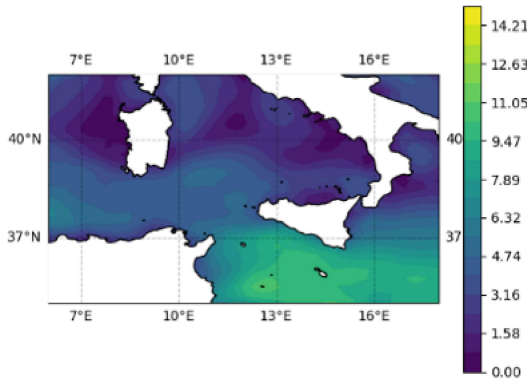
Figure 2.2: Wind speed at 100m in m/s.
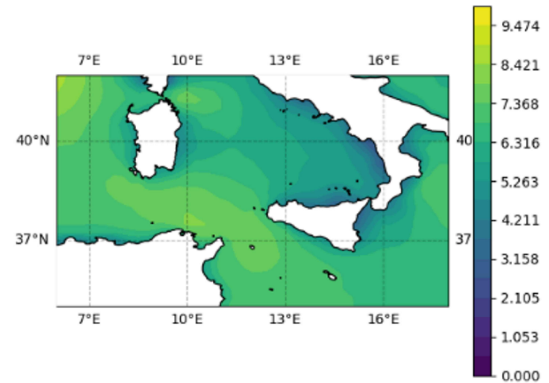
Figure 2.3: Mean wind speed [m/s].
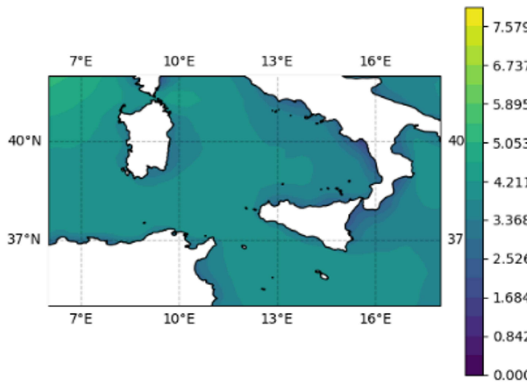
Figure 2.4: Standard deviation of wind speed in m/s.
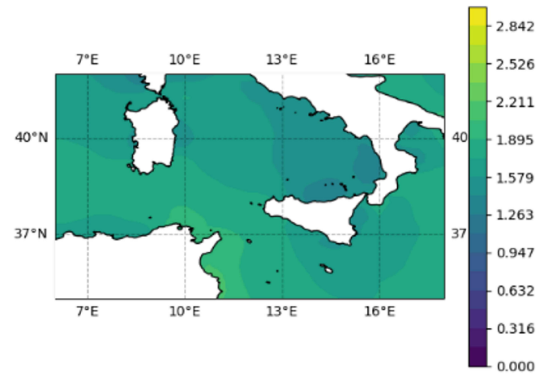
Figure 2.5: Ratio of mean over std.

From Fig. 2.2 it can be observed that the predominant range for wind speed velocity is in the range between 5 m/s and 8 m/s, as confirmed with Fig. 2.5. The
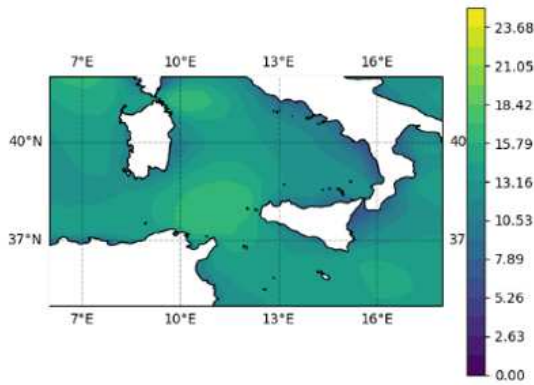
Figure 2.6: 95th percentile of wind speed at 100m in m/s.
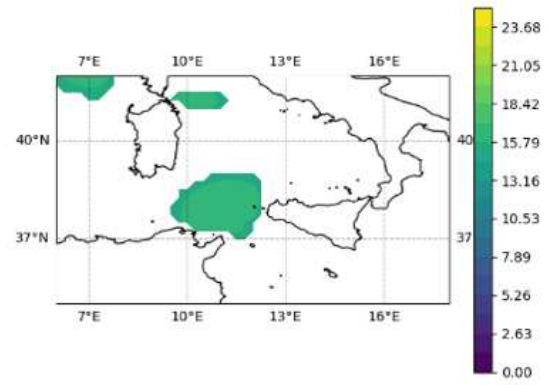
Figure 2.7: 95th percentile of wind speed higher than 15 m/s.
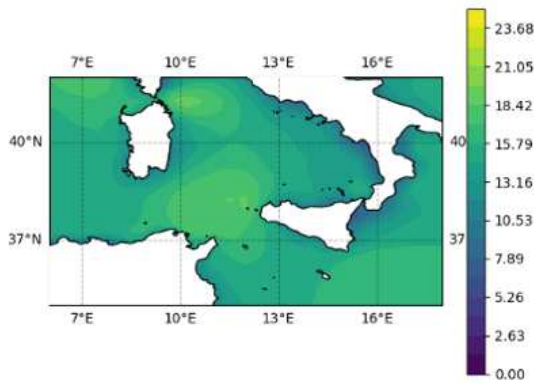
Figure 2.8: 97th percentile of wind speed [m/s].
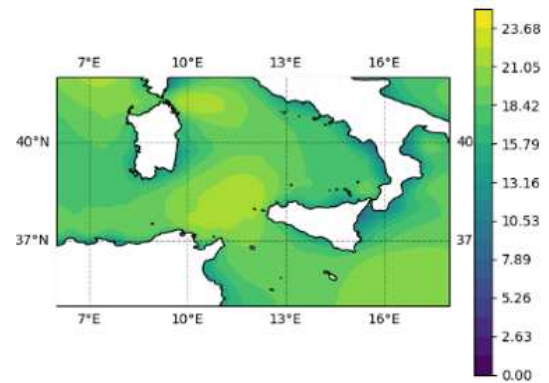
Figure 2.9: 99th percentile of wind speed [m/s].

Fig. 2.5 is useful to evaluate the location with the most stable wind in terms of values, because a greater number will mean a lower dispersion.

The next step was to consider a turbine type from windpowerlib in order to calculate its power production and consequently the energy produced over an year, just integrating the value of the power. The turbine chosen for the simulation is a Siemens SW120/3600 turbine, with a rotor diameter of 120 meters and a nominal power of 3.6 MW.
Windpowerlib is a software package in Python that provides tools and functions for simulating and analyzing wind power systems. It is specifically designed for modeling wind turbines and wind farms to estimate their power output and assess their performance. [35] In Fig. 2.10 the power curve of the mentioned turbine:
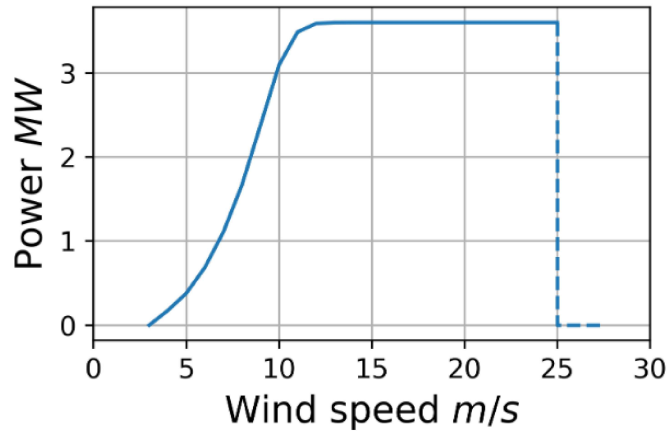
Figure 2.10: power curve for the Siemens SW120/3600 turbine. Cut-in wind speed, the minimum wind speed at which a wind turbine begins to generate electricity corresponds to 3 m/s, while cut-off wind speed is the maximum wind speed at which a wind turbine operates safely, and it's 25 m/s. And the rated wind speed is the level at which the wind turbine operates at its rated capacity.

With all the useful parameters, the final value for energy obtained from that wind power plant is shown in Fig. 2.11.
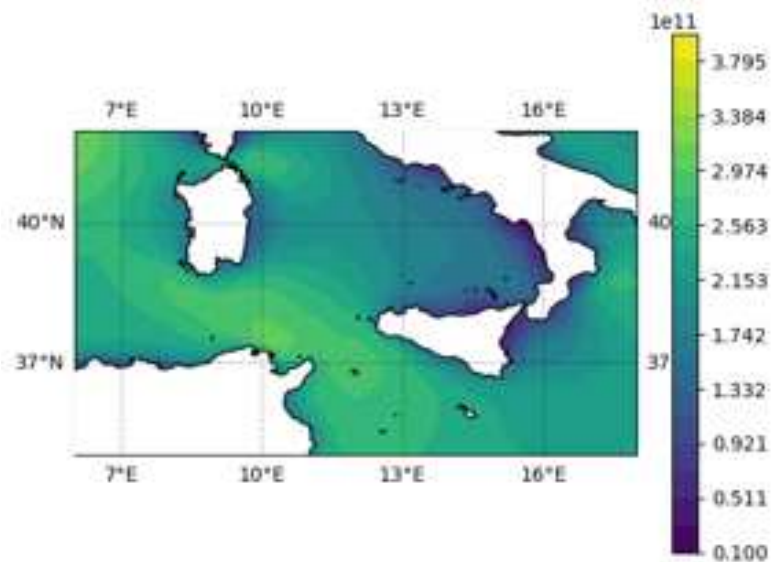
Figure 2.11: energy produced in joule.

A similar procedure is carried out regarding the wind direction, shown in Fig. 2.12, and subsequently the standard deviation is calculated to identify areas with less directional variability. Fig. 2.13.

Wind direction is here represented on a circular scale ranging from $-\pi$ to π, where 0 corresponds to the north direction. Positive values indicate a clockwise direction, while negative values represent a counterclockwise direction. Using a circular scale allows for a more intuitive representation of wind direction, as it captures the continuous nature of the circular motion. It enables the calculation of the angular differences and identify patterns and trends in wind direction over time or across different locations.
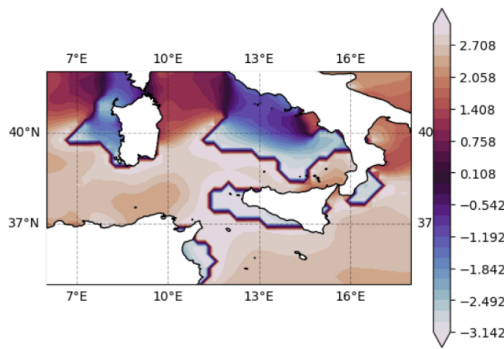
Figure 2.12: Wind direction at 100m.
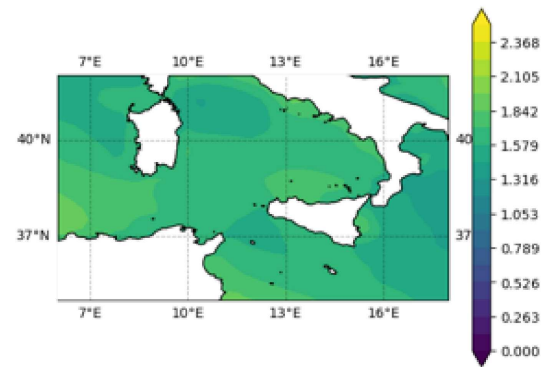
Figure 2.13: Standard deviation of wind direction.

Wind power generation

For the evaluation of the power production, a wind farm turbine has been selected with the software FLORIS.

Regarding the producibility analysis in the Mediterranean area around Sardinia, the offshore wind farm project - NoraEnergia2, found in the MISE official website, `https://va.mite.gov.it/it-IT/Oggetti/Info/8940`, has been considered as a reference case for modeling the fuel production facility.

The aforementioned project aims to create an offshore wind farm consisting of 40 wind turbines, with a total capacity of 600 MW. It will be located in the sea area within the Strait of Sardinia and southeast of the Gulf of Cagliari, approximately 30 km south of Cape Carbonara, at water depths ranging from approximately 170 m to 530 m. Fig.2.14

Figure 2.14: Location of NoraEnergia2 wind power plant.

In the NoraEnergia2 project, the selection of power and size of wind turbines have been hypothesized as reasonable in the market at the time of the project's execution phase, corresponding to a quite big turbine with a nominal power of 15 MW.

The entire wind farm will occupy a sea area of about 110 km^2, and there will be a distance of approximately 2 km between each wind turbines, corresponding to a distance of 7.5 times the rotor diameter. The arrangement of the turbines is visible in Fig.2.15

The technology used for these wind turbines is floating wind turbine technology. This technology allows the installation of wind farms in deep waters with negligible environmental impact. The chosen implementation method enables the optimal utilization of wind resources in locations that would otherwise be unused due to water depth. In general, the choice between installing a fixed structure or a floating structure depends primarily on the water depth at the site of interest. As a general guideline, floating structures are preferred for water depths exceeding 100 m, as it is the case here.

In this specific case, the wind turbine tower has a height of 150 m, reaching a total height of 268 m when considering the length of each blade, which is 118 m.

The estimate of the gross production of the site was obtained by intersecting the power curve of a hypothetical 15 MW turbine with the wind distributions of the site. This allowed determining the annual energy produced by each individual wind turbine and then multiplying it by the total number of wind turbines to obtain the
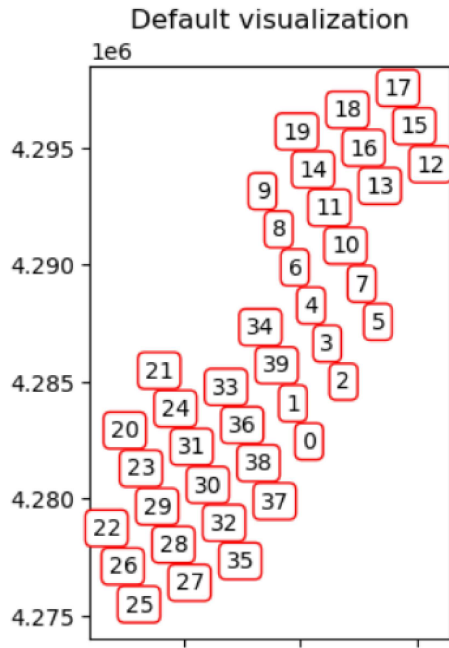
Figure 2.15: Layout of NoraEnergia2 project, coordinates on the axis.
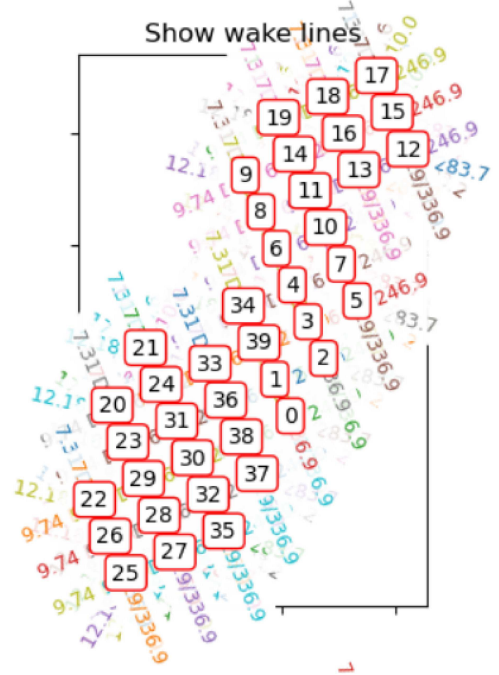
Figure 2.16: Layout of NoraEnergia2 with wake lines.

gross annual production of the park. It is then necessary to apply a reduction to the gross production (which considers the maximum energy that the wind turbine can produce) for energy losses (associated with wake effects between wind turbines, downtime and maintenance, electrical losses in transmission, grid restrictions, etc.).

Based on the analyses considered in the study, it was possible to estimate a site producibility of 1999.1 GWh/year, corresponding to a capacity factor of 38%.

Once the reference model was chosen, namely the plant described by the NoraEnergia2 project, an attempt was made using the FLORIS package to calculate the layout and precise location of the analyzed park. After obtaining the power values and overall producibility it was evaluated whether the simplified model used in this study could have approximated the detailed and more in-depth model used for the actual NoraEnergia2 project with a good level of accuracy.

To do this, the blade tip speed, the producibility of each individual turbine with those wind values, and the overall producibility of the entire wind farm were calculated based on the wind data obtained from the ERA5 software.

2.6.2 Wave

The description of water waves can be done considering them travelling along the water surface with a sinusoidal profile. The parameter useful to describe them is the distance between successive crests, called wavelength, λ, and the time between them, called period, T. Fig. 2.17.

Considering deep water, which it's the case of this application, it is possible to obtain several useful formulas for their characterization. Before falling into a more detailed description of this type of waves, it's important to clarify the difference with shallow water waves. When waves approach the shore, their height H, which is the distance between the crest and the trough, reduces progressively. If

$$H > \frac{\lambda}{2} \tag{2.3}$$

it is considered a deep water wave. A shallow water wave follows instead the relation:

$$H < \frac{\lambda}{20} \tag{2.4}$$

and all the values in between are representative for intermediate water cases.
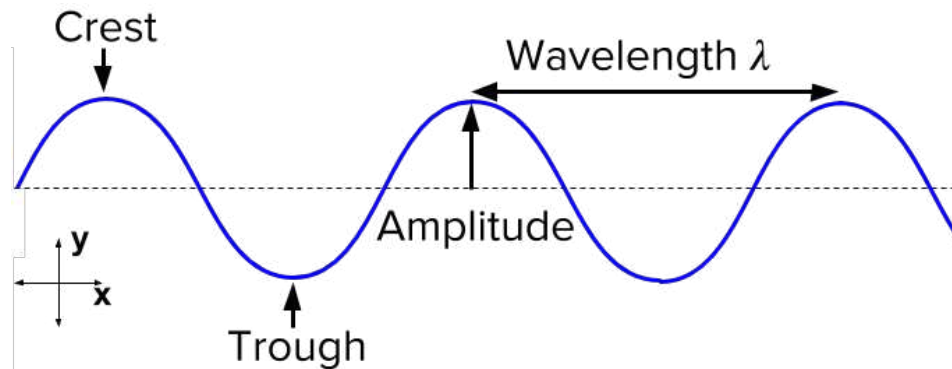
Figure 2.17: wave characteristics. Wavelenght is the distance between two consecutive crests or troughs. Amplitude is the distance from the highest point (crest) to the lowest point (trough). Larger amplitude waves generally carry more energy.

So, dealing with deep waves their wavelength is represented following the formula:

$$\lambda = \frac{gT^2}{2\pi} \tag{2.5}$$

and the velocity of the wave as:

$$C = \frac{\lambda}{T} \tag{2.6}$$

For what concern the dispersion relation, it can be expressed as:

$$\omega^2 = g \cdot k \tag{2.7}$$

where k is the wave number, obtained as:

$$k = \frac{2\pi}{\lambda} \tag{2.8}$$

About the power, considering a more realistic case with irregular waves instead of regular ones, it would be extracted following respectively the law:

$$P = \frac{\rho g^2 H^2}{64\pi} \cdot T \tag{2.9}$$

where ρ is the density of sea water and P is expressed per unit crest length of the wave. [36]

Other parameters usefuel for the evaluation regard the characteristic of the wave motion. Specifically are the periods associated with significant wave height H_s. They are the significant period T_s, calculated as the average of the periods associated with the heights used to compute the significant wave height, and the peak period T_p. The significant wave height H_s is usually defined as the average of $\frac{1}{3}$ of the highest waves. For practical purposes, $H_s = \frac{H_1}{3}$ can be replaced, with little difference, by H_{m0}, the wave height calculated from the zero-order spectral moment and therefore representative of the spectral energy. The definition of maximum wave height H_{max} to be associated with the extreme significant wave height H_s is generally made according to the relationship:

$$H_{max} = 1.87 H_s \tag{2.10}$$

This relationship is derived by considering the validity of the Rayleigh distribution [37].

Wave power generation

For the calculation of the power potential from waves in the selected area the program Copernicus CMEMS (Copernicus Marine Environment Monitoring Service) has been used.

The data extracted, useful for the power calculation, are the sea surface wave significant height H_{m0}, and the sea surface wave period at spectral peak, which represent the peak period T_p, the wave period associated with the most energetic waves in the total wave spectrum at a specific point. Fig. 2.18 It's important to clarify that the significant wave height describes the mean height of the highest one-third of waves in a given wave system. It represents a statistical value that provides a useful indicator of the overall wave conditions.

Statistical Wave Distribution
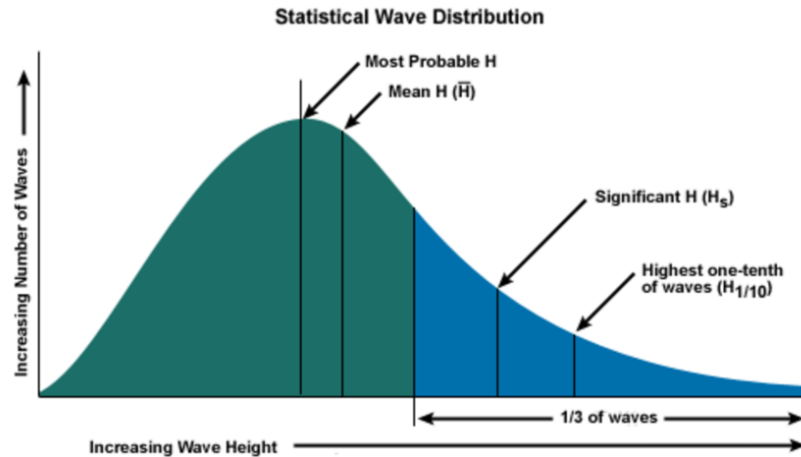
Figure 2.18: Wave statistical distribution. The interaction between wind speed and wind direction influences the generation of wind waves on the sea surface, generating wind waves that follow a Rayleigh distribution. [38]

To model the wave energy distribution in the ocean, JONSWAP and Bretschneider spectra are the most used methods, describing their distribution based on their frequency content. The JONSWAP spectrum is characterized by an higher spectral peak and a narrow bandwidth in Fig. 2.19.
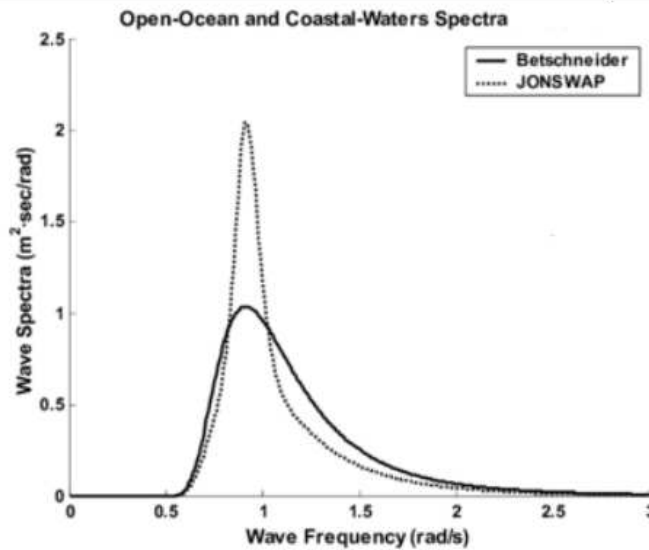
Figure 2.19: JONSWAP and Bretschneider spectra.

Hence, the majority of power available for the spectrum is within the range of

frequencies. Instead, Bretschneider has a wider bandwidth with a lower spectral peak , which means that the bulk of the wave energy is distributed in a wider range of frequencies that can make the energy capture more difficult. [39]

Bretschneider is useful to describe irregular waves in open sea, where wind is blowing regularly, so it's suitable for ocean's description.
JONSWAP is more suitable for seas where waves have a more regular behaviour, like for North sea and Mediterranean sea. In fact, in this analysis the JONSWAP spectra has been used.

For the calculation the python package MHKiT-Python has been utilized, a software library designed for Marine and Hydrokinetic (MHK) data analysis and visualization. MHKiT is developed as a collaboration between the National Renewable Energy Laboratory (NREL), Pacific Northwest National Laboratory (PNNL), and Sandia National Laboratories (Sandia, SNL). The resource sub-module of the wave package contains functions to compute wave energy spectra and metrics. In particular, the calculation of JONSWAP Spectrum follows the IEC TS 62600-2 ED2 Annex C.2 (2019).
Once obtained the spectral density S $\left[\frac{m^2}{Hz}\right]$, it is possible to calculate the wave period T_e, the time it takes for successive wave crests (or troughs) to pass a fixed point and the omnidirectional wave energy flux of the spectra J $\left[\frac{W}{m}\right]$.

2.6.3   Environmental constraints

When selecting the optimal location where to put the floating plant, several factors related to environmental constraints, economic considerations, existing maritime activities and lines need to be taken into account. Basing on several project for offshore wind farm already presented for the Sardinia region, found in the official site of Ministry of Environment and Energy Security [40], it has been possible to understand which constrains were important to analyze for the final selection. One of the first criteria to consider is the visual impact the future plant will have, in fact the wind farm should be situated in a way that minimizes its visibility from the coastline and neighboring areas. The distance from populated areas, tourist attractions, and protected sites should be considered to preserve the aesthetic appeal of the region, remaining of course within the Exclusive Economic Zone of the country.

After that there is the bathymetry analysis which refers to the analysis of seabed topography to identify areas with suitable water depths for wind turbine installation. This ensures that the foundation of the wind farm can be securely established. The bathymetry for the area under study was obtained from the Navionics ChartViewer available on the website: `https://webapp.navionics.com/`.

For what concern the geological and geomorphological framing, it's involves the evaluation about the stability and suitability of the seabed for the plant placement. In the case of Sardinia, the region is situated in the central-western Mediterranean. It is a crustal block, approximately 30 kilometers thick, that is adjacent to two regions characterized by extensional tectonics. These regions are the Liguro-Provençal basin in the west and the Tyrrhenian basin in the east. Over the past 20 million years, the crust in the Liguro-Provençal basin has experienced stretching, while the stretching in the Tyrrhenian basin occurred approximately 8 million years ago. [41]

Plus it's fundamental to assess the seismic activity in the region for ensuring the safety, resilience, and long-term viability of new plant constructions. Italy is divided into different seismic regions based on the level of seismicity. The classification is typically based on the Italian Seismic Hazard Map, which takes into account historical seismic data, geological characteristics and seismological studies. Fig. 2.20.

The classification is as follows:

- Zone 4: Negligible Seismic Hazard Areas with very low seismic activity and minimal risk.

- Zone 3: Low Seismic Hazard Areas with low to moderate seismic activity and

a relatively low risk of earthquakes.

- Zone 2: Moderate Seismic Hazard Areas with moderate seismic activity and a moderate risk of earthquakes.

- Zone 1: High Seismic Hazard Areas with high seismic activity and a significant risk of earthquakes.
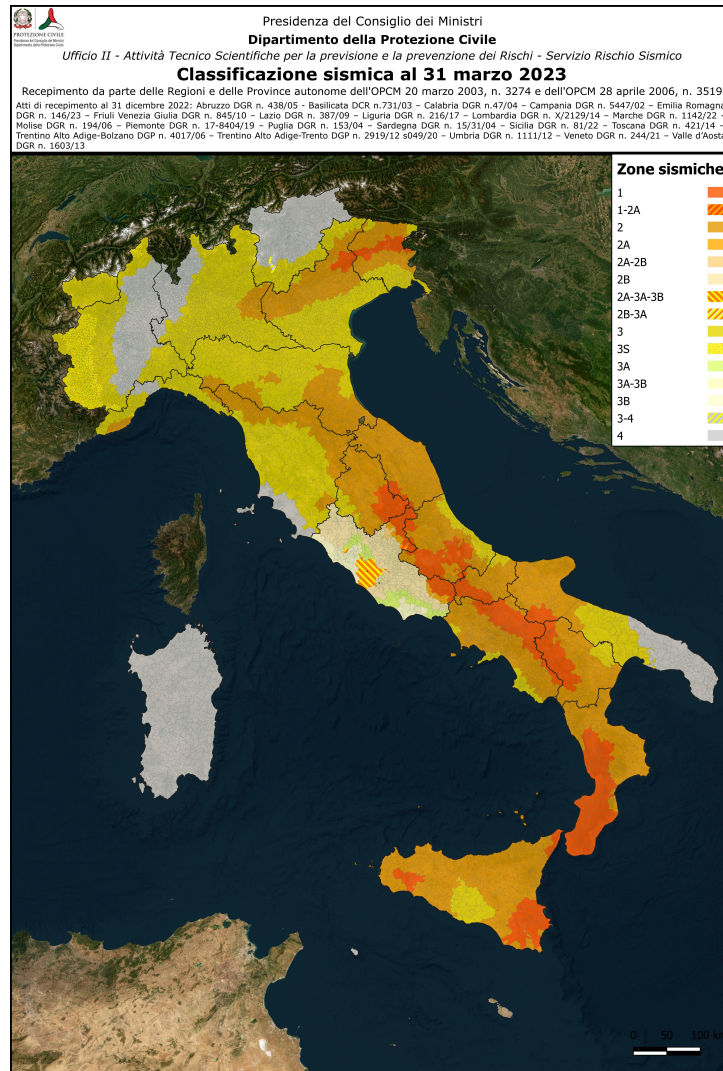
Figure 2.20: Seismic classification of Italy.

It is important to note that the classification may vary within different regions of the country, as seismicity can vary significantly from one area to another. Local geological conditions, fault lines, and historical earthquake records are also taken

into account for a more detailed assessment of specific locations within each zone. [42]

Then the meteomarine framing which involves the evaluation of meteorological conditions such as wind speed, wind direction and extreme weather events. The wind and wave data used in this study were extracted from ECMWF ERA5 databases.

- WAVE MOTION:

  This part considers wave parameters as the significant wave height H_s, the significant period T_s, and the peak period T_p. Plus it needs to evaluate also the maximum wave height for structural and safety reasons. The randomness of maximum waves can introduce uncertainties in engineering structures. To avoid this, it is common practice in design to estimate a value for H_{max} based on both the duration of a particular sea state and the number of individual waves.

- MARINE LEVEL:

  The factors influencing variations in sea level are complex, as there are multiple phenomena that can generate or alter the movement of water masses. When each phenomenon is considered as causing a distinct effect, the sea level can be envisioned as a combination of various vectors.

  $$V = \sum \eta i \tag{2.11}$$

  The temporal sequence of $\eta(t)$, representing the sea level, can be seen as the outcome of a linear combination of two independent components: the deterministic part and the stochastic part:

  $$\eta(t) = \eta T(t) + \eta s(t) \tag{2.12}$$

  The deterministic component encompasses tidal oscillations, while the stochastic component ηs is primarily influenced by wind and barometric gradients.

- MARINE CURRENT:

  Due to the absence of direct current measurements, the dynamic behavior can be reconstructed by utilizing wind and tidal data. Much like sea level, the overall current can be portrayed as a summation of vectors:

  $$V = \sum V i \tag{2.13}$$

  Although this representation assumes linearity and the independence of different phenomena, it lacks strict rigor. Nonetheless, it offers a valid and

reasonably accurate methodology for studying marine currents. In this context, currents can be classified into two fundamental categories, which stem from completely distinct causes: the deterministic component, driven by tidal currents and the non-deterministic or stochastic component, encompassing factors such as wind and slope-induced effects.

At any given moment, disregarding interaction effects, the current value V(t) can be understood as the linear combination of two independent parts:

$$V(t) = VT(t) + VS(t) \tag{2.14}$$

The deterministic part relates to tidal currents, while the stochastic component VS can be further decomposed into two constituents:

$$VS(t) = VWind(t) + VSlope(t) \tag{2.15}$$

Here, the wind-induced component reflects the impact of wind, while the slope-induced component is influenced by the presence of the coastline.

Complementary to this section there is the evaluation of the oceanographic framing, for the analysis of local oceanographic conditions including temperature of the water, salinity and torbidity.

A big chapter is then required for the evaluation of habitats and biotypes that characterize the area, which is based on the analysis of Natura 2000 Network. It is the world's largest coordinated system of protected areas, covering a total surface of more than 1.2 million square kilometers, or about 18% of the total land area of the European Union. For this reason, Natura 2000 is an invaluable example of a large-scale coordinated reserve network developed and operated to address major conservation issues that might help to guide large-scale conservation efforts in other regions. [43].

This network includes sites of community importance (SCIs) and special areas of conservation (SACs), identified under the provisions of the Habitats Directive, as well as special protection areas (SPAs) designated under the "Birds" Directive (Directive 2009/147/EC). A SCI refers to a site that plays a significant role in maintaining or restoring natural habitats to a favorable conservation status. While a SPA is set up to safeguard bird species threatened with extinction, vulnerable to habitat changes, or considered rare due to their small populations or restricted local distribution. Member States are required to designate the most suitable areas as SPAs based on scientific data. [44] Plus, they are responsible for designating and managing Natura 2000 sites within their territories. They are required to establish conservation measures and management plans to maintain or restore the habitats and species present in these areas. The network also promotes cooperation and

coordination among Member States to ensure the effective protection of the shared natural heritage.

Additionally, in order to provide a general overview of the distribution of marine mammals and sea turtles in the study area, the information available from the EUROBIS database extracted from EMODnet (The European Marine Observation and Data Network) , `https://emodnet.ec.europa.eu/geoviewer/#!/`, are taken into consideration. EMODNet is a network supported by EU's integrated maritime policy, with the purpose of furnishing users with an extensive array of information concerning marine organisms and circumstances.

Other constrains to add are the ones related to the exiting fisheries economic activities, analysed again accessing the data published by EMODNET Human Activities. Same for the evaluation of the existing BPZs, Biological Protection Zone, existing in Sardinia to prevent exploitation of the trawling fishing allowing only the traditional way.

Moreover a section referred to the existing maritime trafic and marine infrastructure is required. For what concern flights, the flight restriction map, Fig. 2.21, is considered to take into account the regulations that govern the flight operation in the region. For military activities, in Fig. 2.22, there are certain coastal areas in Italy that are designated for occasional naval activities such as surface and submarine exercises, shooting and bombing drills, dredging operations, and amphibious exercises. These zones are subject to specific regulations, which are communicated to mariners through special Notices to Mariners.

To proceed, the presence of gas pipelines, power lines and telecommunication lines are evaluated to find the infrastructure constraints in the area, because avoiding interference with them is crucial when deciding the location for an offshore plant. In fact, they may incur in several issues like the ones of safety risks damaging and/or disrupting gas lines, electric hazards or power outages. Furthermore an accidental damage to gas lines can result in the release of harmful gases into the environment, contributing to air pollution and potentially harming marine life as well as the disruption of telecommunication cables could also affect communication systems vital for maritime operations, search and rescue efforts, and coastal monitoring.

In section 3.3, the analysis of the existing lines will be performed considering carefully all the existing infrastructures and communication lines actually present and under development as future projects.

Finally, the last consideration is about the marine areas open to hydrocarbon exploration, Fig. 2.23. They are locations designated for activities related to the exploration and extraction of oil resources. In Italy, the definition and regulation of oil exploration areas are determined by the Ministry of Economic Development, which grant mining permits in areas of Italian continental shelf established through laws and ministerial decrees, known as "Marine Zones".
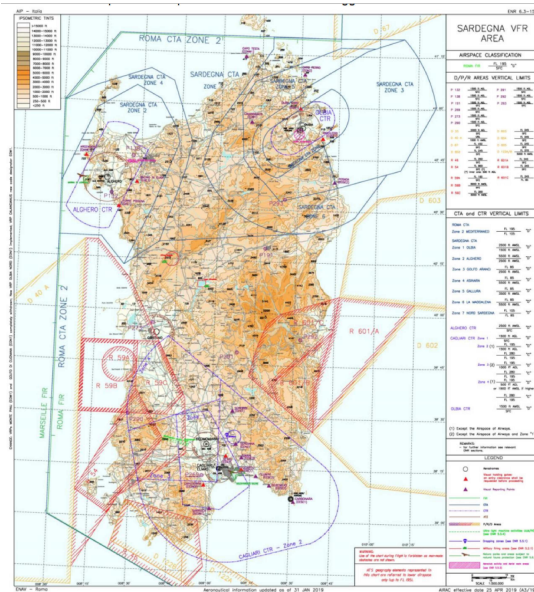
Figure 2.21: Flight restriction map. A geographical representation that displays areas where certain flight restrictions or limitations are in effect.
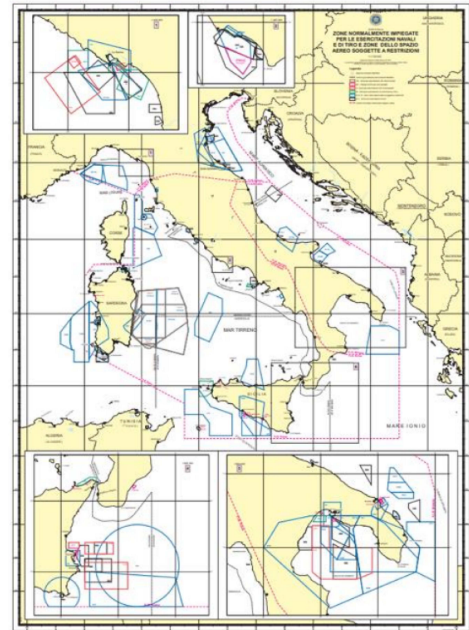
Figure 2.22: Areas for naval shooting exercises and restricted airspace. Typically established to ensure safety and security in and around bodies of water where naval forces conduct training and operations.
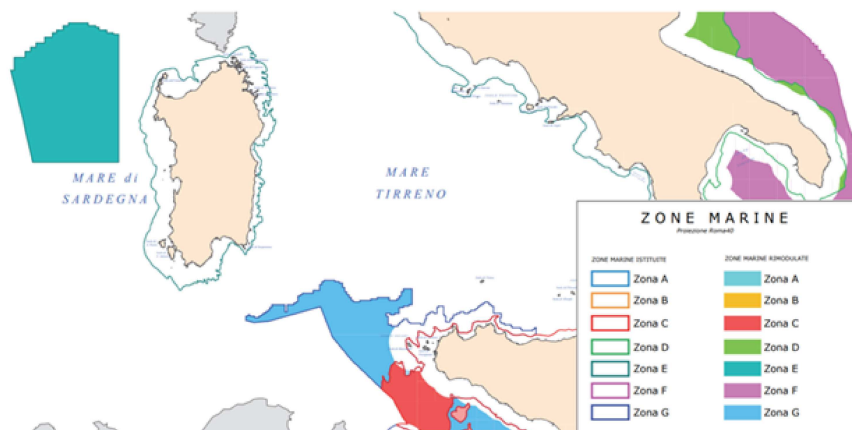
Figure 2.23: Oil exploration areas. Regions where companies and governments conduct surveys, drilling, and other activities to locate and extract oil reserves beneath the Earth's surface.

2.6.4   Pyseafuel

The core of this study concerns the evaluation of the devices implemented to calculate the synthetic fuel production. To perform that, the python package Pyseafuel has been used.

The pyseafuel package simulates the four subprocesses involved in fuel production. Once again, the main concept is a marine-based floating island on which, thanks to wind energy, it will be possible to convert it into electrical energy to produce H_2 and extract CO_2 from seawater, where it is in equilibrium with the atmosphere. These two gases are then let react to form the energy carrier methanol, which could be conveniently shipped to end consumers. These subprocesses are degassing, desalination, electrolysis, and the final reaction, as it is visible in Fig. 2.24 Firstly, seawater is divided into separate streams and fed into the degasser and desalinator. The degasser removes CO_2 from the seawater, which is then directed to the reactor. The degassed seawater is instead discharged at this stage.

Simultaneously, the seawater enters the desalinator where it undergoes a purification, with the brine being returned to the ocean. The purified water is then passed through an electrolyzer, which separates it into hydrogen and oxygen. The oxygen is released into the atmosphere, while the gaseous hydrogen is conveyed to the reactor alongside the carbon dioxide. In the reactor, these components react with each other for the formation of the synthetic fuel which, in this study, has been considered to be methanol CH_3OH.

Methanol is also known as MeOH, representing the most basic carbon-derived fuel option, remaining in liquid form under typical environmental circumstances. With an energy density of approximately half that of gasoline (15.6 MJ/L compared to 32.4 MJ/L), it possesses the potential to fuel existing gas turbines, modified diesel engines, and direct methanol fuel cells . Moreover, it can function as a raw material for the majority of petrochemical goods, and through a straightforward dehydration process, it can be transformed into dimethyl ether, an appealing substitute for natural gas and other hydrocarbon fuels. The production of methanol can be accomplished by catalytic hydrogenation of CO_2. [45]

$$3\,H_2 + CO_2 \longrightarrow CH_3OH + H_2O \tag{2.16}$$

showing an exothermic behaviour with a variation of entalphy of ΔH = -49.3 kJ/mol. [46]

The ideal production of 1 mol of CH_3OH necessitates 3 mol of H_2 and 1 mol of CO_2, both of which pose significant electrochemical challenges during extraction from seawater.
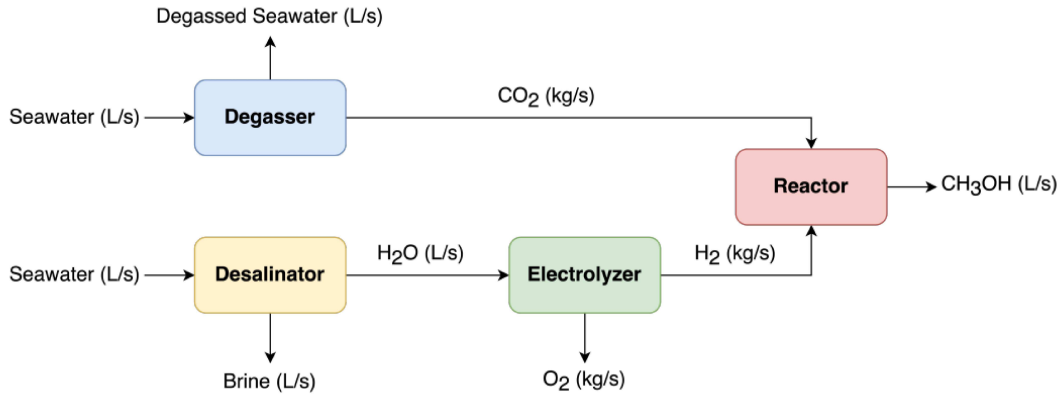
Figure 2.24: Scheme of fuel production plant with methanol as output. Seawater enters in the degasser and desalinator. At the output, respectively, carbon dioxide and purified water. This last will enter in the electrolyzer for the producion of hydrogen and finallu, with CO_2 in the reactor.

An important clarification needs to be made regarding the choice of the final fuel. In this chapter, the hypothetical production of methanol will be considered as the final product of the production facility. However, the actual and decisive selection of the fuel type and output will require further investigation, based on the current economic status for its production and the goals of the Sardinian region in terms of synthetic fuels.

Degasser

The degasser is a fundamental step in order to extract CO_2 from seawater useful later in combination with H_2 from the electrolyzer. This process will have as second output degassed seawater which will be re-injected in the sea. CO_2 traditionally is separated from a gas in two steps: first the selective capture of carbon dioxide and then the desorption of pure CO_2 from the absorber or adsorber. Important to notice is that CO_2 in the atmosphere is in equilibrium with the total dissolved inorganic carbon (DIC) present in the sea. Where:

$$DIC = CO_2 + HCO_3{}^- + CO_3{}^{2-} \tag{2.17}$$

$$CO_2 = CO_2(aq) + H_2CO_3 \tag{2.18}$$
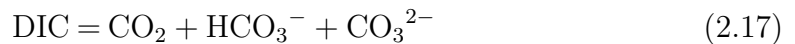
When carbon dioxide dissolves in the seawater, these are the reactions that describe the equilibrium in detail from Lueker et al. (2000): [47]

$$CO_2(g) = CO_2(aq) \tag{2.19}$$

$$CO_2(aq) + H_2O = H_2CO_3 \tag{2.20}$$

$$H_2CO_3 = H^+ + HCO_3^- \tag{2.21}$$

$$HCO_3^- = H^+ + CO_3^{2-} \tag{2.22}$$

Having in mind that the notation (g) and (aq) refers to the state of the species. But, since it's difficult to distinguish between $CO_2(aq)$ and H_2CO_3 they are usually referred together as CO_2^*.

$$CO_2(g) = CO_2^*(aq) \tag{2.23}$$

$$CO_2^*(aq) = H^+ + HCO_3^- \tag{2.24}$$

The method used to extract CO_2 from seawater is based on Eisaman et al. (2012), [48], and consist of the utilization of a BPMED, a bipolar membrane electrodialysis, visible in Fig. 2.25 Seawater is pumped through the bipolar membrane electrodialysis system, splitted in two streams, one of acidified seawater and the other of basified. The acidified stream undergoes a process where the HCO_3^- and CO_3^{2-} ions present in the input seawater are converted into dissolved CO_2. The precise reactions that happens in the acidic compartements are:

$$CO_3^{2-} + 2\,H^+ \rightleftharpoons HCO_3^- + H^+ \rightleftharpoons CO_2 + H_2O \tag{2.25}$$
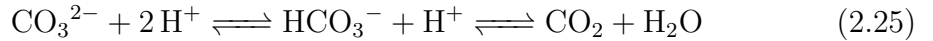
This dissolved CO_2 is then extracted through a vacuum stripping process, resulting in a stream of pure CO_2 gas. The acidified solution, now depleted of CO_2, can be combined with the basified solution to create a neutral-pH solution that can be safely discharged back into the sea. As the acid solution pH drops, the rate of CO_2 gas extraction increases until the solution pH values and the CO_2 extraction rate reach steady-state values.
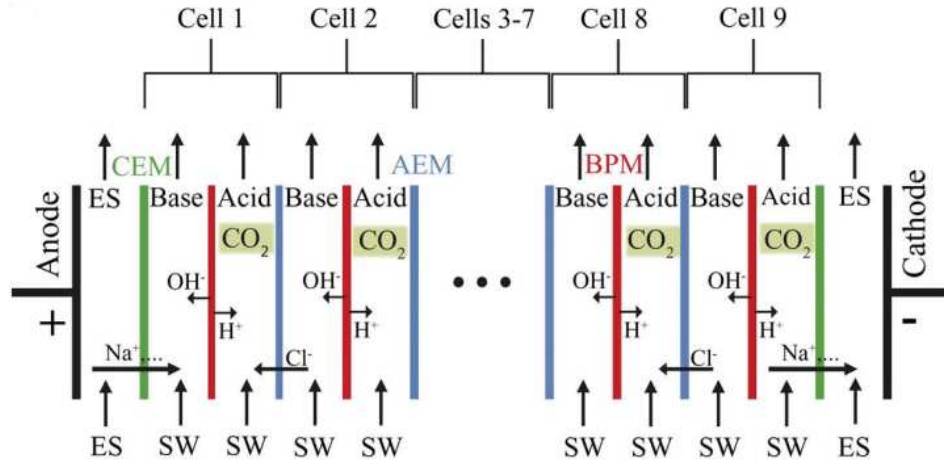
Figure 2.25: Scheme of BPMED unit. ES = electrode solution, SW = seawater, CEM = cation exchange membrane, AEM = anion exchange membrane, BPM = bipolar membrane. Image from Eisaman et al. (2012).

When an electrical potential is applied to the BPMED stack and the current density surpasses the maximum allowable current density for the BPM (typically less than 10 mA/cm^2), it initiates the dissociation of water within the BPM. This generates H$^+$ and OH$^-$ ions, which migrate in response to the applied electric field: H$^+$ ions move towards the negatively charged cathode, while the OH$^-$ ions move towards the positively charged anode. A theoretical minimum polarization of 0.83 V per BPM is required to induce significant water dissociation at room temperature, with higher voltages required at higher current densities. So this water dissociation results in acidification with H$^+$ and basification with OH$^-$ ions. The presence of a AEM next to each BPM allows anions of input seawater as Cl$^-$ to be transported across the membrane towards the positively-charged anode. Doing that, H$^+$ and Cl$^-$ will contribute to the acidified compartments, let OH$^-$ ions replacing Cl$^-$ ions in the basified compartments. At each end of the membrane stack there is a CEM that separates the alternating stack of BPMs and AEMs from the electrode compartments. This means that Na$^+$ and other cations from the anode compartment are transported across a CEM from the anode compartment into the adjacent base compartment towards the cathode compartment.

To compute the module on Python, have been used the values found in Eisaman et al. (2012) basing on experimental curves obtained with different tests performed at different constant flow rates for the acid, base, and electrode solution; 3.1 lpm, 3.6 lpm, 4.1 lpm, and 6 lpm [litres per minute]. Considering the CO$_2$ extraction

efficiency at several values of pH, the CO_2 rate output and the final electrochemical energy needed to acidify the incoming solution to a desired pH, these curves have been reproduced with fitted quadratic curves, called also quadratic regression curve, to mathematically model the relationship between the data points in the scatter plot.
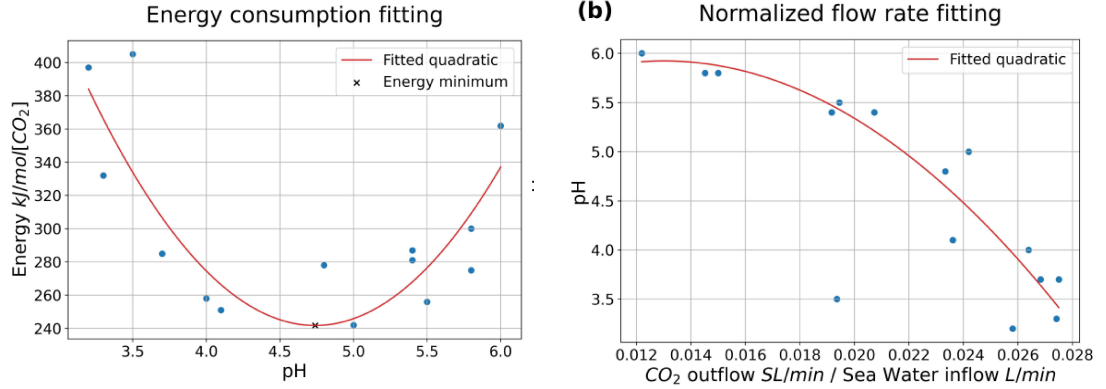
Figure 2.26: Energy consumption per mole of extracted CO_2 depending on pH of the acid output solution. The minimum amount of energy to obtain a certain pH level is the one that corresponds to approximately pH = 4.7.

Figure 2.27: Relation between pH and ratio of outflow of CO_2 over inflow seawater. Decreasing the pH of the output solution will increase the ratio.

For energy consumption in Fig. 2.26:

$$58.29x^2 - 524.44x + 1423.21 = 0 \qquad (2.26)$$

with x = pH, and for the flow rate fitting in Fig. 2.27:

$$-1195.47x^2 + 311.11x + 3.90 - pH = 0 \qquad (2.27)$$

with x = CO_2 outflow / seawater inflow ratio, and the final power consumed is calculated multiplying the energy in $\frac{J}{kg}$ by mass of carbon dioxide at the output, with this output mass obtained as flow ratio multiplied by the volume of seawater at the inlet and then converted using its density ρ.

Desalinator

On the other path, desalination is a process that removes dissolved minerals from seawater, brackish water, or treated wastewater. Seawater contains various particles within it that can hinder the proper functioning of electrolysis processes. This is especially true concerning the presence of chlorine in the water. During the electrolysis of seawater, chlorine evolution reactions (CER) can take place, which hinder the correct progression of the oxygen evolution reaction (OER), which involves the generation of oxygen gas from water when an electric current is applied, resulting in the production of a highly corrosive gas.

$$CER = Cl^-_{aq} \longrightarrow \frac{1}{2} Cl_{2(g)} + e^- \tag{2.28}$$
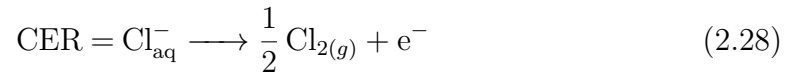
A simple, cost-effective, and efficient way to address this issue is to carry out a desalination process before the operational phase of the electrolyzer.

One method of desalination is exploiting the electrodialysis. The desalination technologies commonly used and commercially proven can be classified into two categories: thermal (evaporative) methods and membrane-based methods. Membrane methods, such as reverse osmosis and electrodialysis, are less energy-intensive compared to thermal methods and since their lower energy requirements, so more cost-effective, membrane methods are quite diffuse.

Electrodialysis is a membrane-based separation process that utilizes an electric field to selectively remove ions from water. The process involves the use of two types of membranes: cation exchange membranes, CEMs and anion exchange membranes, AEMs, called generally ion exchanged membranes, IEMs. These membranes are selectively permeable, allowing the passage of either positive or negative ions. A stack of alternating CEMs and AEMs is placed between two electrodes, creating compartments known as cells. The seawater to be desalinated is fed into the cells and when an electric current is applied, the positive ions are attracted to the negative electrode, while the negative ions are attracted to the positive electrode. Specifically the positively charged cations move toward the cathode, passing through the negatively charged CEM and then they are retained by the positively charged AEM, while the opposite for negatively charged anions. At the end, ion concentration increases in alternate compartments with a simultaneous decrease of ion concentration in other compartments. [49]

52
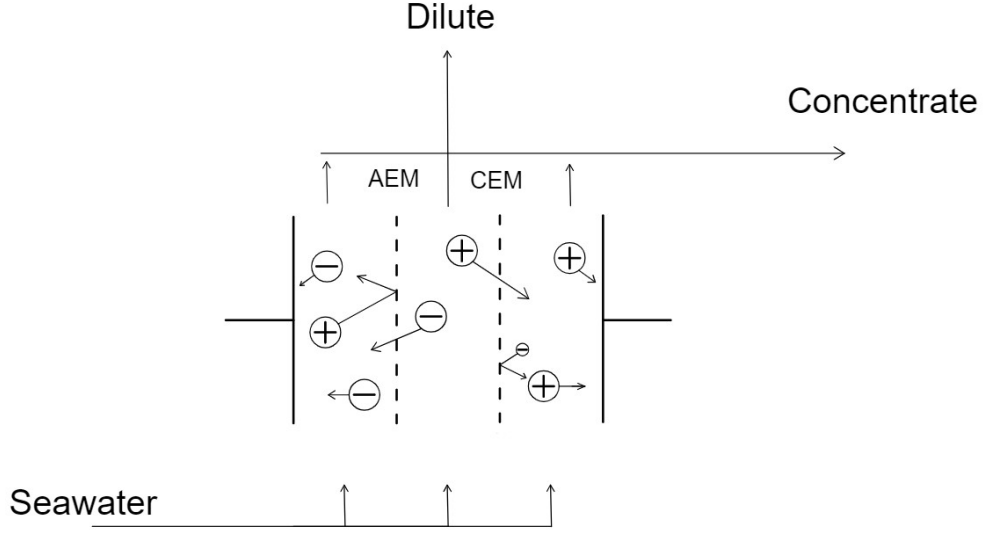
Figure 2.28: Schematic perspective of an electrodialysis cell for the separation and motion of charged ions through selective ion-exchange membranes, allowing for the desalination of the solution.

As the water passes through the electrodialysis stack, the cation exchange membranes allow the positive ions to pass through, while blocking the negative ions. Similarly, the anion exchange membranes allow the negative ions to pass through, while blocking the positive ions. The desalinated water and the concentrated brine (containing the removed salts) are collected separately. Fig. 2.28

The expression for the specific energy consumption, SEC, of ED is obtained using Wang et al. (2020) [50] In single stage operation, the applied voltage is equally distributed between cell pairs. In order to get a specific salt removal value, the applied voltage has to be larger than the equilibrium voltage at the end of the separation. Hence, a practical minimum voltage, ΔE_1, can be determined for a target salt separation.

$$\Delta E_1 = 2\frac{RT}{F} \cdot \ln \frac{c_b}{c_p} \tag{2.29}$$

where R is the ideal gas constant (taken as 8.3145 $\frac{J}{mol \cdot K}$), T is the temperature of the feed flow in Kelvin, c_b is the brine flow in $\frac{mol}{L}$, c_p is product flow in $\frac{mol}{L}$ and F the Faraday constant. The minimum value for the entire membrane stack is obtained multiplying by the number of cell pairs. Then, the transferred electrical charge, Q, at the end of separation is equal to the transferred ionic charge:

$$Q = V_p(c_f - c_p)F \tag{2.30}$$

Finally the minimum SEC is calculated multiplying practical minimum voltage and Q, normalizing by V_p, which represents the volume of product water:

$$SEC = 2RT(c_f - c_p) \ln \frac{c_b}{c_p} \tag{2.31}$$

When considering a multistage ED, energy consumption will be lower, having the product stream of one membrane stack entering as a feed in the stack subsequent. The energy consumption for multistage operation becomes smaller than that for single-stage operation. Plus, operating with multiple stages reduces the excess voltage and so saves energy.

Here, the model equation used is derived from Wang et al. (2020), [50] [51]

$$SEC = 2RTc_f \zeta \ln \left(\frac{1}{(1-\zeta)(1-R_w^{1/n})} - \frac{R_w^{1/n}}{1-R_w^{1/n}} \right) \sum_{i=1}^{n} (1-\zeta)^{i-1} \tag{2.32}$$

Electrolyzer

The electrolysis of seawater is a process which uses an electric current to decompose seawater into its constituent elements, namely hydrogen and oxygen gases. Let's take in mind that seawater is a mixture of water and various dissolved salts, including sodium chloride (NaCl), other minerals and sediment, microorganisms, and complex ion species.

The process of water electrolysis involves two primary half-reactions known as the hydrogen evolution reaction (HER) and the oxygen evolution reaction (OER), which involve the transfer of electrons. At the cathode, where reduction occurs, the HER can be described by the following equations in both acidic and alkaline environments:

Acidic conditions:

$$2\,H^+ + 2\,e^- \longrightarrow H_2 \tag{2.33}$$

Alkaline conditions (basic conditions):

$$2\,H_2O + 2\,e^- \longrightarrow H_2 + 2\,OH^- \tag{2.34}$$

In the acidic environment, where pH is less than 7, two hydrogen ions (H^+) gain two electrons (e^-) to form hydrogen gas (H_2) at the cathode. On the other hand, in an alkaline environment, pH higher than 7, two water molecules (H_2O) gain two electrons to produce hydrogen gas (H_2) and two hydroxide ions (OH^-) at the cathode. Regarding the anode in water electrolysis, the oxygen evolution reaction (OER) takes place. The OER process can be expressed by the following equations under acidic and alkaline conditions:

Acidic conditions:

$$2\,H_2O \longrightarrow 4\,H^+ + O_2 + 4\,e^- \tag{2.35}$$

Alkaline conditions:

$$4\,OH^- \longrightarrow O_2 + 2\,H_2O + 4\,e^- \tag{2.36}$$
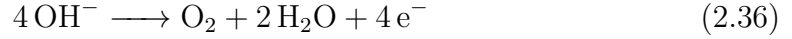
In the acidic environment, two water molecules (H_2O) undergo a decomposition reaction at the anode. This results in the formation of four hydrogen ions (H^+), one molecule of oxygen gas (O_2), and the release of four electrons (e^-).

In an alkaline environment, four hydroxide ions (OH^-) participate in the reaction at the anode. This leads to the generation of one molecule of oxygen gas (O_2), two water molecules (H_2O), and the liberation of four electrons (e^-). These equations illustrate the electrochemical processes that occur at the anode during water electrolysis under both acidic and alkaline conditions, where the OER is responsible for the production of oxygen gas and the release of electrons. [52]

To perform a water electrolysis, technologies that can be used are classified on the basis of the type of electrolyte they use.

- Direct seawater electrolyzer (DWE)

- Proton exchange membrane water electrolyzer (PEMWE)

- Alkaline Electrolysis (AWE)

- Solid Oxide Electrolysis (SOWE)

The first three operate at low temperature conditions, under 100 °C, the last one is instead at temperature of 700-800 °C. In the DWE, the electrolyte is the seawater itself. For AWE liquid water is the feed and the electrolyte is a concentrated caustic, usually NaOH or KOH, but for this case a PEM is the solution adopted.
PEMWE uses liquid water as feed. This type of technology features a solid polymer as an electrolyte, with a high proton conductivity. It is characterized by a low temperature around 40 °C - 80°C, the possibility to obtain H_2 at high pressure and s state of the art which is at commercial level with order of production of kWe to MWe. Its scheme in Fig. 2.29.

Unsupported or carbon-supported platinum, Pt, nanoparticles are commonly employed at the cathode for the HER, while supported or unsupported iridium dioxide (IrO_2) are predominantly used at the anode for the OER. Both catalytic layers are designed to be microscopically porous to facilitate gas evolution and contain a combination of catalyst particles, support particles, and ionomer. The ionomer, by acting as a binder, helps in creating a cohesive structure within the

catalytic layers, ensuring strong adhesion between the catalyst particles, support particles, and other components. This enhances the stability and durability of the cell. Moreover these kind of electolyzer are very compact and modular thanks to the concept of zero-gap architecture. This means that there is a single piece unit, called Membrane-Electrode Assembly (MEA), that connects all the elements in a three-layer sandwich. Due to that, they ensure a homogeneous contact between bipolar plates and the porous electrode. Because of that PEMWE are more expensive but less maintenance is required. Last but not least, important to mention that this presents a slightly bigger degradation rate than AWE leading to a lower efficiency. [53]
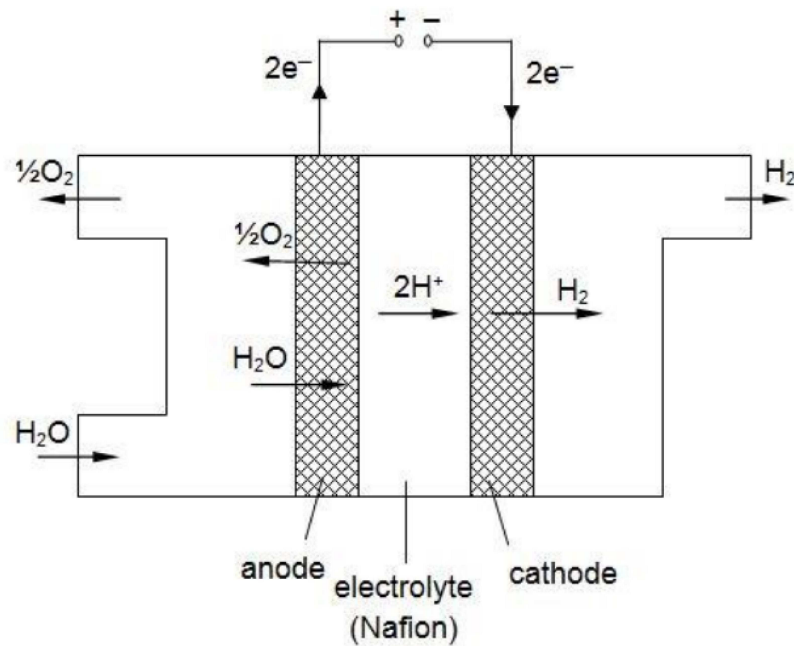
Figure 2.29: Scheme of a Proton Exchange Membrane Water Electrolyzer. Water is split into hydrogen and oxygen gases, with a proton-exchange membrane facilitating the process.

The model used to describe the PEMWE power consumption is derived by Shen et al. (2011) [54]

$$P = K(V - Ir - E_0)^2 \tag{2.37}$$

Where V is cell potential (V), E_0 is the water dissociation potential (V), Ir is ohmic voltage drop or potential drop over the total resistance where r is the cell resistance including electrode resistance, electrolyte resistance and the interfacial

resistance (Ω) and finally K is a proportional coefficient of power conversion which reflects the capability of an electrolytic cell to convert electrical energy to chemical energy (Ω^{-1}).

From that it's possible to obtain the relation between current and potential as:

$$I = \frac{V + 2Kr(V - E_0) - \sqrt{V^2 + 4KrE_0(V - E_0)}}{2r(1 + Kr)} \tag{2.38}$$

Reactor

Finally there is the reactor section, the device used to facilitate chemical reactions happening. It provides an environment where reactants can interact and transform into desired products. In this specific case, H_2 coming from the electrolyzer and CO_2 coming from the degasser interact with the catalyst to combine to produce CH_3OH. Normally the catalyst is one of $Cu/ZnO/Al_2O_3$ type.

Once again the reaction that happens is the hydrogenation of CO_2 following a direct path:

$$CO_2 + 3\,H_2 \longrightarrow CH_3OH + H_2O \tag{2.39}$$
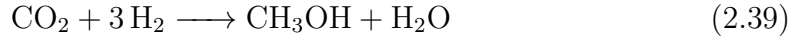
an exothermic reaction, ΔH = -49.3 kJ/mol. According to Le-Chatelier's principle, due to exothermic nature and a lower number of moles in the product, low temperature and high pressure are required to shift the reaction's equilibrium towards a forward direction. [16] But it's important to consider the existence of the Reverse Water Gas Shift Reaction (RWGS) which is endothermic, reducing the effectiveness of the hydrogenation of carbon dioxide. Therefore, increasing the reaction temperature will lead to an increase in the formation of CO hindering the direct hydrogenation of CO_2 to CH_3OH.

$$RWGS = CO_2 + H_2 \longrightarrow CO + H_2O \tag{2.40}$$
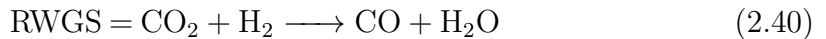
with a ΔH = +41.2 kJ/mol.

Currently, methanol is produced via synthesis processes operating at pressures of 50–100 bar and temperatures of 200°C–300°C. As introduced before the catalyst generally used is $Cu/ZnO/Al_2O_3$ essential for the shift reaction. In spite of thermodynamic considerations suggesting the operation at lower temperatures possible, the methanol synthesis process is conducted at approximately 200°C–300°C due to the catalyst's activity being confined within this temperature range. However, it is important to note that thermodynamic equilibrium constraints and catalyst deactivation significantly impact the overall methanol production. A good catalyst should remain active for several years (up to 4 years). [55]

The type of reactor adopted is a Plug-Flow reactor (PFR), a continuous flow reactor, where all the reactants and products flow over one or more parallel tubes at a constant total mass flow rate, shown in Fig. 2.30.
The description follows the model adopted by Terreni et al. (2020) [56]

Figure 2.30: Scheme of a Plug Flow Reactor, PFR, where reactants flow through a channel, moving at the same velocity and experiencing similar reaction conditions, resulting in efficient and predictable chemical reactions. Image from Terreni et al.(2020).

Where:

$$\dot{N}^{out} = PFR[\dot{N}^{in}] \tag{2.41}$$

$$\text{molar flow rates: } \dot{N} = (\dot{N}_{CO}, \dot{N}_{CO_2}, \dot{N}_{H_2}, \dot{N}_{H_2 0}, \dot{N}_{CH_3OH}) \tag{2.42}$$

$$\text{reduced partial pressure: } p = \frac{P}{P_0} \frac{\dot{N}}{\sum_{j'}(\dot{N}_{j'})} \tag{2.43}$$

$$\dot{N} = \frac{\dot{m}p}{\sum_{j'}(p_{j'}m_{j'})} \tag{2.44}$$

$$\text{mass flow: } \dot{m} = \sum_{j'}(\dot{N}_{j'}m_{j'}) = \frac{v_{flow}A_{tubes}}{RT} \sum_{j'}(p_{j'}^{in}m_{j'}) \tag{2.45}$$

where T is the absolute temperature, R is the gas constant, $p_{j'}$ is the array of reduced partial pressure, vector $\dot{N}$ is the molar flow rate in $\frac{mol}{s}$, P is the reaction pressure (bars), P_0 the atmospheric pressure (bars), m_j is the molecular weight and A_{tubes} is the cross sectional area of all the tubes. The index j' stands for all the components involved in the reaction.

So, the kinetics of the reduction of CO_2 to methanol have been modeled by Graaf et al. (1988), [57]. They described the rates, r_j of the three reactions that could happen in the reactor.

$$\text{Direct hydrogenation}: \mathrm{CO_2 + 3\,H_2 \longrightarrow CH_3OH + H_2O} \qquad (2.46)$$

$$\text{RWGS}: \mathrm{CO_2 + 3\,H_2 \longrightarrow CO + 2\,H_2 + H_2O} \qquad (2.47)$$

$$\text{MeOH synthesis}: \mathrm{CO + 2\,H_2 \longrightarrow CH_3OH} \qquad (2.48)$$
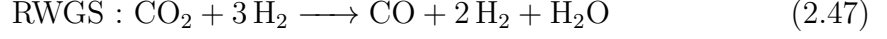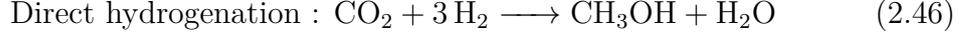
The reactions involved in methanol formation (Direct hydrogenation and MeOH synthesis) are exothermic and result in a reduction of moles. Thus, the transformation of reagents is facilitated by low temperatures and elevated pressures. Nowadays synthesis processes take place at lower pressures, in the range of 50–100 bar, allowing the reduction of the costs of gas compression. Nevertheless, when employing lower pressure methods, the synthesis gas conversion tends to be reduced, typically around 10%. Consequently, the implementation of a recycling loop becomes essential to achieve the desired level of yield. So, the rates are modeled by:

$$r_1 = k_1 K_{CO} \left[p_{CO} \cdot p_{H_2}^{\frac{3}{2}} - \frac{p_{CH_3OH}}{p_{H_2}^{\frac{1}{2}} \cdot K_1^{eq}} \right] / D \qquad (2.49)$$

$$r_2 = k_2 K_{CO_2} \left[p_{CO_2} \cdot p_{H_2} - \frac{p_{H_2O} \cdot p_{CO}}{K_2^{eq}} \right] / D \qquad (2.50)$$

$$r_3 = k_3 K_{CO_2} \left[p_{CO_2} \cdot p_{H_2}^{\frac{3}{2}} - \frac{p_{CH_3OH} \cdot p_{H_2O}}{p_{H_2}^{\frac{3}{2}} \cdot K_3^{eq}} \right] / D \qquad (2.51)$$

$$D = (1 + K_{CO} \cdot p_{CO} + K_{CO_2} \cdot p_{CO_2}) \cdot \left[p_{H_2}^{\frac{1}{2}} + \left(\frac{K_{H2O}}{K_{H_2}^{\frac{1}{2}}} \right) \cdot p_{H_2O} \right] \qquad (2.52)$$

And consequently R, a 5-component vector giving the net production rates for the individual chemical species, is equal to:

$$(R_{CO}, R_{CO_2}, R_{H_2}, R_{H_2O}, R_{CH_3OH}) = (-r_1 + r_2, -r_2 - r_3, -2r_1 - r_2 - 3r_3, r_2 + r_3, r_1 + r_3)$$
$$(2.53)$$

Once again it's important to remember that the efficiency of converting CO_2 to methanol is highly influenced by the operating pressure and temperature of the reactor, along with the initial molar flow ratio of CO_2 and H_2 ($r = \dot{N}^0_{H_2}/\dot{N}_{CO_2}$).
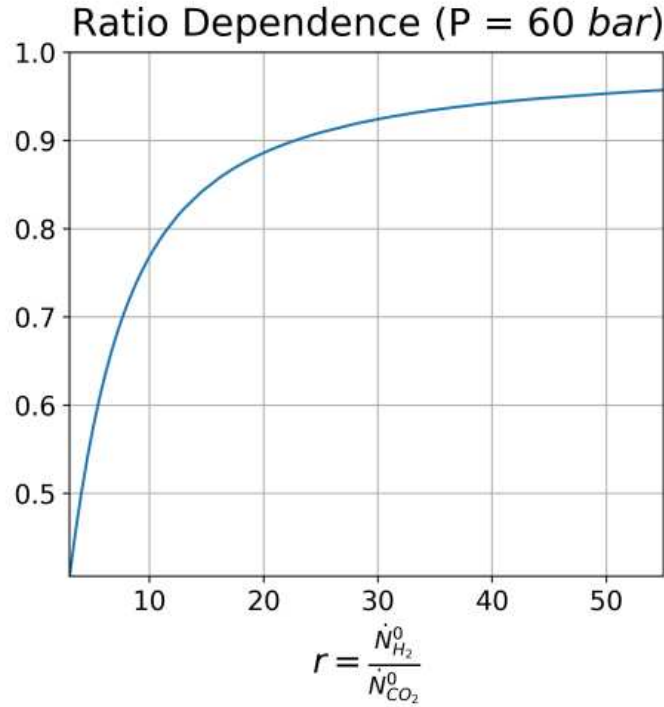
Figure 2.31: conversion factor ξ and $r = \dot{N}^0_{H_2}/\dot{N}_{CO_2}$ relationship, where increasing the amount of H_2 will benefit the final conversion of CO_2 into methanol.

In Fig. 2.31, on the y-axis, there is ξ, the conversion factor, indicating the moles of CO_2 converted into CH_3OH in percentage. Calculated from Terreni et al. (2020) [56], maintaining pressure = 60 bar and varying the ratio r. When examining the ratio, enhancing the reaction with H_2 leads to an improvement in ξ up to a certain threshold, beyond which there are diminishing returns as the ratio increases. Later on it will be illustrated that generating H_2 demands a substantial amount of power, so a consequent reasonable r must be balanced with the power consumption.

2.6.5 Dymethyl ether synthesis

A further consideration which could be done in the analysis is the synthesis of dimethylether. As seen in section 1.6.2 numerous are its advantages and applications, and the following is the procedure to be carried out in order to synthesise it. The procedure to obtain DME involves the integration of a methanol synthesis catalyst

based on $Cu/ZnO/Al_2O_3$ with a methanol dehydration catalyst. Fig. 2.32 This combination operates optimally at temperatures ranging from 240 °C to 280 °C and pressures between 30 bar and 70 bar. The reaction is:

$$2\,CH_3OH \longrightarrow CH_3OCH_3 + H_2O \tag{2.54}$$
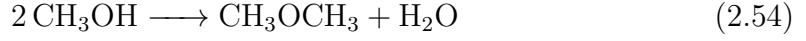
Which is the bimolecular dehydratation of methanol to DME, carried out catalyticaly by solid acids like alumina or phosphoric acid modified γ-Al_2O_3. This reaction is slightly exothermic ΔH = -24 kJ/mol.
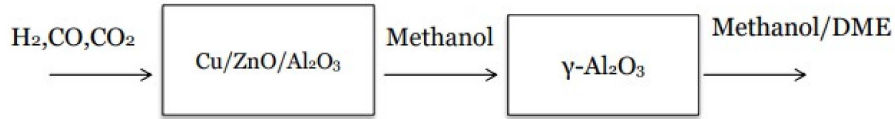
Figure 2.32: Dimethyl ether synthesis in two steps, starting from CO_2 to methanol and then MeOH to DME.

The rate of reaction, r, of the MeOH dehydratation is described by the formula:

$$r_{MeOh_{dehydratation}} = \frac{k_6 \cdot K_{CH_3OH}^2 - [C_{CH_3OH}^2 - (C_{H_2O} \cdot \frac{C_{DME}}{K_{eq,3}})]}{(1 + 2\sqrt{K_{CH_3OH} \cdot C_{CH_3OH}} + K_{H_2O} \cdot C_{H_2O})^4} \tag{2.55}$$

or in the Arrhenius form:

$$r = A(i) \cdot exp(-\frac{Ea}{RT}) \tag{2.56}$$

Using the data provided in Tab. 2.1.

	A	Ea
k_6	$5.35 \cdot 10^{13}$ kmol/(kg$_{cat}$ · h)	-143665.92 J/mol
K_{CH_3OH}	$5.39 \cdot 10^{-4}$ m3/kmol	70560.918 J/mol
K_{H_2O}	$8.47 \cdot 10^{-2}$ m3/kmol	42151.98 J/mol

Table 2.1: Values for rate of reaction of MeOH dehydratation.

And finally an evaluation about the effect that CO_2 and H_2O has on the output of the reactor in Fig. 2.33 and Fig. 2.34.
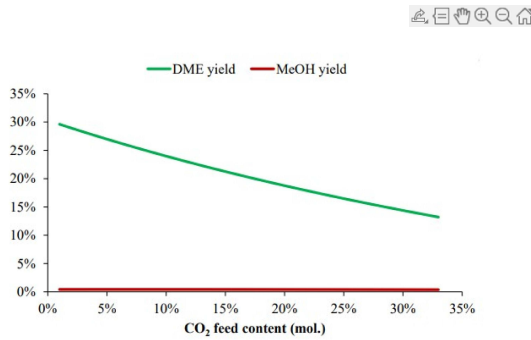
Figure 2.33: Influence of CO_2 on DME at T=250°C and p=50 bar. Increasing that value is not beneficial for the final DME synthesis.
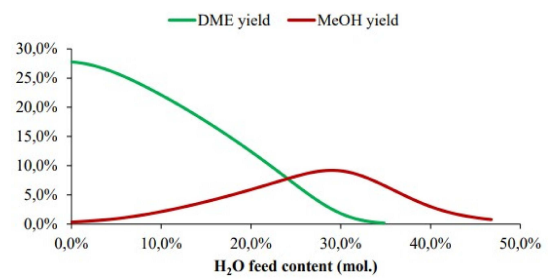
Figure 2.34: Influence of H_2O on DME at same conditions. As well as CO_2, greater amount of H_2O are not beneficial.

Where it is possible to see that increasing CO_2 in molar fraction will push back the reaction decreasing the DME output as well as for H_2O, that inhibits DME synthesis.

Chapter 3

Results and Discussion

The upcoming chapter will delve into a detailed exploration of the outcomes that led to the selection of the final location in the Mediterranean sea for the offshore wind farm installation. This pivotal decision enabled the calculation of the final methanol output, powered by the same wind energy source. Furthermore, a brief investigation into the marine characteristics of the chosen area has been provided and a discussion over the potential implementations of marine energy capture devices.

3.1 Wind

This section will examine closely the assessment of wind aspects and unveil the outcomes derived from a comprehensive analysis of the wind's values. Basing on the data in 2.6.1, where the precise methodology employed and the instruments utilized for calculating the essential parameters in the process were meticulously described, now it is possible to see the results obtained from that.

With a sound understanding of the data collection approach and parameter calculations, the study will proceed to showcase the results obtained from that rigorous investigation. The figures provided in the previous chapter, Fig. 2.3, Fig. 2.4, Fig. 2.2, Fig. 2.5, Fig. 2.6, Fig. 2.11 and Fig. 2.13, serve as visual representations of the wind-related data, offering valuable insights into the patterns and trends observed, since a detailed investigation of wind characteristics, such as speed, direction and availability is basic for the final selection. [58]

However, merely presenting the raw data is not enough to draw conclusive judgments about the feasibility of utilizing the location's wind resources. To determine the viability and potential for exploitation, certain minimum benchmarks have to be set. These benchmarks act as reliable indicators, providing a basis for assessing whether the wind conditions meet the necessary criteria to support

sustainable and efficient utilization.

In this context, the imposed constraints have been thoughtfully selected to ensure an optimal and satisfactory level of power production for the wind turbine. To guarantee effective turbine operation, a minimum condition was set, mandating that the wind speed must exceed the turbine's cut-in velocity, fixed at 3 m/s as visible in Fig. 2.10. This ensures that the turbine initiates power generation at wind speeds above this threshold. To strike a balance between site availability and energy potential, the selected wind speed value was further increased to 6.5 m/s. This choice allows for a reasonably large area for site selection. Going beyond this value would unduly restrict the available area, potentially compromising the overall feasibility of the project.

A similar approach was employed while determining other constraints crucial to turbine performance. Each constraint was carefully assessed to ensure it contributed positively to the turbine's power production while still maintaining practicality and site suitability. [59] [60]

- Wind speed $> 6.5 \frac{m}{s}$ in Fig. 3.2

- Mean wind speed over its standard deviation > 1.8 in Fig. 3.1

- Energy $> 2.5 \cdot 10^{11}$ J in Fig. 3.3

- Wind direction standard deviation < 1.7 rad

By establishing these minimum criteria, the aim was to ascertain that the location is not only reliable but also suitable for harnessing wind energy.

In Fig. 3.4 is shown the combination these constraints.

After identifying a potentially suitable area for the wind plant installation based on the calculated parameters, it becomes crucial to further investigate additional factors, such as wave behavior and environmental constraints within the selected region.

However, before delving into these aspects, it is pertinent to address the security concerns related to the maximum extreme wind speed that the wind plant can endure without compromising its stability. Fortunately, in the area of our interest, which is visible in detail in Fig. 3.5, it is noteworthy that the maximum survival wind speed for a turbine, which commonly stands in the region of 60 m/s, [61] [62], has never been recorded. This information provides reassurance regarding the plant's security and allows to focus the attention on assessing other vital aspects, including wave patterns and environmental considerations.

By conducting a comprehensive analysis of these factors, it is possible to ensure that the chosen location not only possesses suitable wind conditions but also aligns with safety standards and environmental sustainability, ultimately paving the way
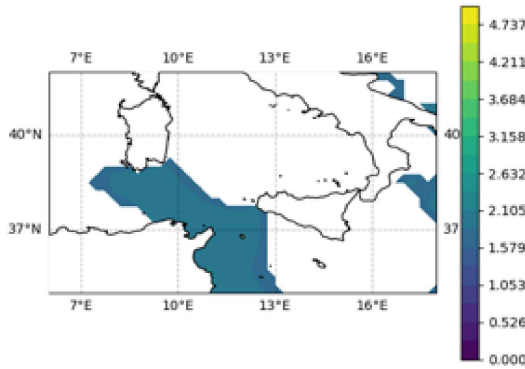
Figure 3.1: Mean WS / Std > 1.8. Bigger amount means bigger stability of the wind behaviour.
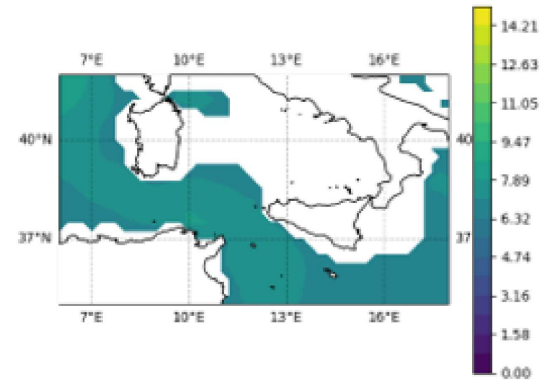
Figure 3.2: Areas where wind speed is higher than 6.5 m/s.
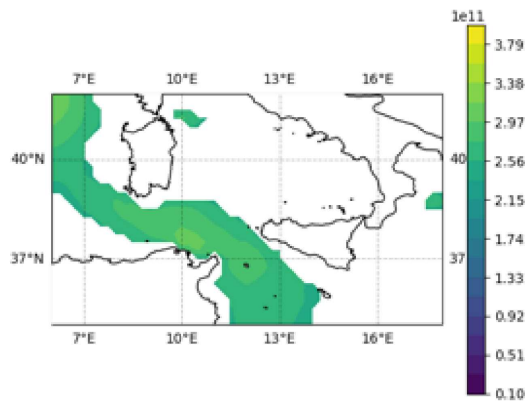
Figure 3.3: locations with energy production higher than $2.5 \cdot 10^{11}$ J.
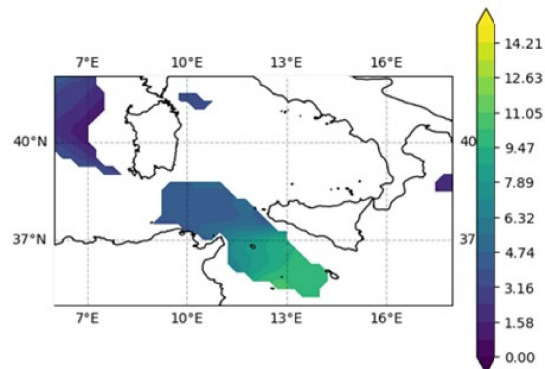
Figure 3.4: Final location with the mentioned constraints. The pickable options fall in the southern part of the region, a portion in the northeast near Corsica, and to the west but significantly farther from the coast.

for a successful and resilient wind energy project.

As referenced in section 2.6.1, the power calculation for the wind energy project was carried out using representative values from the well-established NoraEnergia2 project. Leveraging the advanced capabilities of the Floris package, the net annual energy production was successfully determined, corresponding to a value of
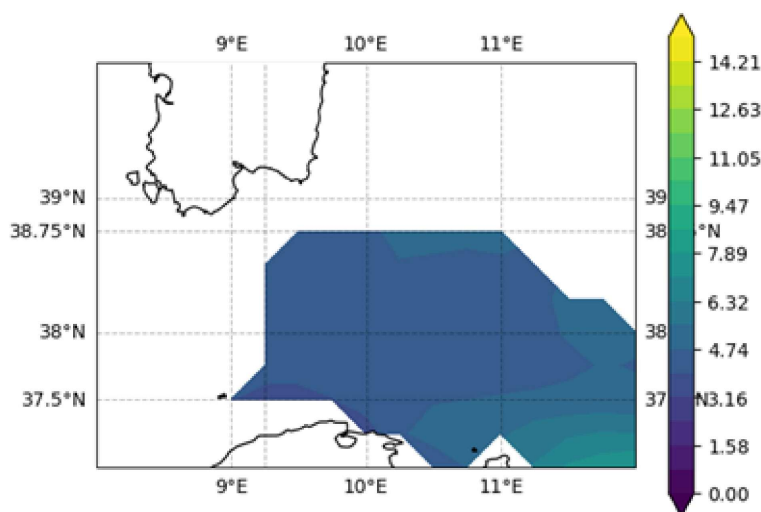
Figure 3.5: Zoom of the final location around the island of Sardinia. It has been selected the southern option due to the larger available area at a reasonable distance from the coast.

2021.6 GWh/yr, a remarkably close match to the project's reported value of 1999.1 GWh/yr. The alignment between the result of this research and the established data from the NoraEnergia2 project provides strong evidence supporting the reliability of this simplified method for power calculation. It instills confidence in the accuracy of the approach and validates its suitability for use in subsequent calculations and analyses. Building upon this outcome, the investigation has progressed culminating in the computation of the capacity factor equal to 39%. In Table 3.1 the results are shown.

	NoraEnergia2	FLORIS simulation
Net Annual Energy Production [GWh/yr]	1999.1	2021.6
Capacity Factor	38%	39%

Table 3.1: Comparison between NoraEnergia2 project and FLORIS simulation.

While focusing on the power production of the plant per day, considering the 40 turbines installed, it provides a value of roughly 230.8 MW, amount which will be used for the final calculation of the fuel output. Additionally, other functions of the Floris package were being explored to gain deeper insights into each turbine's rated annual energy. By discerning the specific energy production potential of individual turbines, a comprehensive understanding of the distribution and performance of

the entire wind farm was gained.

Fig. 3.6 represents the projected annual energy generation that the wind plant can potentially achieve under given conditions for each turbine of the plant at different levels of wind speed, where the precise value of 7.91 m/s of wind speed has been the one used in the NoraEnergia2 project and Fig. 3.7 shows the wake of each of the wind plant's turbines.
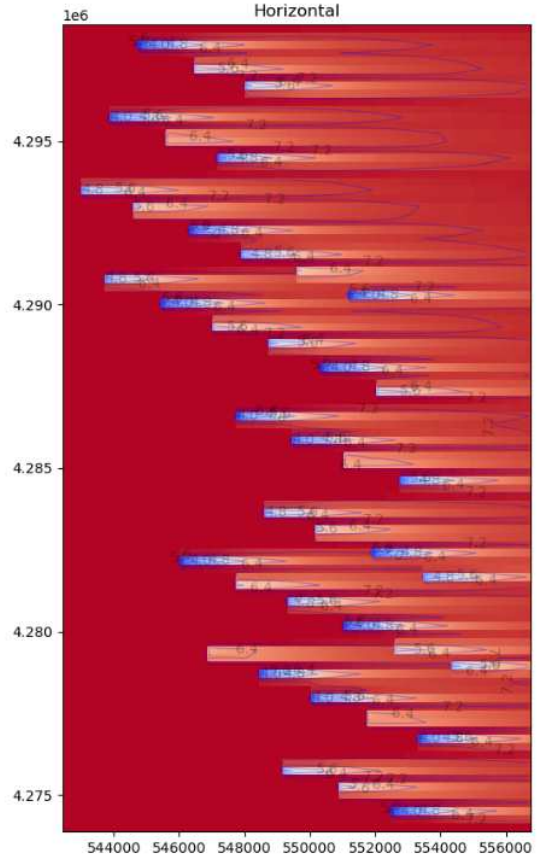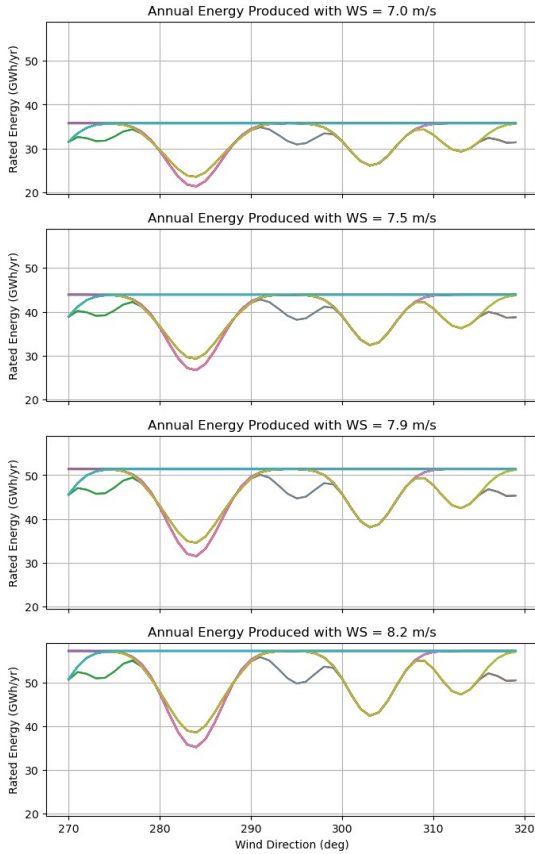
Figure 3.6: annual rated energy production of each turbine at wind speed of 7 m/s, 7.5 m/s, 7.91 m/s and 8.2 m/s.

Figure 3.7: Horizontal wake of offshore wind plant obtained with FLORIS simulation. Along the axis the coordinates of each turbines.

3.2 Wave

Regarding the wave results, an extensive calculation has been carried out to determine the wave energy matrix within the designated area. The process begins by extracting essential data from Copernicus, which provides valuable information, including the peak period of the waves and the spectral density expressed in square meters per hertz $\frac{m^2}{Hz}$.

To obtain the spectral density, the JONSWAP spectrum model was employed, which facilitated the calculation of the energy period (T_e) in seconds, as well as the omnidirectional wave energy flux (J) in watts per meter ($\frac{W}{m}$). The JONSWAP spectrum model is particularly useful in characterizing wave energy behavior and accurately predicting the energy distribution across different wave frequencies. Mean significant wave height (H_s) appears to correlate with the spatial pattern of average wind speed, while the energy period (T_e) exhibits a distinct behavior. In open sea regions exposed to the vast Atlantic fetch, T_e falls within the range of 9 to 10 seconds, indicating a prevalence of swells. However, in semi-enclosed and closed basins, the mean wave periods are shorter, typically less than 7 seconds. In these areas, the wave field evolution is predominantly influenced by local wind patterns, whereas in open seas, it is primarily governed by the distant generation of swells. [63]

Ultimately, the outcome of these computations is the wave energy flux matrix, denoted as JM. This matrix serves as a crucial foundation for subsequent calculations, especially when evaluating the performance of a wave energy converter. By combining the wave energy flux matrix with specific parameters of the chosen wave energy converter such as its capture length, it becomes feasible to determine the wave power matrix, enabling a comprehensive assessment of the system's efficiency in harnessing wave energy. The power matrix represents the amount of energy that can be delivered from the system, based on the probabilities of occurrence as estimated by the joint distribution of H_s and the period T.

By analyzing the wave power matrix, it becomes possible to assess the potential of the wave energy resource in the specific location, identifying suitable sites and estimating the potential energy production, maximizing the overall output and return on investment.

In Fig. 3.8 there are the results obtained, where the waves with the highest mean annual energy are characterized by an energy period around 6 s and a significant wave height slightly lower than 2 m.
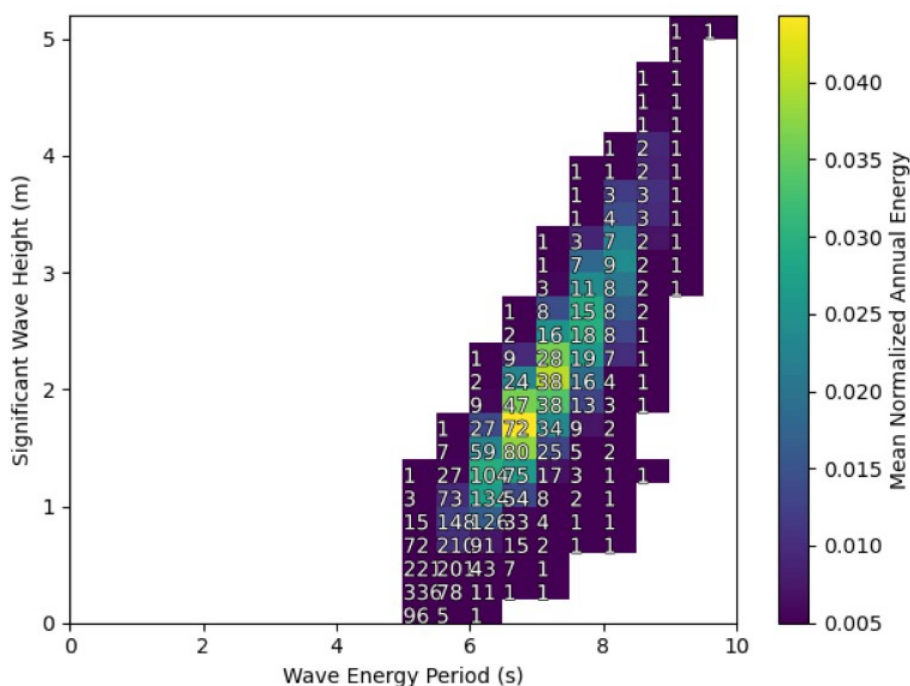
Figure 3.8: Annual wave energy flux matrix with index equal to significant wave height from spectra bins [m] and energy period from spectra bins [s].

Once seen the values obtained it should be fundamental the choice of the WEC to install in the location. There are many concepts and designs of WEC as introduced in section 2.6. Many of the designs have remained at the design stage, laboratory test stage, or prototype testing stage, while only a few have been deployed.

3.2.1 Possible Wave Energy Converter applications

The Oscillating Water Column (scheme in Fig. 3.9) is one of the first identified methods by which energy can be extracted from ocean wave and it could be applied in this situation. It consists of an underwater structure with an opening in its submerged section to capture air above the water's surface. The trapped air inside the structure moves in response to the oscillating motion of the water column, propelling a turbine positioned within the structure. This setup allows the turbine to harness the kinetic energy of the moving air and the linear up and down of the water pressurizes and depressurizes the air inside the chamber generating a flow through the turbines and converting it into usable mechanical or electrical energy.

A floating OWC could be the Backward Bent Duct Buoy (BBDB), Fig. 3.10, where the OWC duct is bent backward from the incident wave direction or the simplest possible concept is the OWC Spar Buoy, in Fig. 3.11, [64], an axisymmetric device, hence insensitive to wave direction, made of a vertical tube submerged open at both ends fixed to a floater. Here the resonance frequency of the water column inside is determined by the length of the tube. The air flow then will drive the air turbine.[65] [66] Since the spar buoy is non sensitive to wave directions it could be suitable in this offshore location where water depth can accomodate the drafts of the vertical tube with more powerful waves.[67] [65]

Figure 3.10: Schematic representation of the Backward bent-duct Buoy (BBDB).

Figure 3.9: Oscillating water column principle.

Other devices possible to use are the oscillating body systems which move in sync with the ocean waves, displaying either translational movements (like heave) or rotational movements (like pitch), visible in Fig. 3.12. [68]
These systems can either float on the water's surface or be submerged beneath it. Regions with significant water depth are particularly well-suited for this capture method as they experience more powerful waves. The resonance between the oscillating body and the ocean waves is crucial for maximizing power capture, leading to more efficient energy conversion. [69]

There are several possibilities of exploitation of seawater displacements. Surging devices take advantage of the longitudinal motion of waves, pitching devices deal with the tilting motion, and heaving devices the up-and-down motion. So heaving systems can take the form of single-body heaving buoys, Fig. 3.13. The heaving body moves in relation to a fixed frame of reference. The relative motion between

Figure 3.12: Pitch, heave and surge responses of a floating object to incident waves.

Figure 3.11: OWC spar-buoy geometry.

the oscillatory part and the fixed part drives a PTO system or a turbine, allowing the system to harness the kinetic energy of the waves and convert it into usable power.
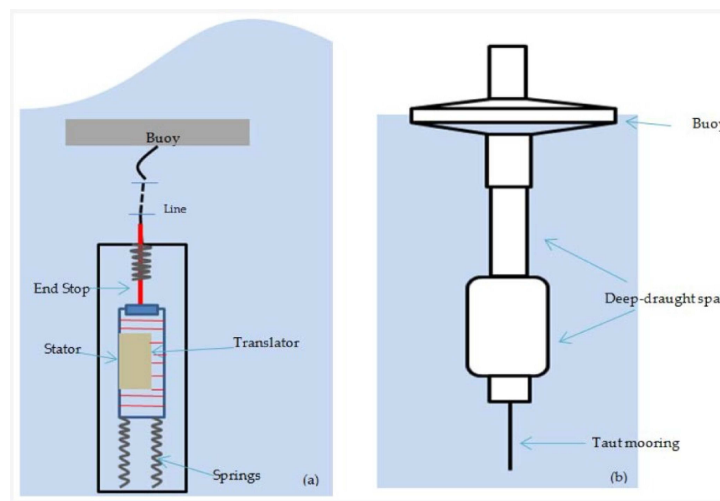
Figure 3.13: Single body heaving buoy is a floating device designed to move vertically in response to wave motion. The buoy's heaving motion helps it remain stable in rough seas.

71

Furthermore, heaving systems can be designed to operate fully submerged, where the lower portion is anchored to the seabed, while the upper segment undergoes vertical oscillations in response to the wave movements. As the buoyant upper part moves up and down, it imparts motion to a generator located in the lower section of the device. This generator efficiently converts the kinetic energy derived from the buoyant part's motion into useful mechanical or electrical power.

A research done by Lavidas et al. (2020) [70] shows the application of different types of WEC put in several locations of the North Sea, so this could be taken as as hint for a possible application in the aforesaid case study, seeing how the Pelamis could be a solution for deep water case. In Fig. 3.14 it is possible to see the results obtained.
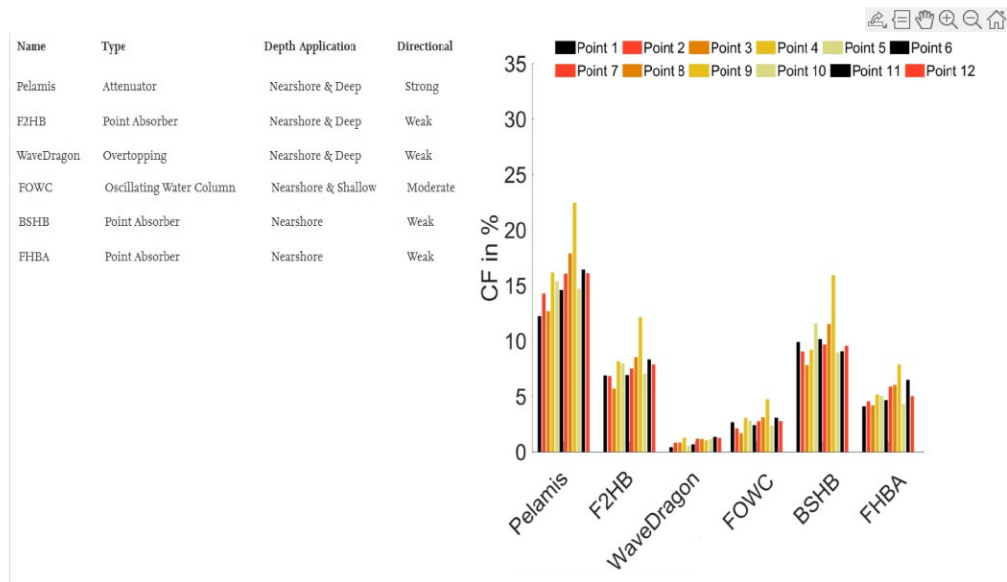
Figure 3.14: Capacity factor of different WECs in 12 different locations of North Sea. The Pelamis performs better than the other devices.

The Pelamis wave energy converter is an attenuator, which means that it extracts energy as the wave passes through its length. It employs a series of semi-submerged cylinders interconnected by hinged joints, enabling it to float and move with the waves. The movement of these joints is counteracted by hydraulic rams. These rams push pressurized oil through hydraulic motors that operate electric generators. Its scheme in Fig. 3.15 To optimize its performance, the Pelamis can be engineered to resonate at a frequency that matches the prevalent wave patterns of the environment it will be deployed in, adjusting the PTO. [71]
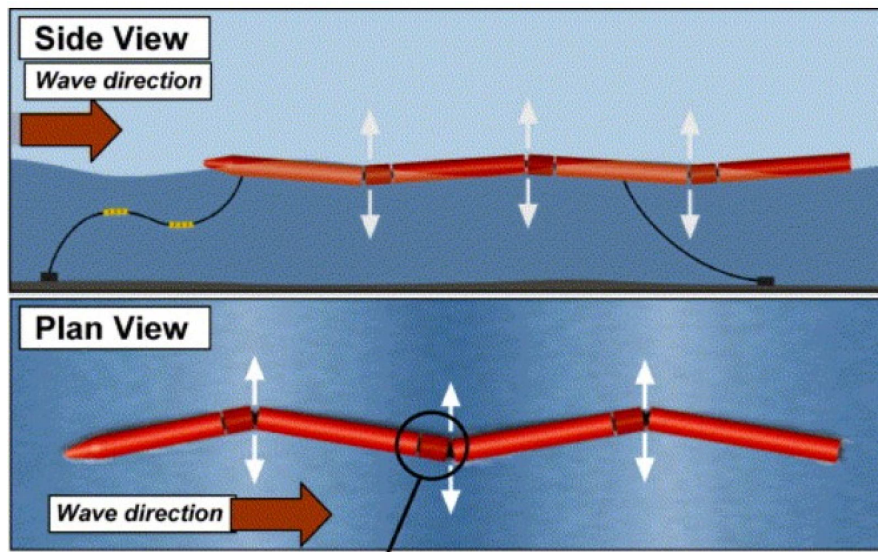
Figure 3.15: Pelamis Wave Energy Converter views. It consists of a series of connected cylindrical sections that float on the water surface. Each section contains hydraulic cylinders, which move and this motion is used to drive hydraulic motors connected to electrical generators, producing electricity.

Finally, a very interesting solution but yet at the initial stages due to the very high costs and difficult implementation could be an hybrid system exploiting wave and wind energy simultaneously. The combination of wind and wave systems is of particular interest for remote islands, since they could be completely isolated from continental grids. The prospect of sharing infrastructure and O&M costs is an advantage as well as the reduction of energy output variability and zero production time, when compared to standalone devices. [72] Plus this solution can prevent wind and wave variability and the WECs introduction would contribute to the stability of the system.

A project done in this field is the Poseidon project, P37, with 30 kW produced by 10 WECs and 33 kW from three floating wind turbines, located near Lolland, in the Baltic Sea. Fig. 3.16

The wave absorbers consists of a front pivot hinged absorber which can be weighted to adapt to varying wave circumstances. The PTO mechanism involves an oil-powered, multi-cylinder hydraulic system that links directly to the hinge axis of the absorbers. This system is capable of assimilating both the forward thrust and upward force of the waves into a unified mechanical motion, but there are still several problems with the misalignement of wind and wave directions and some fatique stresses over the pivot point. [73]

Figure 3.16: P37 demonstration platform in operation.
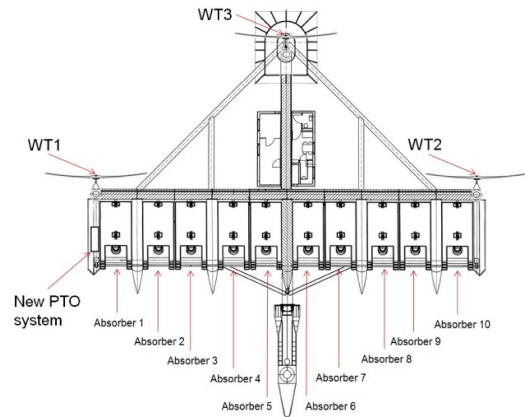
Figure 3.17: Overview of P37 and components.

3.3 Environmental constraints

Once have seen which is the best area for the possible installation of the plant the next step is to check if there are some environmental constraints that impede the realization in that area. This is about the environmental impact, which is a multifaceted factor which is usually a determining aspect of the project success during the planning and acceptance process by the resident population in the neighbourhood. [74] Basing on the path followed and used by existing projects proposed at the Ministry of Environment and Energy Security, extending the concept introduced in the 2.6.3 part, the following aspects have been analysed:

- visual impact

- bathymetric characterization

- seismic framing

- biodiversity

- constraints resulting from economic fisheries and shipping activity

- civil and military aviation activities

- mineral securities for the exploration of hydrocarbons

- cables and submarine lines

3.3.1 Visual impact

The visual impact of offshore wind turbines holds great significance as it has the potential to influence how the public perceives and experiences the scenic beauty of the landscape. While people generally support the concept of renewable energy and wind power solutions in a broad sense, their acceptance tends to decline when actual projects are proposed in their local areas. This phenomenon is commonly referred to as the 'Not In My Back Yard' syndrome, or NIMBY syndrome for short [75]. The underlying idea is that while individuals may support wind energy in principle, they may object to specific local projects due to concerns about potential consequences, especially related to noise and visual effects [76].

To address these concerns, the proposed location for the offshore wind project has been carefully chosen to be situated approximately 35 km from the shoreline, aligning with the guidance of the NoraEnergia2 project. By locating the plant within Italy's Exclusive Economic Zone, Fig. 3.18, the aim is to ensure that potential visual impacts are mitigated and minimize the likelihood of objections from nearby communities.

Figure 3.18: Exclusive Economic Zone of Italy.

The approach used for selecting the proposed location followed a methodical process that involved quantifying the Visual Impact through the identification of specific targets. Two key indices, VP and PTI, were attributed/calculated for this purpose:

- VP, (Landscape Value)

  The VP index represents the value of the landscape in the assessment of visual impact. This index is determined through the analysis of various elements, including the natural characteristics of the landscape, the existing quality of the visible environment, and the presence of areas that might be subject to particular constraints or regulations.

- PTI, (Theoretical Perception of the Installation)

  The PTI index is used to gauge the perceived impact of the proposed structure or installation on the landscape. It takes into consideration the type of structure being introduced and how its characteristics interact with the visual attributes of the surrounding landscape. To define the perception of the structure, the following indices can be utilized:

  - Perceived height H

  - Theoretical visibility level VT

The term "target" is used to describe specific areas that have attributes making them more likely to notice substantial visual changes caused by the introduction of a structure or installation.
These areas typically have potential observers present or passing through, such as cities, towns, residences, roads, or railways. Once the targets are identified, the visual impact assessment is conducted for each of them.

3.3.2 Bathymetric characterization

Bathymetry framing, which refers to the understanding and analysis of the seabed topography or underwater landscape, is of utmost importance for the selection of an offshore wind farm. It evaluates the suitability of the foundation and the stability of it avoiding sensitive areas.

The data shown in this section have been acquired and made available online within the scope of:

- EMODNet (European Marine Observation and Data Network) Bathymetry and coastline (cell resolution from $1/8 \cdot 1/8$ to $1/16 \cdot 1/16$ arc minutes) [77] `https://emodnet.ec.europa.eu/geoviewer/`

- EMODNet (European Marine Observation and Data Network) geology [78]. This portal focuses on providing access to geological data related to the European marine environment. It aims to centralize and make available geological information about the seafloor, sub-seafloor, and the geological processes that shape the European continental margins and seabeds.

For the possible final location, two options have been evaluated with their relative elevation profiles.

1. Option 1 in Fig. 3.19.
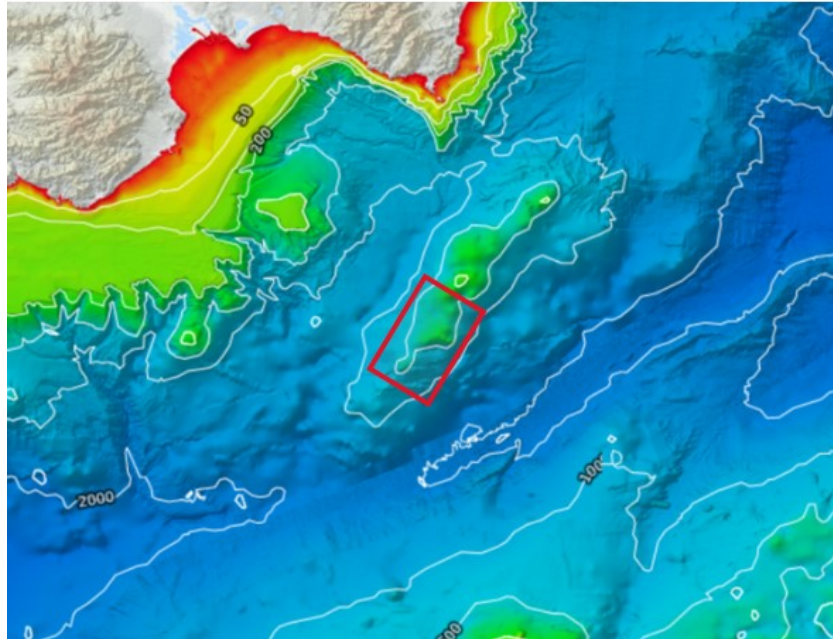
Figure 3.19: Bathymetry of option 1, obtained from EMODNet Map Viewer. Different colors represent different marine depths.

In this specific geographic location, the water depth varies ranging from approximately -500 meters to -300 meters below sea level.

The average distance from the closest land is around 35 km and the dimension of the area available at quite same depth and elevation is approximately 6 kilometers in width and from 10 to 15 kilometers in length.

Figure 3.20: Longitudinal section of the elevation profile of option 1.
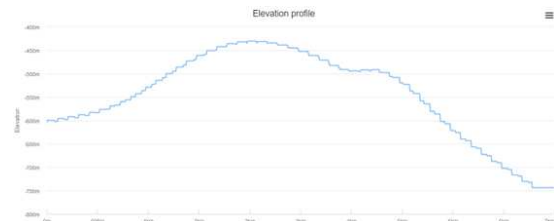
Figure 3.21: Transversal section of the elevation profile of option 1.

2. Option 2 in Fig. 3.22
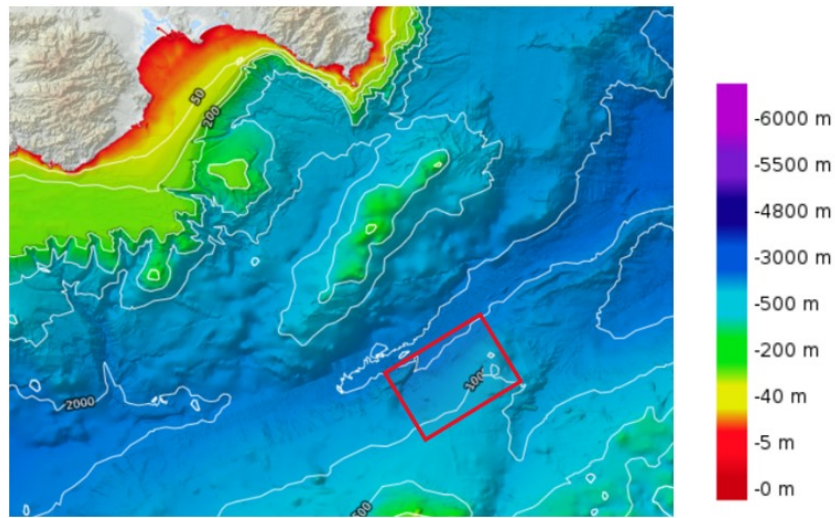
Figure 3.22: Bathymetry of option 2 from EMODNet Map Viewer

Here the water depth is between -1500 m and -1000 m. The average distance from the closest land is around 70 km and the dimension of the area available is bigger than the previous case.
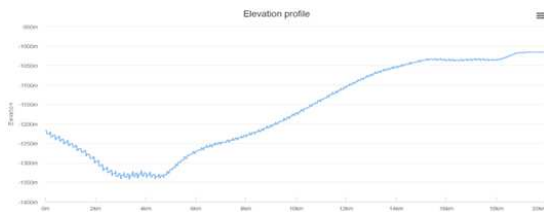
Figure 3.23: Longitudinal section of the elevation profile of option 2.
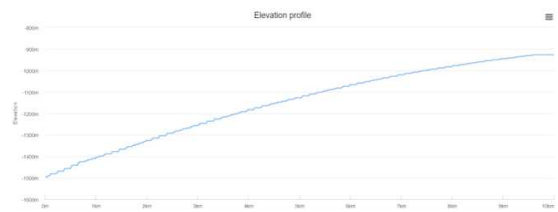
Figure 3.24: Transversal section of the elevation profile of option 2.

Due to its shorter distance from the mainland, option 1 was preferred, ensuring minimal visual impact. This proximity reduces the required length of underwater cables, leading to cost savings in transmission infrastructure and more efficient maintenance and logistics operations. To support this decision, it was noted that the NoraEnergia2 project was designed in a very close area to the one chosen in this project, precisely in the portion of sea within the Sardegna Channel and the southeast of the Gulf of Cagliari, pinpointed approximately 30 km to the south of Cape Carbonara, demonstrating that the option of this study is technically feasible.

3.3.3 Seismic framing

About the risk of seismic events it's worth to cite that the region experiences minimal seismic activity, which can be attributed to geological factors. The Sardinian-Corsican Block, in its entirety, is recognized as one of the most seismically calm areas in the Mediterranean basin, remaining stable for the past 7 million years. The occurrence of earthquakes on the island has been infrequent, and when they do happen, they tend to be of low intensity. These rare events are typically associated with the activity of fault lines that border the Sardinian-Corsican Block, particularly on the eastern and southern sides. [79] In accordance with the Prime Minister's Decree 3274 of 2003, which establishes the new criteria for the seismic classification of the Italian territory, the region of Sardinia (both in the offshore and onshore sectors) is designated as Zone 4 (ag ≤ 0.05). This classification is due to the very low likelihood of an earthquake occurring in the area, Fig. 2.20. Moreover,
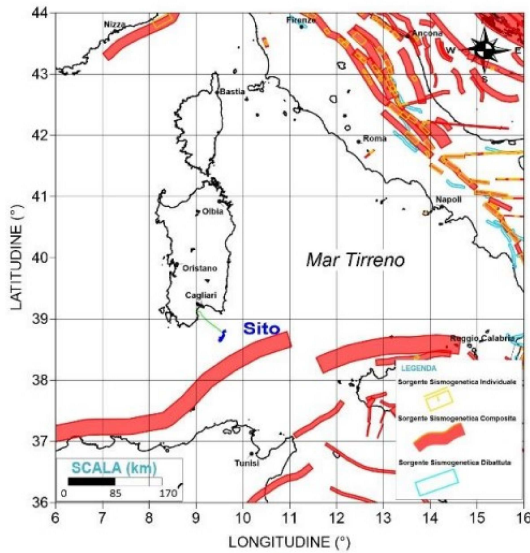
Figure 3.25: DISS (Database of Individual Seismogenic Sources). Red line stands for a composite seismogenic source, a region where earthquakes can originate due to the interaction of multiple geological features or fault systems. [80]
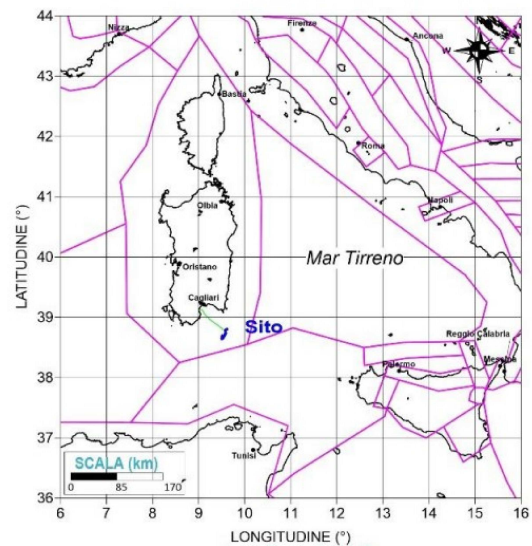
Figure 3.26: Seismic Hazard Harmonization in Europe (SHARE) model. [81]

from Fig. 3.25 and Fig. 3.26, it is possible to notice how the area selected does not fall within individual or composite seismogenic sources and, therefore, does not

exhibit faults.

3.3.4   Biodiversity

Once again. the main instrument to evaluate the biodiversity that is present in a location is using the Natura 2000 Network , the main tool of the European Union's biodiversity conservation policy. It is an ecological network spread across the entire EU territory, established under Directive 92/43/EEC "Habitats" to ensure the long-term preservation of threatened or rare natural habitats and species of flora and fauna at the community level.

The Natura 2000 Network in Sardinia consists of 31 sites of SPAs, 87 sites of Community Importance, which cover roughly 20% of the regional territory, 56 sites of SACs and 6 of them where SACs/SPAs coincide. Furthermore, with Ministerial Decree on August 8, 2019, another 23 Special Areas of Conservation and 2 more sites of coincident type were designated.
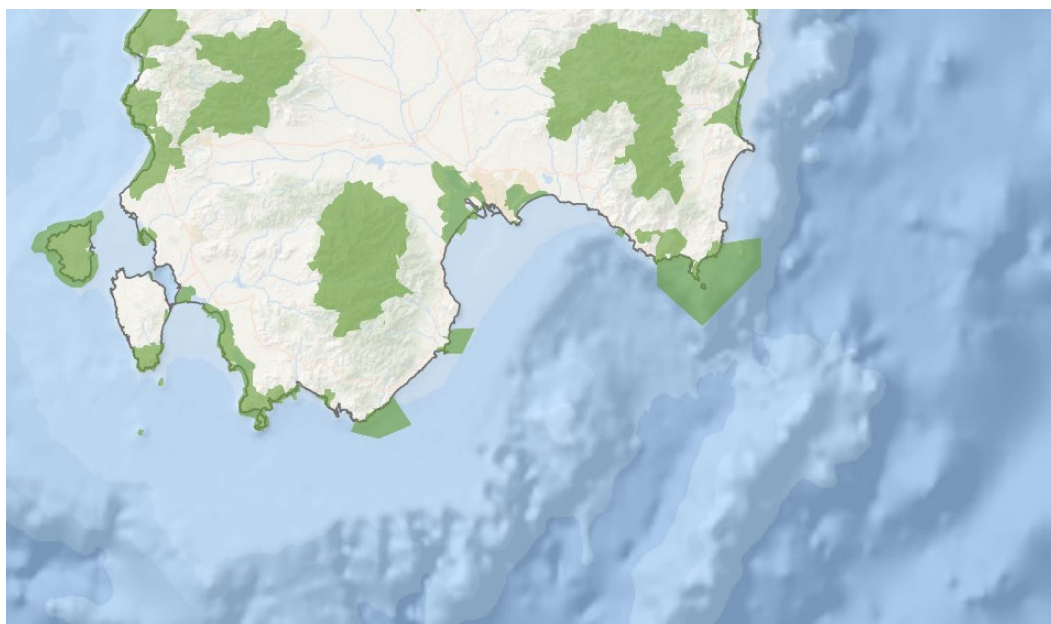
Figure 3.27: Natura2000 Network in Sardinia island.

As it is possible to see from Fig. 3.27 the absence of Natura 2000 Network areas in the offshore region of interest presents a significant advantage for the offshore wind project. But these areas will be an essential factor in determining the location for the onshore substations to connect the offshore facility with the mainland, facilitating the connection between the two. The onshore substations are not analyzed in this work but act as connection points between the offshore

plant and the onshore power grid. The strategic placement of onshore substations is critical for efficient energy transmission and distribution.

Other important parameters to take into account deal with the presence of Coralligenous and other calcareous bioconcretions in the area, as well as for the biogenic substrates in Fig. 3.28, which do not affect the location of interest.

Figure 3.28: Biogenic substrate map. Biogenic substrates are natural or biological materials that form the physical foundation or structure of an ecosystem, serving as habitats for various marine organisms.
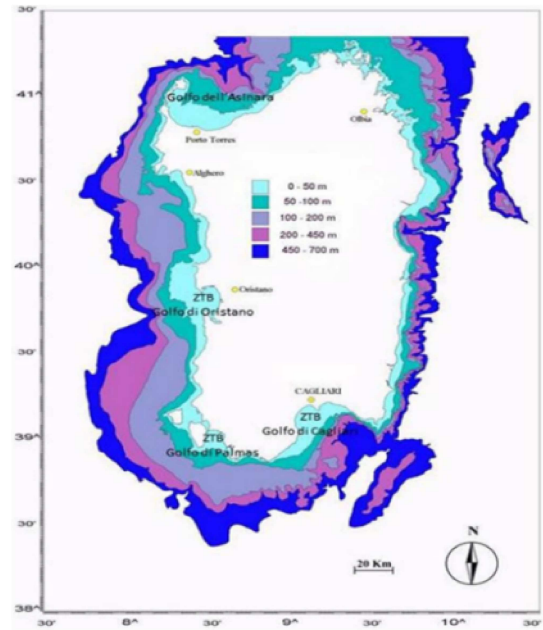
Figure 3.29: Biological Protection Zones, ZTB. [82]

Plus, the constraints resulting from economic fisheries and shipping activity can be found looking at the presence of three BPZs in operation in Sardinia, closed to bottom trawling fishing activities by regional law 7th August 1990, n. 25, with the aim of establishing repopulation areas and one of that is located in the Gulf of Cagliari but it doesn't affect the project. Fig. 3.29.

3.3.5 Civil and military aviation activities

The presence of existing traffic and marine infrastructure is an important factor when positioning an offshore wind farm. Several key elements need to be carefully considered to ensure the successful integration of the wind farm with other maritime activities and to address concerns related to flight and military operations. Firstly the farm must be placed in a location that does not obstruct the maritime traffic, avoiding shipping lanes and shipping routes. Also the fishing activities have to be

checked since they are common in many offshore areas. The purpose is to identify and avoid fishing grounds and areas important for aquaculture which can reduce conflicts with existing marine industries, preserving the livelihoods of fishermen. Also wind turbines can affect air traffic especially near airports or military airfields and a final analysis is the evaluation of the influence it could have on military operations.
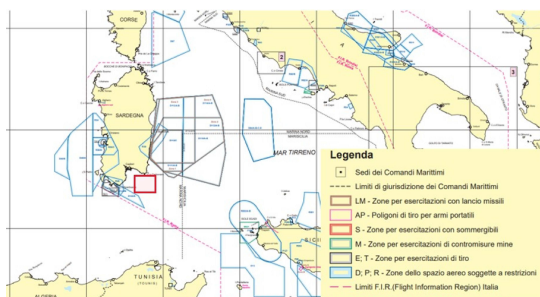
Figure 3.30: Areas dedicated to naval shooting exercises and restricted airspace.

Figure 3.31: Visual Flight Rules (VFR) of Sardinia. VFR are the rules that govern the operation of aircraft in Visual Meteorological Conditions. [83]

So, using the picture already provided section 2.6.3, namely Fig. 3.30 and Fig. 3.31, the location of the floating plant has been set, seeing how it wont affect these dedicated special areas.

3.3.6 Cables and submarine lines

Using the site Submarine Cable Map, `https://www.submarinecablemap.com/`, the only submarine cable encountered in the comprehensive assessment is Janna, owned by EXA Infrastructure, Region Sardinia, Tiscali, WINDTRE (including Wind and 3 Italia) which plays a crucial role in linking Cagliari with Mazara del Vallo, facilitating communication and data exchange across these locations but is far from the area of interest. Fig. 3.32. [84]

For what concern other connections, it is worth mentioning that Sardinia lacks gas-lines, which alleviates any concerns regarding their impact on the location selection process. With no existing gas-lines in the region, the focus can be directed towards addressing other vital factors related to the proposed offshore wind farm. Fig. 3.33.

Regarding electric connections, the scenario is little constrained, with just one prominent electric connection situated in the northern part of Sardinia, known as Sa.Pe.I. This infrastructure plays a pivotal role in electricity transmission within

the northern region, in the area of Fiumesanto, contributing to power distribution and supply reliability. Moreover, in the northern part of Sardinia, there is a project known as "Sa.Co.I.3" that involves the renewal and modernization of the existing HVDC (High Voltage Direct Current) electrical connection between Sardinia, Corsica, and mainland Italy. These information have been found on the Terna website. To provide a visual representation of the electric grid planning Fig. 3.33 displays also the 2023 Planning of the Electric Grid, helping the selection of the plant site. [85]

Figure 3.33: Electric connections actually present and future planning.
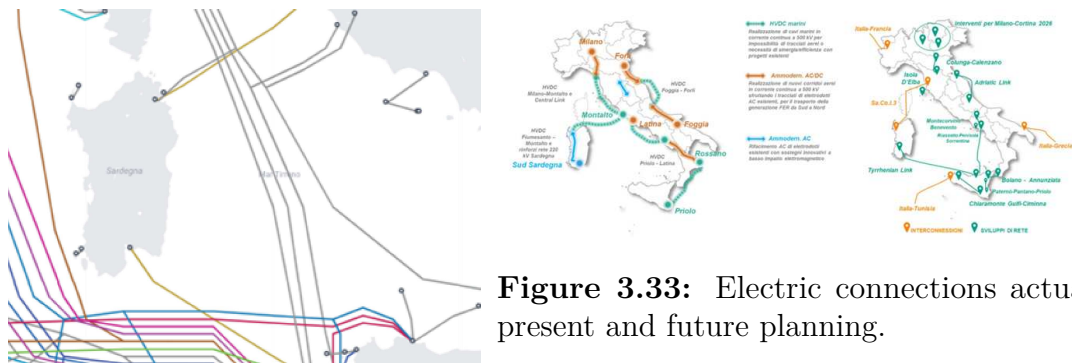
Figure 3.32: Submarine cables.

Finally the last aspect deals with the oil exploration areas, defined by the Ministry of Economic Development. These areas are designated for potential oil and gas exploration and extraction activities, aiming to assess and utilize Italy's hydrocarbon reserves, but the zone is not affected. [86] While the mining titles for the exploration and cultivation of hydrocarbons in the sea, which are conferred by the same Ministry in areas of the Italian continental shelf established by laws and ministerial decrees, called "Marine Zones" and identified by letters of the alphabet, are not a problem neither. Fig. 3.34.

As shown in Fig. 3.35, the wind farm is located outside the current mining concessions. The project area is developed outside the boundaries of ZONE E. So, considering the aspects related to the existing mining titles in the investigation area, there are no particular constraints on the construction of the project's facilities.

Figure 3.34: Oil exploration areas.
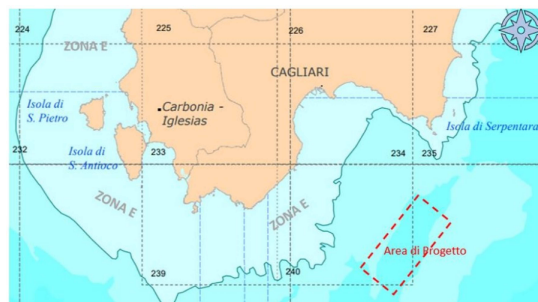
Figure 3.35: Mining titles.

3.4 Pyseafuel

The concepts described in this section relate with the analysis of results obtained from the methanol plant, showing which have been the inputs to run out the simulation.

In the case of the degasser an input flow of 10 L/s of seawater with a pH of 4.5 is considered. The pH value indicates the acidity of the seawater. Taking in mind that the average value of pH for the Mediterranean sea is around 8, [87], [88], [48], from Eiseman et al. (2012) three experiments have been performed to see the effectiveness of the degassification process at different level of pH reached. For an obtained pH of 6, 5, and 4, respectively 50%, 91% and 99% of the DIC was in the form of dissolved CO_2. That's why it was assumed a good value of pH = 4.5. The degassing process, with that quantities, resulted in a power consumption of 2618 W.

The desalinator, the main component responsible for removing salt from seawater, takes an input flow of 0.01 L/s with a salinity of 38 psu (practical salinity units) [89], [90] and a temperature of approximately 291 K, equivalent to average Mediterranean temperature which oscillates between 18°C and 19°C [91] [92]. As also visible in detail in Fig.3.37.

The desalination process involves multistage electrodialysis, but for this application a single stage is considered for ease of execution. However, it is important to note how increasing the number of stages is beneficial for the entire process in terms of reducing energy consumption, as demonstrated in Fig. 3.38 from Wang et al. (2020)
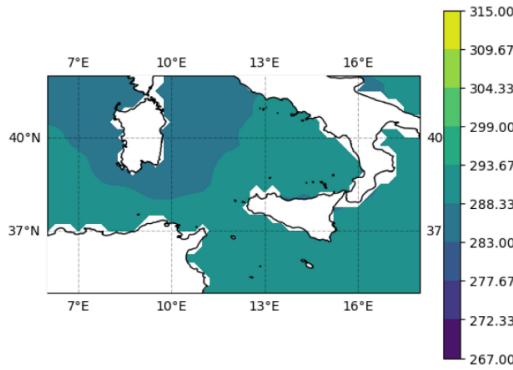
Figure 3.36: Temperature of the Mediterranean sea [K] from ERA5 data.
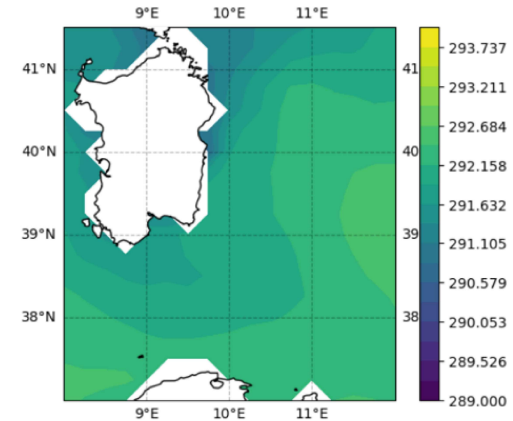
Figure 3.37: Average temperature of the Mediterranean sea [K].
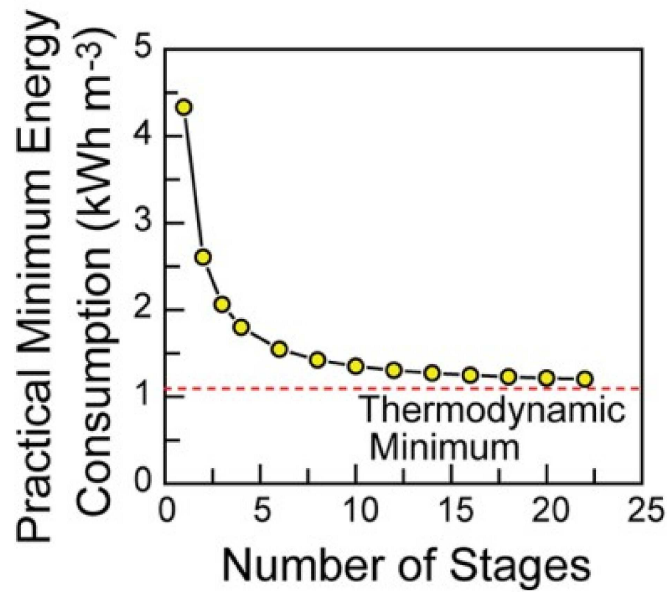
Figure 3.38: Min energy consumption as a function of the number of stages. Diagram referred to feed concentration of 600 mM, water recovery 50%, and salt rejection 99%. Image from Wang et al. (2020).

The salt removal value, ψ, which indicates the percentage of salt removal in terms of concentration for the output flow, is set at 0.99, indicating a significant reduction in salt content. The water ratio, the ratio of the inflow separated into pure water R_w, between [0, 1], is set at a value of 0.5 suggesting that for every unit

of water produced, half a unit of seawater is consumed. So, with these values the desalinator has a power consumption of 165 W.

Then the Shen electrolyzer model, which utilizes an electrolyte to convert electrical energy into chemical energy, specifically to produce hydrogen gas. The three parameters that influence the performance of an electrolytic cell are respectively E_0, r and K.

From Sheng et al. (2011) [54], the value of the kinetic parameter K has a significant impact on both the steepness and shape of the electrolysis curve within the range of $0 \leq K < \infty$. If K is equal to 0 it means that I = 0 A. This indicates that the electrochemical cell experiences no current flow and no electrochemical reaction occurs when the electrodes lack kinetic activity. Inversely, as K approaches infinity the electrochemical cell's performance mimics that of a pure resistance. When platinum, Pt, is used as cathode and metal iridium is used as anode, so as in this case, the water dissociation potential is 1.4 V, hence the cell potential E_0, parameter defined by the material properties of the cell, is set equal to 1.4 V. For this water electrolysis simulation performance, the average value for the cell internal resistance r is considered as 0.15 $\frac{\Omega}{cm^2}$ and a power conversion coefficient K of 27.8 $\frac{1}{\Omega \cdot cm^2}$.

The final power consumption of the electrolyzer is 2888 kW, by far bigger than the previous amount of the degasser and desalinator unit, exceeding their energy consumption by a considerable margin. This is due to its crucial role in producing the necessary hydrogen for the reactor. To ensure an optimal value for the overall methanol production efficiency, it's crucial to balance the need to improve the conversion factor ξ increasing the amount of hydrogen to carbon dioxide ratio and the the overall cost that will increase with the increase in demand for produced hydrogen.

The plug flow reactor is employed as final part of the system. It is a type of chemical reactor where the fluid flows through the reactor without any mixing. From Terreni et al. (2020), the reactor has been considered with a total area of 3.14 m^2, having 10000 tubes with a diameter of 2 cm, and a length of 3 m. The density of the catalyst $Cu/ZnO/Al_2O_3$ is 1000 kg/m^3, which indicates its mass per unit volume. The temperature and pressure conditions inside the reactor are specified as 180°C and 60 bars, respectively.

So, considering all the parameters mentioned above, the final value of methanol per power required to produce it, primarily attributed to the energy demand of the electrolyzer, amounts to $11.96 \frac{\mu L}{day \cdot W}$.

Input parameters					
Degasser					
Inflow	pH				
10 L/s	4.5				
Desalinator					
Inflow	Salinity	T	n stages	ψ	R_w
0.01 L/s	38 psu	291 K	1	0.99	0.5
Shen Electrolyzer					
E_0	r	K			
1.4 V	0.15 Ω/cm^2	27.8 $1/(\Omega \cdot cm^2)$			
Plug Flow Reactor					
Total area	ρ Cu/ZnO/Al$_2$O$_3$	T	P		
3.14 m^2	1000 kg/m^3	180 °C	60 bars		

Table 3.2: Input parameters for the devices responsible for the methanol production.

This quantity represents an energy efficiency of the methanol production process. Taking into account the power that the offshore wind plant could generate in that area, which results to be around 231 MW, the resulting daily production of methanol would be approximately 2800 liters per day.

It's important to say that the sufficiency of the methanol production depends on the specific demand and applications within the given context. For a smaller-scale applications or research purposes, this output might be more than sufficient. However, for larger-scale industrial uses or widespread adoption as a fuel alternative, which is the field of this study, it might be necessary to scale up the production process to meet higher demands since the final production is quite scarce.

Chapter 4

Conclusion

A comprehensive analysis has been conducted to explore the feasibility of establishing a floating wind turbine facility along the coastlines of Sardinia island. The primary objective behind this attempt is to supply the energy needs for a series of devices implemented in the production of a synthetic fuel. This innovative project capitalizes on the abundant wind resources available in the region. The design of the project involves exploiting the power of the wind to drive a complex series of processes including a degasser, a desalinator, an electrolyzer, and a reactor, each playing a vital role in the overarching scheme. The heart of the operation is the wind turbines, strategically positioned offshore to catch the energy of the wind. This energy powers the capture of hydrogen gas through the electrolyzer while the degasser comes into play to efficiently extract CO_2 from seawater. This is necessary for the subsequent production of the synthetic fuel.

Starting with a meticulous examination of the wind resource around the island, leveraging data from ERA5 and processing it using Python programming language, this approach was further complemented by a rigorous assessment of the stringent natural constraints present throughout the territory. In parallel, an analysis of wave energy resources was undertaken, exploring their potential for a possible future incorporation into the project.

Through this, the most optimal site for the establishment of the plant was pinpointed. Following the identification of the ideal location, a comparative analysis was drawn with the NoraEnergia2 project, found on the MISE official website. Using detailed simulation techniques provided in section 2, a potential estimate of the energy production of the park was simulated. By leveraging the energy output from the wind park, an evaluation of the methanol production potential of the facility was conducted.

The outcomes of the simulation have culminated in a final power request for

methanol production of $11.96 \frac{\mu L}{day \cdot W}$, correspondig to a value of 2800 liters per day using the power produced by the wind plant. Given the substantial overall power capacity of the selected wind plant, the result falls notably short of economic viability. It is essential to remember that the economic aspects were omitted from this project's analysis, as the primary aim was to explore a future prospective path for the creation of synthetic fuel sources.

It is worth delving deeper into the significance of the outcome. While the initial methanol production amount may appear modest, it represents a critical proof of concept. It underscores the feasibility of using wind energy to synthesize valuable fuels like methanol. The potential lies not only in the quantity but also in the quality of the fuel produced, as methanol holds immense promise as a sustainable and versatile energy source. A comprehensive cost-benefit analysis would be essential to determine whether the methanol production output aligns with economic sustainability, considering factors such as initial capital investment, operational costs, and market competitiveness. Such an analysis, while beyond the scope of this particular project, would be pivotal in determining the practicality and long-term success of this innovative approach. Furthermore, in consideration of factors just mentioned, the choice of the final output can be adapted to align with changing priorities and market dynamics. One alternative could be the production of DME, due to its clean combustion characteristics and reduced emissions profile, better explained in section 2.6.5.

Ultimately, there's yet another promising pathway that warrants exploration, even though it demands additional time and investment in both technical and economic realms. This involves the concept of integrating a wave energy converter alongside the wind facility. By doing so, this hybrid system would have a potential to ensure a more stable and reliable energy output, mitigating the intermittency challenges associated with wind power. Plus it holds the promise of cost reduction, potentially enhancing the overall efficiency of the system and reducing operational costs. Nonetheless, it is imperative to acknowledge that this concept remains in its early stages and necessitates significant research and development efforts.

In conclusion, this project serves as a valuable stepping stone towards the potential future of green fuel production through wind energy. It highlights the promise of harnessing renewable resources for sustainable fuel synthesis while acknowledging the critical role of economic analysis in translating these promising concepts into real-world applications.

Appendix A

Wave script

```python
import matplotlib.pyplot as plt
import matplotlib.ticker as mticker
import numpy as np
from pathlib import Path
path = Path(r'C:\Users\cella\ubuntu')
paths = sorted(path.glob('*.nc'))
import math
import pandas as pd
import types
from scipy.stats import binned_statistic_2d as \
_binned_statistic_2d
import mhkit
from mhkit import wave
from os.path import join
import xarray as x
import netCDF4

data = xr.open_mfdataset(paths)

#to obtain an annual average value
Tp0 = np.nanmean(data.VTPK, axis=(1,2), dtype= float)
Hs0 = np.nanmean(data.VHM0, axis=(1,2), dtype= float)

ind = np.where(np.isnan(Tp0) | np.isnan(Hs0), False, True)
Tp0 = Tp0[ind]
Hs0 = Hs0[ind]

time = data.time.values[ind]


```

```
30  #evaluate  which  model  describes  the  situation ,  Jonswap  or
         Pierson_Moskowitz ,  to  obtain  Spectral  Density ,  S  [m2/Hz]
31
32  #water  depth  [m]
33  h  =  350
34
35  #cut  off  frequency  [Hz]
36  fc  =  1.25/(2∗math. pi)
37
38  f  =  np.arange(0 ,  fc ,  0.2/(2∗math. pi))
39
40  Jonswap  =  True
41
42  J_list=  []
43  Te_list  =  []
44
45  for  i ,  _  in  enumerate(time ) :
46
47      if  Jonswap :
48          S  =  mhkit.wave.resource.jonswap_spectrum(f ,  Tp0[ i ] ,  Hs0[ i ] ,
      gamma=None)
49
50          print(S)
51
52  #to  calculate  wave  energy  period  Te  [ s ]
53          Te  =  mhkit.wave.resource.energy_period(S,  frequency_bins=None
      )
54          Te_list .append(Te.Te. values [0])
55
56  #calculation  of  the  omnidirectional  wave  energy  flux  of  the  spectra
57          J  =  mhkit.wave.resource.energy_flux(S,  h ,  deep=False ,  rho
      =1025,  g=9.80665,  ratio =2)
58          J_list .append(J.J. values [0])
59
60  #Convert  Te  and  J  from  pd.DataFrame  to  np.array
61          S0  =   pd.DataFrame(S) . to_numpy()
62          Te0  =  pd.DataFrame(Te) . to_numpy()
63          J0  =  pd.DataFrame(J) . to_numpy()
64
65      else :
66          S  =  mhkit.wave.resource.pierson_moskowitz_spectrum(f ,  Tp[ i ] ,
      Hs[ i ])
67  #to  create  an  average  annual  energy  matrix  with  frequency  of
      occurance
68  fig  =  mhkit.wave.graphics.plot_avg_annual_energy_matrix(Hs0,  Te_list ,
       J_list ,  time_index  =  time ,Hm0_bin_size  =  .2 ,  Te_bin_size  =  .5    )
```

Bibliography

[1] Atika Qazi, Fayaz Hussain, Nasrudin ABD Rahim, Glenn Hardaker, Daniyal Alghazzawi, Khaled Shaban, and Khalid Haruna. «Towards sustainable energy: a systematic review of renewable energy sources, technologies, and public opinions». In: *IEEE access* 7 (2019), pp. 63837–63851 (cit. on p. 1).

[2] Raif Cergibozan. «Renewable energy sources as a solution for energy security risk: Empirical evidence from OECD countries». In: *Renewable Energy* 183 (2022), pp. 617–626 (cit. on p. 1).

[3] Seyed Ehsan Hosseini. «Transition away from fossil fuels toward renewables: lessons from Russia-Ukraine crisis». In: *Future Energy* 1.1 (2022), pp. 2–5 (cit. on p. 2).

[4] Constanze Fetting. «The European green deal». In: *ESDN report* 53 (2020) (cit. on p. 2).

[5] Joeri Rogelj et al. «Mitigation pathways compatible with 1.5 C in the context of sustainable development». In: *Global warming of 1.5 C.* Intergovernmental Panel on Climate Change, 2018, pp. 93–174 (cit. on p. 2).

[6] Detlef P Van Vuuren, Sebastiaan Deetman, Jasper van Vliet, Maarten van den Berg, Bas J van Ruijven, and Barbara Koelbl. «The role of negative CO 2 emissions for reaching 2 C—insights from integrated assessment modelling». In: *Climatic Change* 118 (2013), pp. 15–27 (cit. on p. 2).

[7] *Piano Nazionale Intergrato per l'Energia e il Clima.* Ministero dello Sviluppo Economico, Ministero dell'Ambiente e della Tutela del Territorio e del Mare, Ministero delle Infrastrutture e dei Trasporti. 2019 (cit. on pp. 3, 6, 8).

[8] George A Olah, Alain Goeppert, and GK Surya Prakash. «Chemical recycling of carbon dioxide to methanol and dimethyl ether: from greenhouse gas to renewable, environmentally carbon neutral fuels and synthetic hydrocarbons». In: *The Journal of organic chemistry* 74.2 (2009), pp. 487–498 (cit. on pp. 4, 21).

[9]   Éverton Simões Van-Dal and Chakib Bouallou. «Design and simulation of a methanol production plant from CO2 hydrogenation». In: *Journal of Cleaner Production* 57 (2013), pp. 38–45 (cit. on pp. 4, 18).

[10]   *Piano Energetico Ambientale della Regione Sardegna, 2015-2030, terzo rapporto di monitoraggio.* Regione Autonoma della Sardegna. 2023 (cit. on pp. 7, 17).

[11]   *Emission Trading europeo.* ISPRA, Istituto Superiore per la Protezione e la Ricerca Ambientale. URL: https://www.isprambiente.gov.it/it/servizi/registro-italiano-emission-trading/contesto/emission-trading-europeo (cit. on p. 9).

[12]   Giorgio Osti. «The uncertain games of energy transition in the island of Sardinia (Italy)». In: *Journal of Cleaner Production* 205 (2018), pp. 681–689 (cit. on p. 14).

[13]   M Mureddu, A Porcu, F Ferrara, A Pettinau, and G Cau. «Scenari energetici sull'utilizzo della CO2 per l'accumulo di energia in Sardegna». In: (2019) (cit. on p. 15).

[14]   Leslie Bromberg and DR Cohn. «Alcohol fueled heavy duty vehicles using clean, high efficiency engines». In: (2010) (cit. on p. 18).

[15]   Leslie Bromberg and Daniel Cohn. «Heavy duty vehicles using clean, high efficiency alcohol engines». In: (2010) (cit. on p. 18).

[16]   Aubaid Ullah, Nur Awanis Hashim, Mohamad Fairus Rabuni, and Mohd Usman Mohd Junaidi. «A Review on Methanol as a Clean Energy Carrier: Roles of Zeolite in Improving Production Efficiency». In: *Energies* 16.3 (2023), p. 1482 (cit. on pp. 18, 57).

[17]   Kimberly M McGrath, GK Surya Prakash, and George A Olah. «Direct methanol fuel cells». In: *Journal of Industrial and Engineering Chemistry* 10.7 (2004), pp. 1063–1080 (cit. on p. 19).

[18]   IRENA and METHANOL INSTITUTE. *Innovation Outlook : Renewable Methanol.* Abu Dhabi: International Renewable Energy Agency, 2021 (cit. on p. 19).

[19]   Andrés González-Garay, Matthias S Frei, Amjad Al-Qahtani, Cecilia Mondelli, Gonzalo Guillén-Gosálbez, and Javier Pérez-Ramırez. «Plant-to-planet analysis of CO 2-based methanol processes». In: *Energy & Environmental Science* 12.12 (2019), pp. 3425–3436 (cit. on p. 19).

[20]   Christopher Consoli. «Bioenergy and carbon capture and storage». In: *Global CCS Institute* (2019) (cit. on p. 19).

[21]   Global Energy Transformation Irena. «A Roadmap to 2050». In: *International Renewable Energy Agency, Abu Dhabi* (2018) (cit. on p. 20).

[22] Constantine Arcoumanis, Choongsik Bae, Roy Crookes, and Eiji Kinoshita. «The potential of di-methyl ether (DME) as an alternative fuel for compression-ignition engines: A review». In: *Fuel* 87.7 (2008), pp. 1014–1030 (cit. on p. 21).

[23] Madis Paas. *Safety assessment of DME fuel. Addendum.* Tech. rep. M. Paas Consulting Ltd., Winnipeg, Manitoba (Canada); Transportation . . ., 1998 (cit. on p. 21).

[24] Yotaro Ohno. «DME in Japan». In: *4th Asian DME Conference.* 2007 (cit. on p. 22).

[25] Dipayan Choudhury, Fei Ji, Nidhi Nishant, and Giovanni Di Virgilio. «Evaluation of ERA5-Simulated Temperature and Its Extremes for Australia». In: *Atmosphere* 14.6 (2023), p. 913 (cit. on p. 26).

[26] *Climate reanalysis.* Dipartimento della Protezione Civile. URL: https://climate.copernicus.eu/climate-reanalysis (cit. on p. 26).

[27] Marıa O Molina, Claudia Gutiérrez, and Enrique Sánchez. «Comparison of ERA5 surface wind speed climatologies over Europe with observations from the HadISD dataset». In: *International Journal of Climatology* 41.10 (2021), pp. 4864–4878 (cit. on p. 26).

[28] Niels Otto Jensen. *A note on wind generator interaction.* Vol. 2411. Citeseer, 1983 (cit. on p. 27).

[29] Ángel Jiménez, Antonio Crespo, and Emilio Migoya. «Application of a LES technique to characterize the wake deflection of a wind turbine in yaw». In: *Wind energy* 13.6 (2010), pp. 559–572 (cit. on p. 27).

[30] Pieter MO Gebraad, Floris W Teeuwisse, JW Van Wingerden, Paul A Fleming, Shalom D Ruben, Jason R Marden, and Lucy Y Pao. «Wind plant power optimization through yaw control using a parametric model for wake effects—a CFD simulation study». In: *Wind Energy* 19.1 (2016), pp. 95–114 (cit. on p. 27).

[31] G.Korres M.Ravdas A.Zacharioudaki D.Denaxa & M.Sotiropoulou. «Mediterranean Sea Waves Reanalysis CMEMS Med-Waves, MedWAM3 system». In: *Copernicus Monitoring Environment Marine Service, CMEMS* (2021) (cit. on p. 27).

[32] DV Bertram, AH Tarighaleslami, MRW Walmsley, MJ Atkins, and GDE Glasgow. «A systematic approach for selecting suitable wave energy converters for potential wave energy farm sites». In: *Renewable and Sustainable Energy Reviews* 132 (2020), p. 110011 (cit. on p. 28).

[33] Marcus Lehmann, Farid Karimpour, Clifford A Goudey, Paul T Jacobson, and Mohammad-Reza Alam. «Ocean wave energy in the United States: Current status and future perspectives». In: *Renewable and Sustainable Energy Reviews* 74 (2017), pp. 1300–1313 (cit. on p. 28).

[34] Johannes Falnes. «A review of wave-energy extraction». In: *Marine structures* 20.4 (2007), pp. 185–201 (cit. on p. 29).

[35] S.Hass U.Krien B.Schachler S.Bot Kyri-Petrou V.Zeli K.Shivam &S.Bosch. «Wind-Python/Windpowerlib: Silent Improvements». In: *Zenodo* 0.2.1.Swizerland (2021) (cit. on p. 32).

[36] Tom W Thorpe et al. «A brief review of wave energy». In: (1999) (cit. on p. 38).

[37] Y Goda. «Random Seas and Design of Maritime Structure", Univ. of Tokyo Press, Tokyo, Japan». In: (1985) (cit. on p. 38).

[38] Nana O. Abankwa, Steven J. Johnston, Mark Scott, and Simon J. Cox. «Ship motion measurement using an inertial measurement unit». In: *2015 IEEE 2nd World Forum on Internet of Things (WF-IoT).* 2015, pp. 375–380. DOI: 10.1109/WF-IoT.2015.7389083 (cit. on p. 39).

[39] James Prendergast, Mingfang Li, and Wanan Sheng. «A study on the effects of wave spectra on wave energy conversions». In: *IEEE Journal of Oceanic Engineering* 45.1 (2018), pp. 271–283 (cit. on p. 40).

[40] Ministero dell'Ambiente e della Sicurezza Energetica. URL: https://va.mite.gov.it/it-IT (cit. on p. 41).

[41] Luigi Carmignani, G Oggiano, A Funedda, Paolo Conti, and Sandro Pasci. «The geological map of Sardinia (Italy) at 1: 250,000 scale». In: *Journal of Maps* 12.5 (2016), pp. 826–835 (cit. on p. 41).

[42] *Classificazione sismica 2023.* Copernicus Climate Change Service. URL: https://rischi.protezionecivile.gov.it/it/sismico/attivita/classificazione-sismica/ (cit. on p. 43).

[43] Thomas Campagnaro, Tommaso Sitzia, Peter Bridgewater, Douglas Evans, and Erle C Ellis. «Half Earth or whole Earth: what can Natura 2000 teach us?» In: *BioScience* 69.2 (2019), pp. 117–124 (cit. on p. 44).

[44] Sabrina Lai and Corrado Zoppi. «The influence of Natura 2000 sites on land-taking processes at the regional level: An empirical analysis concerning Sardinia (Italy)». In: *Sustainability* 9.2 (2017), p. 259 (cit. on p. 44).

[45] Bruce D Patterson, Frode Mo, Andreas Borgschulte, Magne Hillestad, Fortunat Joos, Trygve Kristiansen, Svein Sunde, and Jeroen A Van Bokhoven. «Renewable CO2 recycling and synthetic fuel production in a marine environment». In: *Proceedings of the National Academy of Sciences* 116.25 (2019), pp. 12212–12219 (cit. on p. 47).

[46] Jawed Qaderi. «A brief review on the reaction mechanisms of CO2 hydrogenation into methanol». In: *International Journal of Innovative Research and Scientific Studies* 3.2 (2020), pp. 53–63 (cit. on p. 47).

[47] Timothy J Lueker, Andrew G Dickson, and Charles D Keeling. «Ocean pCO2 calculated from dissolved inorganic carbon, alkalinity, and equations for K1 and K2: validation based on laboratory measurements of CO2 in gas and seawater at equilibrium». In: *Marine chemistry* 70.1-3 (2000), pp. 105–119 (cit. on p. 48).

[48] Matthew D Eisaman, Keshav Parajuly, Alexander Tuganov, Craig Eldershaw, Norine Chang, and Karl A Littau. «CO 2 extraction from seawater using bipolar membrane electrodialysis». In: *Energy & Environmental Science* 5.6 (2012), pp. 7346–7352 (cit. on pp. 49, 84).

[49] Mohtada Sadrzadeh and Toraj Mohammadi. «Sea water desalination using electrodialysis». In: *Desalination* 221.1-3 (2008), pp. 440–447 (cit. on p. 52).

[50] Li Wang, Camille Violet, Ryan M DuChanois, and Menachem Elimelech. «Derivation of the theoretical minimum energy of separation of desalination processes». In: *Journal of Chemical Education* 97.12 (2020), pp. 4361–4369 (cit. on pp. 53, 54).

[51] Douglas Keller Jr, Vishal Somanna, Philippe Drobinski, and Cédric Tard. «Offshore CO2 Capture and Utilization Using Floating Wind/PV Systems: Site Assessment and Efficiency Analysis in the Mediterranean». In: *Energies* 15.23 (2022), p. 8873 (cit. on p. 54).

[52] Fei-Yue Gao, Peng-Cheng Yu, and Min-Rui Gao. «Seawater electrolysis technologies for green hydrogen production: challenges and opportunities». In: *Current Opinion in Chemical Engineering* 36 (2022), p. 100827 (cit. on p. 55).

[53] Rafael d'Amore-Domenech, Oscar Santiago, and Teresa J Leo. «Multicriteria analysis of seawater electrolysis technologies for green hydrogen production at sea». In: *Renewable and Sustainable Energy Reviews* 133 (2020), p. 110166 (cit. on p. 56).

[54] Muzhong Shen, Nick Bennett, Yulong Ding, and Keith Scott. «A concise model for evaluating water electrolysis». In: *international journal of hydrogen energy* 36.22 (2011), pp. 14335–14341 (cit. on pp. 56, 86).

[55] Giulia Bozzano and Flavio Manenti. «Efficient methanol synthesis: Perspectives, technologies and optimization strategies». In: *Progress in Energy and Combustion Science* 56 (2016), pp. 71–105 (cit. on p. 57).

[56] Jasmin Terreni, Andreas Borgschulte, Magne Hillestad, and Bruce D Patterson. «Understanding Catalysis—A Simplified Simulation of Catalytic Reactors for CO2 Reduction». In: *ChemEngineering* 4.4 (2020), p. 62 (cit. on pp. 58, 60).

[57] Geert H Graaf, EJ Stamhuis, and AACM Beenackers. «Kinetics of low-pressure methanol synthesis». In: *Chemical Engineering Science* 43.12 (1988), pp. 3185–3195 (cit. on p. 58).

[58] Mohamad A Alkhalidi, Shoug Kh Al-Dabbous, S Neelamani, and Hassan A Aldashti. «Wind energy potential at coastal and offshore locations in the state of Kuwait». In: *Renewable Energy* 135 (2019), pp. 529–539 (cit. on p. 63).

[59] Merve Cengiz Toklu and Özer Uygun. «Location selection for wind plant using AHP and axiomatic design in fuzzy environment». In: *Periodicals of Engineering and Natural Sciences* 6.2 (2018), pp. 120–128 (cit. on p. 64).

[60] Wojciech Jarzyna, Artur Pawłowski, and Nadzeya Viktarovich. «Technological development of wind energy and compliance with the requirements for sustainable development». In: *Problemy Ekorozwoju–Problems of Sustainable Development* 9.1 (2014), pp. 167–177 (cit. on p. 64).

[61] CCEA rewarding learning. «Energy from the Wind». In: *Environmental Technology, GCE LEVEL* (2014) (cit. on p. 64).

[62] Vestas Wind Systems A/S. «V236-15.0 MW». In: *Vestas Group* (2021) (cit. on p. 64).

[63] Christina Kalogeri, George Galanis, Christos Spyrou, Dimitris Diamantis, Foteini Baladima, Marika Koukoula, and George Kallos. «Assessing the European offshore wind and wave energy resource for combined exploitation». In: *Renewable energy* 101 (2017), pp. 244–264 (cit. on p. 68).

[64] J Henriques, J Portillo, F Fay, E Robles, L Gato, and I Touzon. «On latching control for wave energy converters: the case of an oscillating water column». In: *Proceedings of the 11th European Wave and Tidal Energy Conference, Nantes, France.* 2015 (cit. on p. 70).

[65] Antonio F de O Falcao. «Wave energy utilization: A review of the technologies». In: *Renewable and sustainable energy reviews* 14.3 (2010), pp. 899–918 (cit. on p. 70).

[66] Yuanrui Sang, Hayrettin Bora Karayaka, Yanjun Yan, Nadir Yilmaz, and David Souders. «1.18 Ocean (Marine) Energy». In: *Comprehensive Energy Systems*. Ed. by Ibrahim Dincer. Oxford: Elsevier, 2018, pp. 733–769. ISBN: 978-0-12-814925-6. DOI: `https://doi.org/10.1016/B978-0-12-809597-3.00120-6`. URL: `https://www.sciencedirect.com/science/article/pii/B9780128095973001206` (cit. on p. 70).

[67] Tunde Aderinto and Hua Li. «Ocean wave energy converters: Status and challenges». In: *Energies* 11.5 (2018), p. 1250 (cit. on p. 70).

[68] JCC Portillo, PF Reis, JCC Henriques, LMC Gato, and AFO Falcão. «Backward bent-duct buoy or frontward bent-duct buoy? Review, assessment and optimisation». In: *Renewable and Sustainable Energy Reviews* 112 (2019), pp. 353–368 (cit. on p. 70).

[69] Johannes Falnes. «Principles for capture of energy from ocean waves. Phase control and optimum oscillation». In: *Department of Physics, NTNU, N-7034 Trondheim, Norway* (1997), pp. 1–8 (cit. on p. 70).

[70] George Lavidas. «Selection index for Wave Energy Deployments (SIWED): A near-deterministic index for wave energy converters». In: *Energy* 196 (2020), p. 117131 (cit. on p. 72).

[71] Ross Henderson. «Design, simulation, and testing of a novel hydraulic power take-off system for the Pelamis wave energy converter». In: *Renewable energy* 31.2 (2006), pp. 271–283 (cit. on p. 72).

[72] Daniel Clemente, P Rosa-Santos, and F Taveira-Pinto. «On the potential synergies and applications of wave energy converters: A review». In: *Renewable and Sustainable Energy Reviews* 135 (2021), p. 110162 (cit. on p. 73).

[73] Anders Yde, Mads Mølgaard Pedersen, Sarah Bellew Bellew, Anders Køhler, Rasmus S Clausen, and Anders Wedel Nielsen. «Experimental and theoretical analysis of a combined floating wave and wind energy conversion platform». In: (2014) (cit. on p. 73).

[74] Angel G Gonzalez-Rodriguez, Javier Serrano-Gonzalez, Manuel Burgos-Payan, and Jesus Riquelme-Santos. «Multi-objective optimization of a uniformly distributed offshore wind farm considering both economic factors and visual impact». In: *Sustainable Energy Technologies and Assessments* 52 (2022), p. 102148 (cit. on p. 74).

[75] Paul Gipe. *Wind energy comes of age.* Vol. 4. John Wiley & Sons, 1995 (cit. on p. 75).

[76] Søren Krohn and Steffen Damborg. «On public attitudes towards wind power». In: *Renewable energy* 16.1-4 (1999), pp. 954–960 (cit. on p. 75).

[77] *Bathymetry and Coastline.* EMODNet (European Marine Observation and Data Network), 2021. URL: https://portal.emodnet-bathymetry.eu/ (cit. on p. 76).

[78] *Geology.* EMODNet (European Marine Observation and Data Network), 2021. URL: https://www.emodnet%02geology.eu/map-viewer/ (cit. on p. 76).

[79] Carlo Meletti, Romano Daniele Camassi, and Viviana Castelli. «La sismicità storica dell'isola senza terremoti». In: *Quaderni di Geofisica INGV* (2020) (cit. on p. 79).

[80] Roberto Basili et al. «Database of Individual Seismogenic Sources (DISS), Version 3.3. 0: A compilation of potential sources for earthquakes larger than M 5.5 in Italy and surrounding areas». In: (2021) (cit. on p. 79).

[81] Sinan Akkar. «Seismic Hazard Harmonization in Europe (SHARE)». In: (2012) (cit. on p. 79).

[82] Ippiche e della Pesca. Direzioine Generale della Pesca Marittima e dell'Acquacoltura| Dipartimnento delle Politiche Competitive della Qualit Agroalimentare. «Piano di Gestione Nazionale relativo alle flotte di pesca per la cattura delle risorse demersali nell'ambito della GSA 11 (Sardegna)». In: (2015) (cit. on p. 81).

[83] Istituto Idrografico della Marina. «Premessa agli Avvisi ai Naviganti 2020 e Avvisi ai Naviganti di Carattere Generale». In: (2020) (cit. on p. 82).

[84] *La carte mondiale des câbles de telecommunications sous-marins.* EuraFibre. URL: https://www.eurafibre.fr/la-carte-mondiale-des-cables-de-telecommunications-sous-marins/ (cit. on p. 82).

[85] *TERNA: Presentato il piano di sviluppo 2023 della Rete Elettrica Nazionale.* Terna Driving Energy. URL: https://www.terna.it/it/media/comunicat i-stampa/dettaglio/piano-sviluppo-2023 (cit. on p. 83).

[86] O.Coppi N.Santocchi A.Ligato A.Orlandi and M.P.Pellegrini. «Il Mare supplemento al Bollettino Ufficiale degli Idrocarburi e delle Georisorse». In: *Direzione Generale per le Risorse Minerarie ed Energetiche* -.2 (2013), p. 76 (cit. on p. 83).

[87] Momme Butenschön, Tomas Lovato, Simona Masina, Stefano Caserini, and Mario Grosso. «Alkalinization scenarios in the Mediterranean Sea for efficient removal of atmospheric CO2 and the mitigation of ocean acidification». In: *Frontiers in Climate* 3 (2021), p. 614537 (cit. on p. 84).

[88] Koffi Marcellin Yao, Olivier Marcou, Catherine Goyet, Véronique Guglielmi, Franck Touratier, and Jean-Philippe Savy. «Time variability of the north-western Mediterranean Sea pH over 1995–2011». In: *Marine environmental research* 116 (2016), pp. 51–60 (cit. on p. 84).

[89] P Brasseur, Jean-Marie Beckers, JM Brankart, and R Schoenauen. «Seasonal temperature and salinity fields in the Mediterranean Sea: Climatological analyses of a historical data set». In: *Deep Sea Research Part I: Oceanographic Research Papers* 43.2 (1996), pp. 159–192 (cit. on p. 84).

[90] Michael N Tsimplis and Trevor F Baker. «Sea level drop in the Mediterranean Sea: an indicator of deep water salinity and temperature changes?» In: *Geophysical Research Letters* 27.12 (2000), pp. 1731–1734 (cit. on p. 84).

[91] Mohamed Shaltout and Anders Omstedt. «Recent sea surface temperature trends and future scenarios for the Mediterranean Sea». In: *Oceanologia* 56.3 (2014), pp. 411–443 (cit. on p. 84).

[92] Abdulla Sakallı. «Sea surface temperature change in the Mediterranean Sea under climate change: A linear model for simulation of the sea surface temperature up to 2100». In: (2017) (cit. on p. 84).